Université de Montréal

Optimization of Parameters Used in Predictive Models for Respirator Cartridge Service Life for Toxic Organic Vapors

Optimisation des paramètres utilisés dans les modèles de prédiction du temps de service des cartouches d'appareils de protection respiratoire contre les vapeurs organiques toxiques

par Florence Janvier

Département de santé environnementale et santé au travail
École Santé publique de l'Université de Montréal

Thèse présentée
en vue de l'obtention du grade de Ph.D
en Santé Publique
option Toxicologie et analyse du risque

August, 2017

Résumé

Les appareils de protection respiratoire munis de cartouches chimiques contenant du charbon actif, sont les appareils les plus utilisés en milieu de travail pour protéger les travailleurs contre les vapeurs organiques toxiques. Cependant, étant donné que les indicateurs de fin de service pour les cartouches ne sont pas encore au point, il est recommandé d'utiliser des modèles de prédiction pour estimer la durée de vie des cartouches. Dans le cas des mélanges, ces modèles de prédiction ne tiennent pas compte de la toxicité des contaminants.

Ainsi, l'objectif principal de cette thèse fut d'optimiser les modèles théoriques de prédiction à partir de réalisation de trois sujets de recherche : (1) le développement d'une méthode expérimentale pour caractériser la microstructure des charbons actifs dans des conditions environnementales semblables à celles de leur utilisation; (2) la conception d'une approche expérimentale dans un montage réduit avec une cartouche miniature (Mini) permettant de mieux contrôler les conditions environnementales et de réduire la quantité de solvants utilisés lors des essais ; et (3) l'intégration d'une approche toxicologique qui applique le principe de l'indice de risque (HI) aux mélanges pour l'utilisation sécuritaire des cartouches.

En ce qui concerne la caractérisation de la microporosité des charbons, il a été démontré qu'il était possible d'obtenir des isothermes d'adsorption de type I en exposant les charbons à des vapeurs organiques différentes, ayant des rapports de tensions de vapeurs variant de 0.001 à 0.1. Ces isothermes ont permis d'obtenir les microporosités des charbons et, à l'aide de l'équation de Dubinin-Radushkevich, de calculer les capacités d'adsorption des charbons des cartouches chimiques qui sont semblables aux valeurs expérimentales.

La mise au point d'un système réduit a démontré qu'une cartouche Mini représentant une section de la cartouche de taille réelle était capable de reproduire les temps de claquage à 10% d'un contaminant et la capacité d'adsorption de la cartouche tout en reproduisant des courbes de claquages parfaitement symétriques. Cette approche a permis de mieux contrôler les paramètres expérimentaux (température, humidité et débit d'air) et de diminuer la quantité de solvants utilisés pour les essais, tout en obtenant des résultats plus fiables.

L'étude sur les mélanges de vapeurs comprenant un contaminant très volatil et peu toxique a démontré que l'intégration de l'indice de risque dans le calcul du temps de service pour les mélanges permettait une utilisation efficace et sécuritaire des cartouches. Cette approche est valable lorsque la concentration du contaminant le plus volatil est < 50 ppm et que le rapport des concentrations du contaminant volatil au moins volatil est inférieur à 2.

Ces travaux ont démontré, dans l'ensemble, l'amélioration de l'approche expérimentale et théorique, ce qui apporte une plus haute précision des paramètres des modèles de prédiction du temps de service des cartouches chimiques et par conséquent, une meilleure protection des travailleurs.

Mots-clés : Vapeurs organiques, cartouches chimiques, mélanges, temps de service, charbon actif, capacité d'adsorption, modèles, indice de risque (HI), appareil respiratoire.

Abstract

Air-purifying respirators equipped with activated carbon cartridges are among the most widely used respirators in the workplace to protect against toxic organic vapors. Because end-of-service-life-indicators (ESLI) are limited for organic vapors, mathematical models are recommended to yield the cartridge service life (CSL). Moreover, in the case of mixture contaminants, the toxicity of the breakthrough vapors is not even considered in the estimation of CSL.

Hence, the main objective of this study was to improve predictive models by investigating three research topics: (1) developing an experimental approach to characterize the pore structure of activated carbons in respirator cartridges using adsorption isotherms obtained with different organic vapors of different vapor pressure at environmental conditions similar to the ones found in the workplace; (2) designing a miniaturized (Mini) cartridge device to allow better control of environmental conditions and reducing the amount of solvent used while providing reliable data; (3) integrating a toxicological approach in the estimation of CSL for vapor mixtures by using the Hazard Index (HI) principle to indicate the safe use of respirators.

The characterisation of the microporous structure of the activated carbons showed that a type I characteristic multi-vapor adsorption isotherm can be obtained with organic vapors of relative vapor pressures ranging from 0.001 to 0.1. The obtained micropore values were used in the Dubinin-Radushkevich equation to calculate the micropore volumes and the adsorption capacities of the activated carbons, which showed agreement with the experimental data.

The Mini cartridge device was designed to reproduce a small section of a given respirator cartridge and have the same carbon bed thickness as the full size respirator cartridge. The Mini was able to reproduce symmetrical breakthrough curves of the full size cartridge and gave results comparable to the 10% breakthrough times and adsorption capacities of the cartridges. This efficient approach provided better control over environmental conditions (temperature, humidity, and flow) in breakthrough tests to obtain reliable data, and reduced the amount of solvent used.

The study on vapor mixtures involving a volatile and low toxic component showed that applying the Hazard Index (HI) was suitable for optimal and safe use of respirator cartridges.

This approach was reliable at low concentrations of acetone (< 50 ppm) and when the ratio of the contaminants of the volatile to the less volatile was < 2.

Overall, this thesis has showed that the experimental and theoretical approaches have improved the predictice models for cartridge the service life by improving the precision of the intrinsic parameters of these models to better protect the workers.

Keywords : Organic vapors, cartridge service life, breakthrough time, activated carbon, models, mixtures, adsorption capacity, hazard index, air-purifying respirator.

Table of Contents

List of Tables

List of Figures

List of Abbreviations

AIHA	American Industrial Hygiene Association
ANSI	American National Standards Institute
APF	Assigned protection factor
APR	Air-purifying respirator
BET	Brunauer- Emmett-Teller
BJH	Barrett-Joyner-Halenda
BLS	Bureau of Labor Statistics
CA	Concentration Addition
CNESST	Commission des normes, de l'équité, de la santé et de la sécurité du travail
CSA	Canadian Standards Association
CSL	Cartridge Service life
DCM	Dichloromethane
DFT	Density Functional Theory
DR	Dubinin-Radushkevich
EPA	Environmental Protection Agency
ESLI	End-of-service-life-indicator
FID	Flame Ionization Detector
HI	Hazard Index
IA	Independent Action
IAST	Ideal Adsorbed Solution Theory
IDLH	Immediately dangerous to life or health
IRSST	Institut de recherche Robert-Sauvé en santé et en sécurité du travail
IUPAC	I*nternational Union of Pure and Applied Chemistry*
LDF	Linear Driving Force
LDFT	Local Density Functional Theory
MIBK	Methyl Isobutyl Ketone
Mini	Miniaturized cartridge
MTZ	Mass Transfer Zone
MUC	Maximum use concentration

NDFLT	Non-Local-Functional-Theory
NIOSH	National Institute for Occupational Safety and Health
OSHA	Occupational Safety & Health Administration
OV	Organic Vapor
OEL	Occupational Exposure Limit
PPE	Personal protective equipment
PSD	Pore size distribution
RH	Relative Humidity
RROHS	Regulation Respecting Occupational Health and Safety
TLV	Threshold Limit Value
UF	Uncertainty Factor
US	Unites States
WJ	Wheeler-Jonas Equation

Acknowledgement

There is an African proverb about the pencil effect, which means that a lot of elements have to come into place in order to achieve a big accomplishment such as a thesis. This thesis would not have been possible without the following people and financial support.

I would like to thank my mother, who has gone beyond and above to support me. Without her, this work would not have been possible. I would like to dedicate this thesis to my father who is no longer with us, but has made personal sacrifices for his family. I thank my sister who my role model who also has PhD. She paved the way even before I had embarked in this journey. Finally, my son, the reason I do all of this for. And of course none of this would have been possible without my faith in God.

Furthermore, I would like to thank my advisors and mentors: Dr. Jaime Lara and Dr. Sami Hadadd for their guidance and advice throughout my graduate studies. *L'École de santé publique de l'Univesité de Montréal* (ÉSPUM) and the Department of Environmental and Occupational Health made life as a graduate student easier and more enjoyable. Many aspects of this research were performed in collaboration with the *Institut de recherche Robert-Sauvé en santé et en sécurité du travail* (IRSST) and *Institut de recherche sur l'hydrogène de Université du Québec à Trois-Rivières*. Therefore, I would like to thank Dr. Ludovic Tuduri, Mr. Daniel Drolet, Mr. Ives Cloutier and Mr. Daniel Cossement. I thank my mentor, Mr. Wayne Wood for his guidance. I am thankful for the financial support from the doctoral scholarship of IRSST and Fonds de recherche du Québec – Santé (FRSQ), and ESPUM and the several scholarships and awards earned during my graduate studies (Canadian Centre for Occupational Health and Safety, American Industrial Hygiene Foundation Scholarship, Quebec Black Medical Association Scholarship, Fondation de L'Association québécoise pour l'hygiène, la santé et la sécurité du travail (AQHSST), Arthur Johnson Young Researcher Award from the International Society for Respiratory Protection (ISRP), and the travel scholarships from l'Institut de recherche en santé publique de l'Université de Montréal (IRSPUM)

CHAPTER 1: INTRODUCTION

1.1 Chemical Hazard

Chemical hazards are one of the most severe hazards found in the workplace due to their widespread applications in the chemical and allied industries, research, engineering, construction and manufacturing processes. According to the *Québec Survey on Working and Employment Conditions and Occupational Health and Safety*, over 312,000 (8.8%) workers are exposed to solvents and one in five manual workers are often or always exposed to solvents in their principal line of work [1]. Similarly, in the Unites States (U.S.), 25.0% of the population reported chronic exposure to vapors, dust, gas, or fumes while on their job according to the 2010 *National Health Interview Survey* [2,3].

Every year in the US, 190,000 illnesses and 50,000 deaths are attributed to chemical exposure in the workplace [4]. Exposure to chemical hazard poses a wide range of health effects to the nervous central systems, the peripheral nervous system, effect on the liver and the kidneys, reproductive functions carcinogenicity, lung impairment, and even hearing loss [5–9]. Inhalation is the main exposure route for chemical hazards in the workplace although dermal exposure may be important in some industry such as paints [10].

Thus, the alarming prevalence rate of occupational exposure and health risk of chemicals show the importance for improvements in worker's protection from inhalation of hazardous contaminants.

1.2 Controlling Hazards in the Workplace

Hazards are first controlled by substitution for less hazardous chemicals available in the marketplace [11]. However, when substitution is not feasible, or when engineering or administration control measures are not adequate or while they are being implemented, personal protective equipment (PPE) is required by the *Regulation Respecting Occupational Health and Safety* (RROHS) [12] in Quebec and by the *Occupational Safety & Health Administration* (OSHA) [13] in the U.S. The concept behind the hierarchy of controls (see Figure 1.1) is that the control methods at the top of the list are potentially more effective and protective than those

at the bottom. Following the hierarchy normally leads to the implementation of inherently safer job-sites, ones where the risk of illness or injury has been substantially reduced.

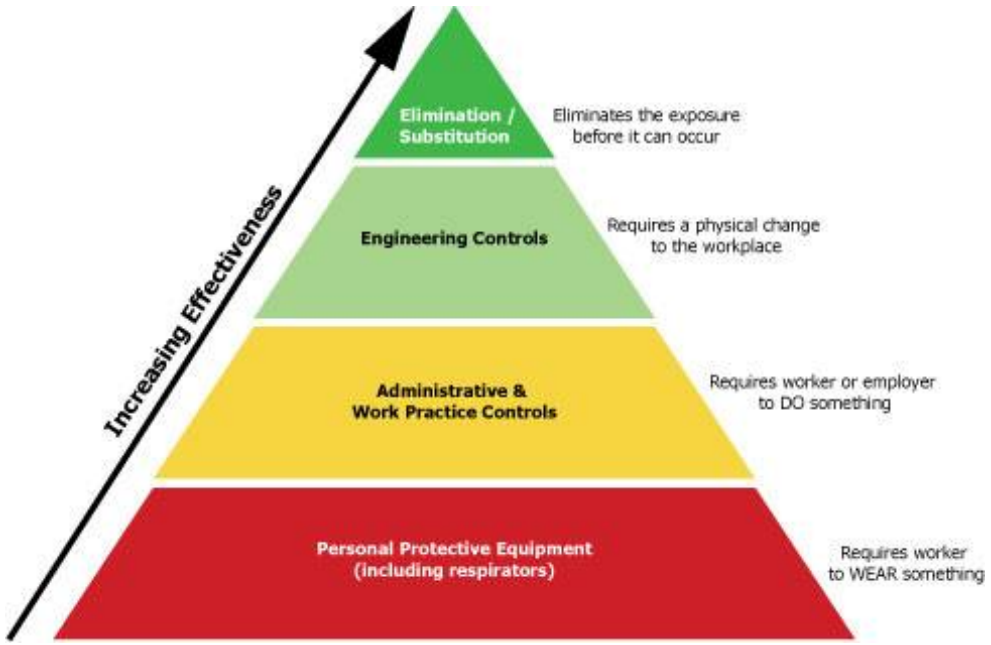

Figure 1.1. Hierarchy of controls adapted from [4]

1.3 Respiratory Protection

The use of respiratory protection is among the most important PPE to protect workers from inhalation of hazardous contaminants. According to the 2001 survey of the National Institute for Occupational Safety and Health (NIOSH) and the U.S. Department Bureau of Labor Statistics (BLS), 3.3 million private sector employees distributed among 281,800 establishments required the use of respirators [14].

An appropriate respirator has to be selected depending on the type of contaminant, concentration, toxicity and regulations. There are two main categories of respirators: air-supplied and air-purifying respirators (APR). Air-supplied respirators provide clean air from an uncontaminated source and may be used for long periods of time in oxygen deficient and other

immediately dangerous to life or health (IDLH) atmospheres when used in conjunction with a 5 minute self-contained air-supply (escape respirator).

Whereas APRs use replaceable filters or cartridges/canisters to remove contaminants from the ambient air, they cannot be used in oxygen-deficient atmospheres, or in atmospheres, which have high concentrations of contaminant. Proper fit of APRs may be required too.

1.3.1 Air- Purifying Respirators (APRs)

Among all the respirators, APRs are the most widely used. In the U.S., from all the private establishments requiring respirator use (emergency and non-emergency), 95% of them required APRs to protect mostly against paint vapors (45.7%), solvents (28.3%), and other dust/mist (24%) [12,13].

However, 78% of all the workplaces requiring the use of APRs had no written change-out schedule as required by law [15]. Moreover, the 2011 survey conducted by the American Industrial Hygiene Association (AIHA) on approximately 6000 members revealed that 69% indicated a need for specific courses with a significant interest in cartridge change-out schedule [16].

Change-out schedule of vapors/gas filtering cartridges for air-purifying respirators is important because the old practice of relying on contaminant odour thresholds as an indicator for determining cartridge service life is no longer acceptable and when end-of-service-life-indicator (ESLI) is not available, the employer is required to establish a change-out schedule for cartridges [13]. The change out schedule allows the replacement of the cartridge before the "service life " has ended.

1.3.2 Activated Carbon Respirator Cartridges

In the case of organic vapors, air-purifying respirators (APRs) are equipped with replaceable filter cartridges, which contain an adsorbent medium to remove toxic vapors from the ambient air by a process known as adsorption. Typically, activated carbon is used as the sorbent material due to its high porosity and surface area, and adsorption capacity, and low cost [17]. Activated carbons are obtained from various precursors, and thus the characterization of the porous structure, which varies based on the activation methods, has proven to be difficult.

However, this filtering process is limited and after the cartridge has adsorbed a particular contaminant to its capacity, it will begin to let the contaminants enter inside the breathing zone, which is referred to as breakthrough. The service life is the estimated or calculated time at which the breakthrough of contaminants is reached for a specific cartridge under specified conditions. Typically 10%, 50%, or 90% of inlet concentration existing the cartridge is considered the breakthrough depending on the Permissible exposure level (PEL). Moreover, the breakthrough or service life of a cartridge depends upon many factors including environmental conditions (concentration, temperature, and relative humidity) [18], breathing rate [19], the physical and chemical characteristics of the adsorbent (activated carbon) [17] and the presence of other contaminants in the air [20]. When a cartridge is saturated, it can no longer provide respiratory protection and all the contaminants will pass through the filtering media.

In the case of exposure to more than one contaminant in the ambient air, which is the most common situation in the workplace environment, the cartridge service life is decreased due to the presence of other contaminants. Furthermore, the concentration of the most volatile contaminant inside the mask can exceed the concentration outside the mask, thus wearing a respirator can become more dangerous than not even wearing one [21].

1.3.3 End-of Service-Life Indicator Cartridges

Currently, there are very few cartridges equipped with National Institute for Occupational Safety and Health (NIOSH) approved end-of-service-life-indicators (ESLIs). ESLIs are limited for organic vapors and typically are effective at specific concentrations. The ESLI technology sensor warns the wearer when it is time to change cartridges often by a color change.

Challenges in the development of ESLI for cartridges have been described [22,23] and typically the disadvantages are that they require active monitoring by the user, presence of lighting, interference by the relative humidity (RH) or other substances and are specific for only a particular chemical functional group.

1.3.4 Predictive Models for Cartridge Service Life

Predictive models, which incorporate physicochemical properties of the adsorbent and cartridge, are recommended to estimate cartridge service life because they are inexpensive and take less time than having to perform a single test for every working situation. Nevertheless, experimental data on the textural properties such as the micropore volume and adsorption capacity of activated carbon is required for identification of parameters and for model validation for various working conditions.

Several authors have described the challenges of developing a mathematical model for cartridge service life. Wheeler-Jonas [24, 25], Yoon [26], Wood [27], Lodewyckx [28] and Vallières [29] all have proposed predictive models to improve cartridge service life estimations. Several of these models lack experimental data and some fitting parameters do not have physical meaning, thus reducing accuracy. Also, they fail to account for mixture of various compounds. The complexity of the adsorption process, however, makes it necessary to use simplifying assumptions in deriving these models without consideration of the role of activated carbon microstructure on organic vapor adsorption.

Recent studies on cartridge service life have focused on the effect of water and adsorption rate coefficient to improve the estimation of cartridge service life. Few scientists have studied the optimization of the adsorption capacity, a crucial parameter in the prediction of cartridge service life, which incorporates activated carbon textural properties. These models have been derived from the performance of a limited number of compounds with limited structural considerations.

Furthermore, establishing cartridge service life for mixtures of contaminants is a complex task. Several prediction tools/software based on these aforementioned models and respiratory selection guidelines have been developed. Aside from the recommendation of not using an APR if the concentration of the contaminant is greater than the occupational exposure limit by a factor of 10 for half-mask and 100 for a full mask, no other consideration of the toxicity of the contaminant have been integrated.

The existing recommendation for multi-component mixtures is to consider the additive concentration effect, using the breakthrough concentration of the most volatile contaminant as

the determinant in the calculation of cartridge service life [20]. This approach is simplistic and typically over-estimates the cartridge service life because is does not take account the quantity and toxicity (e.g. cumulative effect) of the contaminants.

1.4 Research Questions

This thesis aims to improve cartridge service life prediction models by (a) developing an adsorption isotherm by integrating textural properties of activated carbon obtained in environmental conditions similar to field use; (b) designing a miniaturized experimental set-up for better control of experimental conditions; and (c) incorporating a toxicity approach in the case of mixtures. The specific objectives are:

I. Build a so-called universal adsorption isotherm from breakthrough data with different organic solvents of different boiling points obtained from environmental conditions that closely match use in the workplace. A point in the adsorption isotherm, representing the adsorption capacity can be used to predict respirator cartridge service life for any other organic solvent without prior experimentation. Also this approach can provide further understanding of the mechanism of organic vapor adsorption onto activated carbon when comparing with traditional textural characterization method with inert gases (ex. N_2, Ar).

II. Develop and validate an innovative design of a miniaturized (Mini) device, which replicates a small area of a full size respirator cartridge to obtain accurate and reliable data from breakthrough experiments under controlled experimental conditions, which would also translates into a significant reduction in the amount of solvent used.

III. Propose a toxicological approach for multiple contaminants to determine cartridge service life by applying the hazard index principles, which takes into account the breakthrough vapor of the mixture to estimate the cartridge service life.

1.5 Thesis Outline

Chapter 2 surveys the overarching regulations of respiratory protection that apply to Quebec, Canada, and the United Sates and the complementary elements for an efficient respiratory protection. It also explains the properties of activated carbon and adsorption processes fundamental in gaseous filtration. This chapter also provides a critical review of studies in cartridge service life, and model development.

Chapter 3 provides the methods and the experimental procedures used throughout this study.

Chapter 4 compares the micropore characterization of activated carbon in respirator cartridges used in the prediction of the adsorption capacity parameter and proposes a comprehensive model based on the adsorption isotherm of several organic solvents with different vapor pressures. The fundamental concepts, experimental-set up, assumptions, and equations as well as the input parameters used in this model are explained in details in this chapter. The predicted adsorption data obtained from the proposed model are compared with the experimental data for five compounds. This paper was published in the scientific journal Carbon.

Chapter 5 describes and validates the experimental approach of the miniaturized cartridge with a repeatability and reproducibility study. The breakthrough data of the Mini and the full size cartridge are compared. This paper was published in Adsorption Science and Technology.

Following this validation process, Chapter 6 introduces the development of a new toxicological approach for mixtures, and was submitted to the International Society for Respiratory Protection Journal.

Chapter 7 presents the general discussion and conclusions of this study and recommendations for further work on the subject.

1.6 Statement of Authorship

I am the first author of all three publications presented in this dissertation. A version of Chapter 4 has been published (**Janvier, F**., Tuduri, L, Cossement, D., Drolet, D., Lara, J.,

Micropore characterization of activated carbons of respirator cartridges with argon, carbon dioxide, and organic vapors of different vapor pressures, November, Carbon 94, 2015, 781-791.) As the lead investigator, my contribution represented overall more than 80%. I was responsible of the acquisition of the organic vapor data at the *IRSST* laboratory, the analysis and the interpretation of argon, CO_2, and OV data, as well as writing the manuscript composition. Tuduri was involved in the early stages of concept formation and contributed to manuscript edits. Cossement was involved in the data acquisition of Ar and CO_2 data at the *Institut de recherche sur l'hydrogène (IRH)* de *l'Université du Québec à Trois-Rivières*. Drolet was involved in the study concept. Lara was the supervisory author on this project and was involved throughout the project in concept formation and manuscript composition.

A version of Chapter 5 has been published in the *Journal of Hazardous Materials* (Janvier, F., Tuduri L., Cossement D., Drolet D., & Lara J. (2016), *Systematic evaluation of the adsorption of organic vapors onto a miniaturized cartridge device using breakthrough tests in parallel experiment with a full size respirator cartridge*, Adsorption Science & Technology, 34(4-5), 287-306.). My overall contribution represented over 80% of the work. I was the major lead investigator of this project, responsible for all data collection at IRSST, analysis, interpretation, and manuscript composition. Tuduri was involved in the early stages concept and contributed to the manuscript edits. Cossement was involved in the design of the Mini device. Lara was the supervisory author on this project and was involved throughout the project in concept formation and manuscript edits.

I was the lead investigator for the project presented in Chapter 6 and the status of the manuscript is published (Janvier, F., Haddad, S., Lara, J. (2017) *Integrating a Toxicology Approach in the Prediction of Cartridge Service Life for Mixtures*, International Society for Respiratory Protection, 34 (1), 10-25. My overall contribution represented over 85% of the work. I was responsible of the project conception, design, data acquisition, analysis and interpretation as well of manuscript composition. Haddad and Lara were the main supervisors on this project, and were both involved in the project conception and manuscripts edits.

CHAPTER 2: BACKGROUND

2.1 Regulator Drivers

Knowledge of applicable policies in respiratory protection is the underpinning of this thesis. In Quebec, compliance to regulations is a complex task because it makes reference to other jurisdictions such as Canada and the United Sates (U.S.).

In Quebec, the *Commission des normes, de l'équité, de la santé et de la sécurité du travail.* (CNESST) has the responsibility to administer Quebec's occupational health and safety plan in compliance with the law *An Act respecting occupational health and safety* [30,31] for which the articles governing respiratory protection are found in the *Regulation Respecting Occupational Health and safety (RROHS)* [32]. It stipulates that employers are required to provide respirators specific to the intended use according to the *Guide of respiratory protection equipment used in Québec* published by *l'Institut de recherche Robert-Sauvé en santé et en sécurité du travail* (IRSST). In the section on individual protective respiratory equipment article 45 states:

> … the employer shall provide the worker, free-of-charge, with respiratory protective equipment and ensure that he uses it, as indicated in the *Guide des appareils de protection respiratoire utilisés au Québec*, published by the *Institut de recherche Robert-Sauvé en santé et en sécurité du travail* . The equipment shall be selected, adjusted, used and cared for in accordance with the CSA Standard Z94.4-93 *Selection, Use and Care of Respirators*. A respiratory protection program shall be drafted and applied in compliance with that standard [32].

It also clearly underscores that this procedure does not replace the employer's obligation to reduce danger at the source [32].

The Canadian Standards Association (CSA) governs operating procedures in the selection, use, and care of respirators. The RROHS refers to the Z94.4-93 [33], which identifies the need for an effective respiratory protection program and the importance of its administration in the workplace. Its objective is to protect respirator users from any known respiratory hazards. Each province has its own regulations for respiratory protection and most of them refer to the recent Z94.4-11 CSA Standards [34].

All the respirators used in Quebec including all the components such as facepieces, cartridges, connectors, straps, air hoses etc. are classified and certified by the National Institute for Occupational Safety and Health (NIOSH) according to the 42 CFR part 84 regulation. NIOSH also recommends a respiratory selection protocol for choosing respirators based on properties of the contaminants [35]. By contrast the Occupational Safety and Health Administration (OSHA) is the US federal agency that legislates the use of respirators to protect workers from inhaling hazardous substances when engineering controls are not feasible under the 29 CFR 1910.134 standard [13].

Another important regulatory driver worth mentioning is the American National Standards Institute (ANSI). ANSI coordinates the U.S. voluntary consensus standards system, providing a neutral forum for the development of policies on standards issues on a global scale for all industries.

2.2 Description and Selection of Respirators

The selection of an appropriate respirator depends on the level of oxygen in the air being greater than 19.5% for all filtering respirators, types of contaminants, assessment of contaminants concentration, environmental conditions, the exposure limit and the physical properties of the hazard [36]. Furthermore, consideration for work requirements and conditions, the duration of exposure, comfort and proper fit and any additional stress to the respirator user must be given.

All respirators have an assigned protection factor (APF) and depending on the type, it will provide a different level of respiratory protection. The APF is defined as the level of respiratory protection that a properly functioning and fitted respirator is expected to provide to a trained user and is the ratio of the ambient concentration of a given contaminant to that inside a respirator mask [33]. The maximum use concentration (MUC) is the maximum concentration that a worker is expected to be protected against when wearing a respirator and is calculated using APF (i.e. multiplying the occupational exposure limit by the protection factor) [13].

Facepieces of a respirator can either be tight fitting or loose-fitting. Tight-fitting facepieces require a seal around the perimeter of the respirator user's face and must be fit tested prior to use. Fit testing assures that a tight-fitting facepiece respirator is able to provide a good face seal, and has to be performed for each worker who is assigned a tight fitting respirator. Loose-fitting

facepieces cover all the head without sealing directly onto the face and rely on airflow, which generates positive pressures within the facepiece. Tight-fitting or loose-fitting facepieces are illustrated in Figure 2.1:

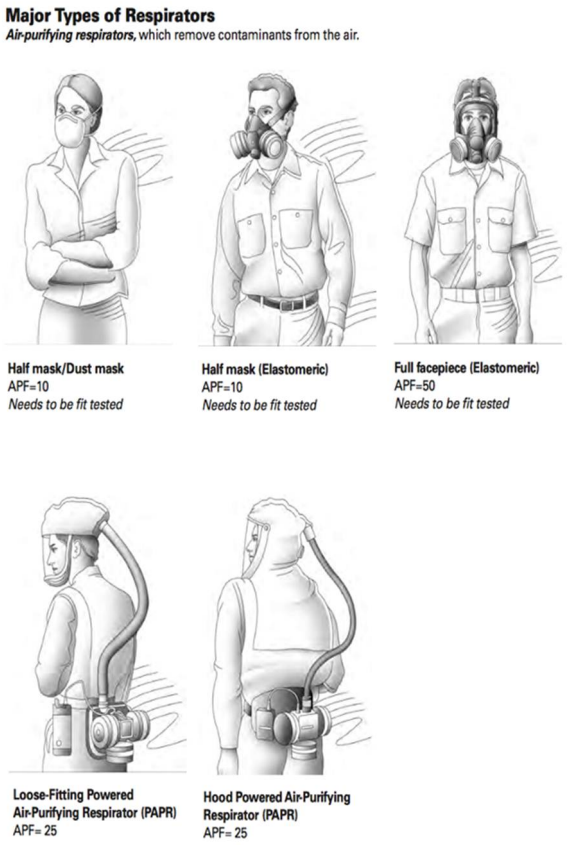

Figure 2.1 Loose and tight fitting Facepiece respirators and their assigned protection factors (APF), taken from [37].

For emergency escape, it is possible to use some respirators that are designed for use during brief periods such as a nose clip and a mouthpiece attached to an air purifying cleaner device.

Respirators may also be classified into two broad categories: air-supplied respirators or atmosphere-supplied respirators and air-purifying respirators (APRs). Air-supplied respirators provided clean airflow from an uncontaminated source and their APF may go up to 10,000 while APRs devices remove contaminants from the ambient air by adsorption, absorption, or filtration and APFs vary from 10-100 (see Figure 2.1) [37].

2.3 Air-Purifying Respirators (APRs)

Air-purifying respirators (APRs) are the most widespread respirators. There are three main categories: particulate removing, vapor/gas removing and combination. Filters are used to remove particulates while canisters/cartridges are used to remove either vapors or gas. The difference between a cartridge and a canister relies mainly on the size, the cartridge being smaller than the canister. Thus, for the simplicity of text, the term cartridge will be employed exclusively. Filters and cartridges are the essential functional parts of an air-purifying respirator and they need to be removed or replaced once the end of their service life has been reached.

Filtering particulate respirators remove particulates by several mechanisms such as interception, impaction, diffusion, electrostatic attraction and gravitational setting.

Respirator cartridges remove vapor/gas through the adsorption process, which is when gas molecules are removed from an air stream by binding to the surface of the sorbent solid [17]. In an adsorption system, the contaminated air stream passes through a layer of solid particles known as the adsorbent bed. As the contaminated air stream passes through the adsorbent bed, the contaminant's molecules adsorbs or binds to the surface of the adsorbent. Eventually, the adsorbent bed becomes filled or saturated with the contaminant and reaches an unacceptable level of exit concentration at a time known as the *breakthrough time* or *service life*.

Furthermore, there are serious limitations to these type of respirators that should be considered here [38][21]:

- They cannot be used for gas or vapors that can have high heats of reaction with the sorbent of the cartridge;
- APR do not supply breathing air, therefore they cannot be used in an atmosphere with an oxygen level smaller than 19.5% except for escape;
- Contaminant exposures cannot exceed the maximum use concentration of the chemical cartridge determined by NIOSH;
- APR should not be used to enter atmospheres immediately dangerous to life or health (IDLH);
- The respirator user should not have medical conditions that would not allow him to detect odor (in certain jurisdictions);

- APR should not be used under conditions when the concentration of the contaminants is not known, or cannot be reasonably estimated;
- The change-out schedule of the chemical cartridge should be based on the end-of-service indicator if available or mathematical models to estimate cartridge service life.

The service life or change-out schedule of the cartridge varies based on the type of contaminants and other variables such as the carbon weight and physical and chemical properties of the vapor and adsorbent, the concentration of vapor in the atmosphere, the relative humidity of the atmosphere, and the breathing rate of the respirator wearer [39]. When filter cartridges become saturated, they must be changed. Unless a proper change-out schedule for the respirator cartridge is established, their protection against harmful chemicals diminishes and may even permit the passage of hazardous agents.

2.4 The Sorbent Media: Activated Carbon

Due to its good adsorption capacity for various organic vapors, and of its low cost, activated carbon makes one of most used adsorbent material for respirator cartridge [40]. Activated carbon materials are characterized by their high specific surface area and their tunable porosity. Activated carbon finds utility in many important technologies, namely oil and natural gas, food, pharmaceuticals, water treatment, hydro metallurgy, gold recovery, and carbon-in-pulp process as well as for the removal of pollutants (both gaseous and liquid) [41].

Depending on the choice of precursor, method of activation, and control of processing conditions, the adsorptive properties of activated carbon can be specifically tuned depending on the desired applications.

2.4.1 Manufacture

Most common feedstocks for the commercial production of activated carbons are anthracite and bituminous coal, lignocellulosic materials (wood, coconut shells, fruits, and pits) [42]. However, for the manufacture of vapor/gas adsorption, coconut shells, coal, peat and petroleum residues are used [43]. Several activating agents have been employed for the formation of activated carbon with desired pore structure.

The goal of activation is to create pores in the carbon material and thereby increases the adsorptive capacity. The activation process can either be classified as either physical activation or chemical activation depending on whether gaseous agents or solid activated agents are used as shown in Figure 2.2. Both methods required high temperature and will have an effect on the properties (porosity, density, hardness) of the activated carbon [44].

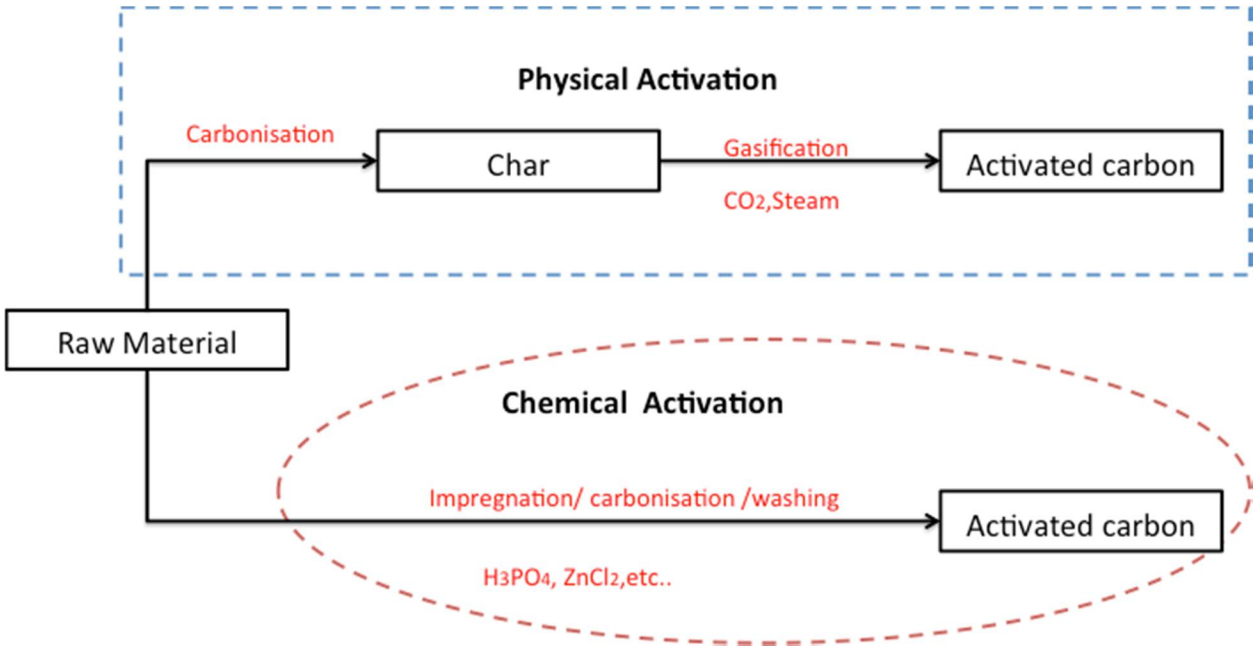

Figure 2.2 Schematic representation of the activated carbon production by physical and chemical activation.

Physical Activation

The physical activation process of activated carbon is characterized by two distinct stages: the carbonization at high temperature (600-650°C) and the activation; however, the yield of activated carbon is low [42]. Carbonization implies the removal of non-carbon materials and the formation of fixed carbon (char) [43]. The subsequent activation of the resulting char is carried out in the presence of carbon gasification reactants namely, steam or carbon dioxide. It is the reaction of the carbon with the oxidizing gas which gives rise to the development and creation of pores. Typically, carbon dioxide mainly develops microporosity whereas steam produces a wider pore size distribution [42].

Chemical activation

Chemical activation involves the process of a single step where the precursor is activated in the presence of chemical agents such as alkali and alkaline earth metal-containing substances and some acids without prior carbonization [42]. This method is usually used when the precursor is a lignocellulosic origin. The activating agents employed have dehydration and oxidation characteristics and function as dehydrating agents that influence pyrolytic decomposition, hence, inhibiting the formation of tar and thereby enhancing the yield of carbon [45]. The reagents that have been used in the industry are zinc chloride and phosphoric acid. The temperatures used in chemical activation are lower than that used in the physical activation process (350-900°C) and contain less water-extractable species due the inherent washing process necessary for the recovering of the chemical agent [43]. As a result, the development of a porous structure is better in the case of chemical activation method; however, large investments are needed for the recovery of the chemical used for the impregnation of the pores [46].

2.4.2 Pore Structure

Activated carbon is found in several forms such as powders, cylindrical extrudates, spherical beads, granules, and fibers. The structure of a typical microporous activated carbon is shown in Figure 2.3. Microporous carbon materials are highly disordered. In general, the structure is comprised of aromatic sheets and strips resembling crumpled papers and wood shavings. The variable voids and gaps of molecular dimensions between such aromatic sheets are considered as pores. Adsorption in micropores theoretically proceeds through the volume filling mechanism [47]. Different pore sizes are used to capture molecules of different volatility. The smaller crevices (gaps) are able to capture and hold the smaller and more volatile molecules. The larger pores are used to capture and hold the larger and less volatile molecules. It is the carbon precursor and the method of preparation which will determine its microporosity [42].

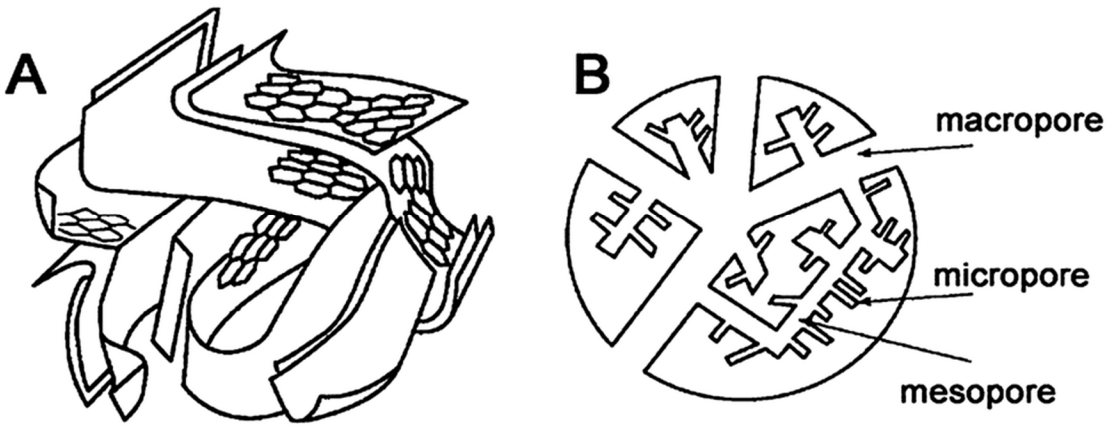

Figure 2.3 Schematic representation of (A) the three-dimensional and; (B) the two-dimension activated carbon, taken from [48].

The adsorptive properties of activated carbon are not only determined by its porous structures but also by its surface composition, which may play an important role. Oxygen functional groups may have a marked effect on adsorption, especially for polar molecules [49]. This is an important consideration for the adsorption of gases in the presence of moisture. The source of these activation groups may come from the original raw material, the activation process, or post-treatment.

2.4.3 Pore Size

The pore size property of activated carbon is of major importance in application practices because it will dictate its usage. The total number of pores, their shape and size determine the adsorption capacity and even the dynamic adsorption rate of the activated carbon [50]. The 1972 *International Union of Pure and Applied Chemistry* (IUPAC) width (w) classification categorizes pores in three groups [51]:

- macropores (> 50nm)
- mesopores (2 - 50 nm)
- and micropores (< 2 nm).

Micropores can be further subdivided into ultra or narrow micropores ($w < 0.7$ nm). The IUPAC classification is mostly based on the different mechanisms occurring in these pores during N_2 isothermal adsorption at 77 K and 1 atm. pressure. Multilayer adsorption, capillary condensation, and micropore filling are the processes that relate to macropores, mesopores, and micropores, respectively [17]. The macropores act as transport pathways through which the adsorptive molecules travel to the mesopores, from where they finally enter the micropores. Below the relative pressure of 0.95, the adsorption in the macropores is irrelevant, and only the adsorption in the micro-mesopores is significant [52]. Hence, the term pore size distribution (PSD) refers exclusively to the distribution in the micro- and mesopores. However, most of the adsorption of gases takes place within the micropores, as a consequence of the enhanced adsorption potential of the pore walls [53]. The micropores usually constitute the largest proportion of the internal surface of the activated carbon and contribute most to the total pore volume. Thus the total pore volume and the pore size distribution determine the adsorption capacity [54].

2.5 Adsorption Process

Adsorption is the process of non-specific loose binding of the adsorbate (gases, vapor, or liquid) to the solid (adsorbent) [49]. The Polanyi adsorption potential theory has been extensively used to describe gas-phase adsorptions [55,56], and the modified version of Manes describes the adsorption of liquid on activated carbon [57]. Essentially, the Polanyi theory is based on the attractive forces between the surface of the adsorbent and gas molecules, which must be greater than the forces that tend to keep the molecules in motion in the air stream. Within the range of the attractive forces of the surface of the adsorbent (the adsorption space), the potential energy of a given gas is reduced. Thus, the gas molecules are adsorbed when their potential energy is at a minimum. The strength of the attractive forces depends on the chemical structure of both the gas molecule and the solid. When molecules are adsorbed, they lose their kinetic energy of motion in the form of heat. Therefore, all adsorption processes are exothermic.

Adsorption processes can be classified as either physical or chemical, the difference being the type of bond that is formed when the gas molecule is adsorbed. In physical adsorption, the interactive forces are weak and are known as van der Waals type interactions with the order of magnitude 4,1840 J/mol and are characterized by the fact that the adsorption process is readily

reversible [49]. Chemical adsorption involves the transfer of electron, which is caused by stronger valence forces in the order of 83,680 – 418,400 J/mol [49].

The adsorption process for organic vapors onto activated carbon used in respirator cartridge is regarded mainly as a physical adsorption process. Thus, adsorption depends on three variables [58]:

i. the physical and chemical characteristics of the adsorbent (activated carbon);

ii. the physical and chemical characteristics of the adsorbate (organic vapors);

iii. the experimental conditions (air flow, relative humidity, temperature, concentration).

2.6 Adsorption Isotherms

Adsorption of gases is one of the most widely used techniques for the characterization of microporous carbon by describing the thermodynamic equilibrium and diffusivities, it measures the kinetic properties of the adsorption [59]. Usually adsorption is described through an isotherm. Adsorption isotherms are a graphical representation of the adsorption capacity, which is usually expressed as the amount adsorbed (mmol/g or ml/g) versus the relative pressure (P/P_o) at a given gas-phase concentration under equilibrium conditions [60]. The adsorption capacity plays a major role in determining the breakthrough times for a given organic vapor and it corresponds to one point on the adsorption isotherm. It is a critical parameter, which must be determine to calculate cartridge service life in prediction models.

Nitrogen (at 77 K) is the recommended adsorbate for obtaining an adsorption isotherm which will be used to determine the surface area and mesopore size distribution, but it is necessary to use other molecular probes to obtain reliable assessment of the micropore size distribution. Alternatively, CO_2 (273 K) can be employed for the adsorption isotherm to provide the volumes of narrow micropores (also called ultra micropores) because its saturation pressure being high at 273 K, it is able to reach its maximum relative pressure at 0.03 [42]. Also, Argon (Ar) is an ideal probe gas for characterizing the microporosity of activated carbon because it is much less reactive (i.e. monatomic, no multipolar moments), of the same size as N_2. Argon adsorption reveals a much more straightforward correlation between the pressure where micropore filling occurs and the pore

size [61]. This assumption together with the higher boiling temperature (87.3 K) shifts argon pore filling to higher relative pressures, which helps to reduce some of the kinetic restrictions usually associated with nitrogen adsorption at 77.4 K [61].

Adsorption isotherms are very useful in screening the best carbon for adsorption or purification needs [62]. Typically, gases/vapors on activated carbon containing micropores have a Type I adsorption isotherm, increasing rapidly at low vapor concentrations, less rapidly at moderate concentrations, and finally reaching a plateau at high concentrations [63] as shown in Figure 2.4

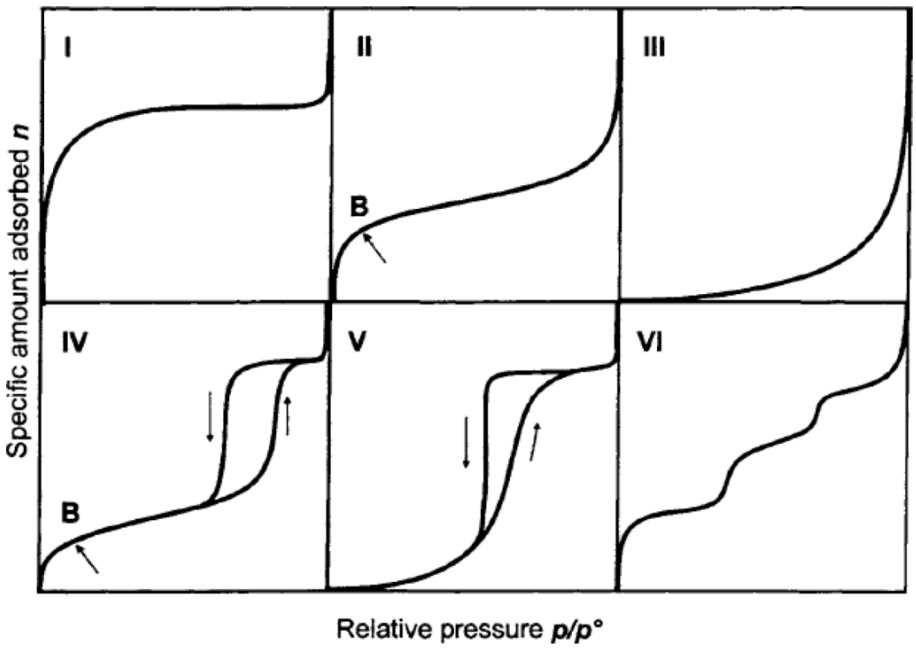

Figure 2.4 Six types of gas physisorption isotherms. Taken from [64] © 1985 IUPAC.

An inherent property of Type I isotherms is that adsorption is limited to the completion of a single monolayer of adsorbate at the adsorbent surface. Also, Type I isotherms are observed for the adsorption of gases on microporous solids whose pore sizes are not much larger than the molecular diameter of the adsorbate. Complete filling of these narrow pores corresponds to the completion of a molecular monolayer [65]. Other isotherms are also illustrated in Figure 2.4 where Type II, and type III describe adsorption on macroporous adsorbent with strong and weak

adsorbate-adsorbent interactions, respectively. The point B shows the stage where monolayer coverage is completed and multilayer adsorption begins. Type IV and V represent adsorption isotherms with hysteresis loop, which is associated with capillary condensation from the adsorption of gases by mesoporous solids. Finally, type VI has steps with represents multilayer adsorption on a uniform non-porous surface [49].

Thus, adsorption isotherms contain a wealth of information about the adsorbate-adsorbent interactions including the porous structure, surface area, pore volume, and pore size distribution for given gas-phase concentration under equilibrium conditions, all which are essential for the characterization of activated carbon to obtain critical parameters for prediction models.

2.7 Characterization of Activated Carbon

Due to the complexity of the porous structure of activated carbons, there is no single experimental method able to measure directly all the information needed to fully characterize the structure of the porosities. However, characterization of the pore structure and its adsorptive properties of activated carbon are important for their application in determining the service life of respirator cartridges [62].

Experimental evaluation of the adsorption isotherm and adsorption capacity is a time consuming and elaborate process. As a consequence, several complex adsorption models have been proposed to describe the adsorption of vapor and gases. The most commonly used are the Langmuir [66], the Brunauer–Emmet–Teller (BET) [67], and the Dubinin-Raduskevish (DR) equations [47]. The Langmuir and BET equations are both derived from similar assumptions. However, the Langmuir equation assumes monolayer adsorption and the BET equation extended the Langmuir model for multilayer adsorption. The Langmuir equation has the following form

$$X = \frac{P/P_{sat}}{A+B\cdot P/P_{sat}} \tag{2.1}$$

The BET has the form:

$$X = \frac{C\cdot P/P_{sat}}{(1-P/P_{sat})[1+(C-1)\cdot P/P_{sat}]} \tag{2.2}$$

where X is the volume of organic adsorbate adsorbed, P is the partial pressure of the adsorbate, P_{sat} is the saturated vapor pressure, A and B are Langmuir constants related to the adsorption capacity and rate of adsorption, respectively, and C is a constant related to the heat of adsorption. The Langmuir equation is valid under low pressure only because it assumes that the adsorbed gas behaves ideally in the vapor phase. There are no interactions between adsorbates and formation of a homogenous layer on the surface with uniform energy is possible under low-pressure conditions only. As the pressure increases, the assumption breaks down, as the organic molecules attract more molecules towards each other to form a multimolecular layer on the surface of the adsorbent and the BET theory is applied. The BET theory has similar limitations to the Langmuir equations such as that all adsorption sites are assumed to be equal in size and shape and have equal affinity for the adsorbate molecules. Though it is known that the underlying BET theory has some shortcomings, it is still useful for determining surface areas of activated carbon [68].

Determination of surface area can be done using the t- and α_s-methods [69]. It is important to note that the micropore volume obtained is dependent on the method and the selected adsorbate because the micropore filling mechanism is a function of the pore width/molecular dimension ratio and not the absolute value of the pore width [42]. Thus, different values may be obtained depending on the procedure employed.

2.7.1 Dubinin-Radushkevich (DR) Equation

Among all the equations, the DR equation is the most used to characterize *Type I* adsorption isotherms. It was developed as a general mathematical form of the Polanyi adsorption potential theory to volume filling of microporous adsorbent including activated carbon [70]. This equation with some recent modifications [71] has been widely used to describe the adsorption of gases and vapors onto activated carbon [72] and is expressed as :

$$W_e = W_o \, exp - \left(\frac{RT}{\beta E_o} \ln\left[\frac{P_{sat}}{P}\right]\right)^2 \tag{2.3}$$

where,

W_e : volume of pores filled at P/Po (cm^3/g).

W_o: micropore volume (or adsorption space, cm^3/g).

Eo : characteristic free energy

β : affinity (or similarity) coefficient of the adsorbate

R : ideal gas constant = 1.987 cal/mole K

T : absolute temperature (K)

P_{sat}/P : inverse of the adsorbate partial pressure

The linear form of DR equation is:

$$\ln(W_e) = lnW_o - B/\beta^2[(RT\ ln[P_{sat}/P])^2] \tag{2.4}$$

where B is a parameter related to the pore size distribution of the activated carbon. By plotting $\ln(W_e)$ versus $(RT\ ln[P_{sat}/P])^2, W_o$ and B/β^2 can be obtained from the intercept and slope, respectively. Alternatively, W_o, which is an activated carbon parameter can be derived from any known isotherm of the activated carbon (e.g. N_2 at 77K). The micropore volume, W_o is a function of only the adsorbent and can be considered to be constant for a given adsorbent [68]. The parameter β is known as the affinity coefficient related to the characteristic of the adsorbate only and describes the adsorptivity of a vapor in comparison to a suitable reference (usually benzene). It has been correlated to several properties of the adsorbate such as liquid molar volume, molecular parachors, and electric polarization [68]. In cartridge service life prediction models, β can be found in the literature or can be calculated by the ratio of the electronic polarization of the adsorbate, to that of the non-polar adsorbate (e.g. benzene) [73] [74]. The molar polarization, P_e (m^3/mol) is calculated with:

$$P_e = \left(\frac{n_D^2-1}{n_D^2+2}\right)\frac{M_W}{\rho} \tag{2.5}$$

$$\beta = {P_e}\Big/{P_{e_{reference}}} \tag{2.6}$$

where n_D is the refractive index, M_W is the molecular weight of the adsorpbate, and ρ is the liquid density. These parameters can be found in the *Handbook of Chemistry and Physics* [75].

The DR equation has several advantages [73] :

- good data fit over a wide concentration range;
- temperature is included as a parameter;
- built around physical parameters;
- easy to apply.

However, it has been observed that the DR equation on the average may give a 5 % error in underestimating of the adsorption capacity, which should be considered for the breakthrough times estimates [76]. Furthermore, there are some issues with respect to the pressure range in which the equation is applied such as the compliance with Henry's law at low pressure, the derived heat of adsorption at very low and very high pressures, and the debate on using a suitable reference for the affinity coefficients [40]. Moreover, the value of β does not take into account the properties of the organic molecules that are important such as solubility, steric configurations, size and polarity, and the nature of the functional group [68]. Because for larger organic molecules, molecular size might be a limiting factor in the accessibility of the pores, adsorption may not take place regardless of the apparent affinity of the carbon for the molecule [68].

2.7.2 Density Functional Theory

Another method for modeling adsorption isotherm and obtaining pore volume and pore size distribution (PSD) is the so-called Density Functional Theory (DFT). Initially Seaton et al. [77] employed this method to describe the adsorption of fluid in meso-micropores range. In their approach the Local Density Functional Theory was used (LDFT), which was a great improvement in the calculation of the pore structure parameters, but was still inaccurate for narrow micropores because the LDFT failed to take into account the short range correlations in these pores [78]. Therefore, the Non-Local-Functional-Theory (NLFDT) was developed in combination with Monte Carlo simulations to accurately describe adsorption in the narrow micropores and both are able to produce oscillation profile at a solid fluid interface [78]. The NLFDT takes into account the

metastability of the confined fluid, pore blocking and network effect as well as the instability of the adsorption film and cavitation of the condensed fluid [79].

2.8 Adsorption Process for a Single Vapor

The adsorption models described in the previous section are able to predict the adsorption capacity for a given carbon, which has been characterized and for which the adsorption of the reference compound is known [68]. As mentioned, the DR equation is the preferred equation for this task. For the application of prediction of cartridge service life, the shape of the contaminant breakthrough curve is required. The time to breakthrough, which is defined by a critical concentration of the contaminant, is defined as the criterion that determines the time at which the carbon filter should not be in service. Before describing the existing breakthrough curve models it is important to understand the dynamic adsorption in a packed activated carbon bed for which the models are derived.

2.8.1 Dynamic Adsorption and Breakthrough Curve in a Packed Carbon Bed

When a contaminated air stream passes through a packed carbon bed, most of the contaminant is adsorbed in the vicinity of the inlet to the bed [80]. The gas then passes on with little further adsorption taking place. Later, when the inlet part of the adsorbent becomes saturated, adsorption takes place deeper inside the bed. As more gas passes through and adsorption proceeds, the so-called mass transfer zone (MTZ) or the adsorption front moves forward until the breakthrough point is reached (see Figure 2.5). The cartridge becomes no longer efficient when the front reaches the end of the bed. If the air stream of the contaminated gas is continued, the front exits the bed (exit concentration) and will rise until it attains the level of the inlet concentration.

The graphical representation of the breakthrough curve is shown in Figure 2.5. The breakthrough fraction or concentration (ratio of the exit concentration to the inlet concentration) is plotted as a function of time. The breakthrough time or the service life, t_b is defined as the point on the curve when the exit concentration is unacceptable for inhaled air [81]. Typically, the cartridge service life is defined as the percentage of the exit contaminant concentration through the cartridge from 1-100% [80] depending on the Permissible Exposure Level (PEL). Thus, predicting breakthrough time(s) is essential to setting change-out schedules and maintaining

worker's protection. Predictive models of service life should incorporate adsorbate properties, adsorbent properties, bed geometries and the conditions of use [82].

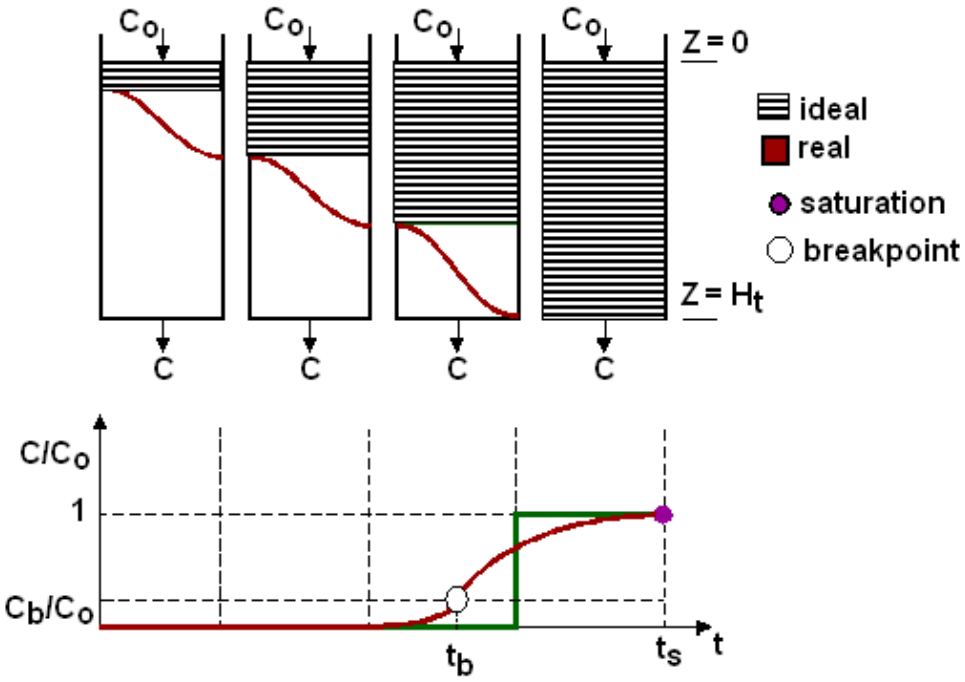

Figure 2.5 Mass transfer zone of the breakthrough curve of a fixed bed where C is the outlet concentration, C_o is the inlet concentration, t_b is the defined breakthrough time of the cartridge, and t_s is the time at 100% saturation, and Z is the Mass Transfer Zone (MTZ) and H_t is the bed height, taken from [83].

In addition, a breakthrough curve may be described by three characteristics: shape, midpoint, and steepness, and a service life model should include all these points [84]. The midpoint is characterized by adsorption capacity of the activated carbon bed for a selected vapor concentration, airflow (breathing rate), and other conditions. The steepness describes the rate (speed) at which the vapor is removed from the air as it flows through the bed, which can also be described as adsorption rate coefficient [81]. If the rate coefficient is constant throughout the breakthrough process, the shape of the breakthrough curve will be symmetrical from as shown in Figure 2.5. Service life models differ on how they describe one or less of these three breakthrough curve characteristics.

2.9 Breakthrough Curve Models for a Single Vapor

Several mathematical models have been proposed for modeling adsorption breakthrough curves for a fixed carbon bed. These models are presented in Table 2.1 and were theoretically addressed to describe the adsorbate diffusion in the porous adsorbent (e.g. activated carbon). It has been shown that breakthrough times (i.e., times to reach defined effluent concentrations) and adsorption capacities (i.e., amounts held at breakthrough) of adsorbent beds for a given adsorbate vapor are functions of the concentration of that vapor in air [85].

In 1920, Bohart and Adams first developed an equation for the ideal symmetrical breakthrough curve of chlorine through charcoal [86]. The Bohart and Adams' equation assumed mass balance and first order adsorption kinetics [81]. Then, Mecklenburg applied this equation to gas mask filtration [87]. Klotz later modified the Mecklenburg equation to obtain a breakthrough time expression as described in Table 2.1 [88]. In this equation, the breakthrough fraction (C_o-C/C) is replaced by C_o/C, by assuming it is very large. This assumption was also incorporated in the best-known breakthrough equation, often called the Modified Wheeler-Jonas Equation (WJ) [25,81] .

2.9.1 Modified Wheeler-Jonas Equation

Among all the predictive models, the modified Wheeler Jonas (WJ) equation is the most widely used to estimate the breakthrough time of organic vapors on activated carbon respirator cartridge. Its simple form and readily available parameters have been able to yield good predictions for breakthrough times [72,89]. The first term of the WJ equation presented in Table 2.1 is the stoichiometric center of the breakthrough curve, which represents the breakthrough time at infinitely fast and large adsorption rate (k_v) [81]. The approximation $ln(C_o/C)$ instead of $ln[(Co-C)/C]$ makes less than 1% difference in the second kinetic term for breakthrough fraction, however, it does change the shape of the breakthrough curve from "S"-shaped to "J"-shaped, approaching infinity instead of a maximum value ($C/C_o = 1$) [72,81]. Overall, this equation is based on the assumption of a constant pattern (in wave front shape) and a constant overall rate coefficient [84]. It also assumes mass balance and first order adsorption kinetics in vapor concentration and first order in concentration of remaining adsorption sites and presumes constant challenge concentration, airflow rate, and temperature over the entire duration [90].

The modified WJ equation can be used to extrapolate experimental data to other environmental condition (varying airflow, concentration, bed depth etc.) And the two parameters W_e and k_v, can be treated as fitted parameters which can be derived from a series of breakthrough experiments. Ideally, one wants to extrapolate these parameters without prior experimental work.

Wood and Moyer [91] have published a review on the WJ equation as it applies to organic vapor respirators. In their study, they varied bed weight, residence time, and fitting the breakthrough curve. They applied these three methods to breakthrough curves, and obtained a common adsorption capacity but varying rate coefficients. The k_v was proportional to the square root of the airflow rate [91].

Dynamic Adsorption Capacity (W_e)

The dynamic adsorption capacity of the carbon bed can be approximated by the static capacity (W_e), which can be given from the adsorption isotherm by using the DR equation in Eq. 2.3 or it can be approximated from the integration of the breakthrough curve with [91]:

$$W_e = \frac{C_o Q t_{b50\%}}{\rho \cdot w} \tag{2.7}$$

where C_o is the inlet concentration in g/cm^3, Q is the flow rate in cm^3/min, $t_{b50\%}$ is the time at 50% saturation, ρ is the liquid density in g/cm^3, and w is the weight of activated carbon in g. Wood has reported on the estimation of adsorption capacity of the activated carbon bed for organic vapors by using previous data by other researchers at high concentrations of 1000 ppm [74], In another study, Wood has compared and reviewed adsorption isotherm equations for activated carbon respirator cartridges for organic vapors concentration between 275 - 2000 ppm at 1% breakthrough concentration [72,91].

Adsorption Rate Capacity (k_v)

The parameter k_v is more difficult to estimate because it is impossible to differentiate between the different diffusion steps involved in the adsorption process; therefore, k_v must be calculated either from the breakthrough time or from breakthrough curves. Consequently, it inevitably carries experimental uncertainties [58,82]. The adsorption rate coefficient is dependent on the velocity, u (cm/min) and several equations have been proposed to relate it to k_v.

Wood and Stampfer [58] proposed an equation based on the fitting of 165 breakthrough curves for 27 hydrocarbons and fluorocarbons with:

$$K_v{}^{-1} = (1 + 0.027u) \times \left[\left(I + S_B \times P_e{}^{-1}\right)\right] \times u^{-1} \qquad (2.8)$$

where $S_B = 0.0063 - 0.0055\, ln[(C_o - C/C)]$, $I = 8.25 \times 10^{-4}$ (min $\cdot cm)/s$ and P_e is the molar polarizability (cm^3/mol). In this study, the adsorption rate constant increased linearly with the linear velocity and no size dependence was observed [58]. More recently, Wood and Lodewyckx [92] incorporated the granule diameter and affinity coefficient in the equation for k_v and it is given by:

$$k_v = 800\beta^{0.33} d_p{}^{-1.5} v_L{}^{0.75} \left(\frac{W_e}{M_w}\right)^{0.5} \qquad (2.9)$$

where,

β is the affinity coefficient of DR equation

$\mathbf{d_p}$ is the mean diameter of the carbon particles (cm)

$\boldsymbol{v_L}$ is the linear velocity of the air stream through the carbon bed ($cm \cdot s^{-1}$)

$\boldsymbol{W_e}$ is the equilibrium adsorption capacity (g vapor/g carbon)

$\boldsymbol{M_w}$ is the molar mass of the organic vapor ($g \cdot mol^{-1}$).

2.9.2 The Extended Wheeler-Jonas Equation

To better describe the asymmetry (skewed) of breakthrough curves, Wood has extended the WJ equation [27,93] (see Table 2.1). The skewed breakthrough curves are steeper at the beginning of breakthrough than predicted by ideal models such as the WJ equation. This asymmetry was attributed to heterogeneity of the activated carbon and its adsorption sites in micropores [94]. Vapors at the wave front of the adsorption as they move through the carbon bed, contact and occupy the most active (by rate and capacity) adsorption sites, leaving the less active ones for subsequently arriving vapors. The advantage of using this equation is that when the *G* and *H* are zero, it reduces the equation to the ideal case; however, these two parameters have not yet been

assigned physical meaning or relation to the physical properties of carbon or the organic vapors [81].

2.9.3 Yoon-Nelson and Linear-Driving Force Models

Other common predictive models are the empirical Yoon-Nelson theory [26] and the Linear-Driving Force (LDF) Model [95,96]. The Yoon-Nelson model is based on the assumption that the rate of decrease in the probability of adsorption for each adsorbate molecule is proportional to the probability of adsorbate adsorption and the probability of adsorbate breakthrough on the adsorbent [68]. The parameters τ and k' have to be obtained from experimental data by plotting t_b versus $ln(C/C_o - C)$ in order to calculate the entire breakthrough curve (see Table 2.1). The Yoon-Nelson model at first glance appears simple than other models, but it is important to note, that this model requires no detailed data concerning the characteristics of adsorbate, the type of adsorbent, and the physical properties of adsorption bed. Also, it is specific for each activated carbon cartridge type.

Alternatively, the LDF mode is governed by the difference between the temporal and the equilibrium concentrations of the gas adsorbate [95] (see Table 2.1). The LDF considers that the adsorbate concentration per mass unit of solid adsorbent changes with time as a function of the adsorbate concentration in the adsorbent. Vallières and coworkers utilized the LDF model to predict the service life of activated carbon cartridges [80,96]. The constant-pattern LDF equation resulted in asymmetrical curves, which required an analytical solution valid for a Langmuir isotherm only or numerical solutions with the DR isotherm [96],. At very low concentrations where the isotherm is linear, the constant pattern no longer exists and the model fails[96].

Table 2. 1 Breakthrough models for prediction of cartridge service life or breakthrough time.

Model	Equation	Parameters
Bohart and Adams [86]	$t_b = \frac{a_o z}{60_{V_L} C_o} - \frac{1}{k C_o} ln\left(\frac{C_o - C}{C}\right)$	C_o is inlet concentration (g/cm³) C is the breakthrough concentration t_b is the breakthrough time a_o is the volumetric capacity (g/cm³) z is the bed length (cm) k is the rate coefficient (cm³/g·min) V_L is the linear airflow velocity (cm/s)
Mecklenburg [87]	$t_b = \frac{a_o A}{C_o Q}[z - I]$	I is the critical bed depth (cm) Q is the volumetric airflow rate (cm³/min) A is the cross section area (cm²)
Klotz [88]	$t_b = \frac{a_o A}{C_o Q}\left[z - \frac{1}{a} Re^{0.41} Sc^{0.67} ln\left(\frac{C_o}{C}\right)\right]$	Re is the Reynold number Sc is the Schmitt number
Wheeler-Jonas [97]	$t_b = \frac{W_e}{C_o Q}\left[W - \frac{\rho_B Q}{K_v} ln\left(\frac{C_o}{C}\right)\right]$	W_e is the adsorption capacity (g/g_{carbon}) W is the weight of carbon (g) ρ_B is the packed bed density (g/cm3) K_v is the adsorption rate coefficient
Wood [27][93]	$\frac{C}{C_o} = \frac{exp\{(t-A)/[B + G(t-A)]\}}{exp\{(t-A)/[B + G(t-A)]\} + \left[(1 - P_s)/P_s exp[-H\ (t-A)/B]\right]}$	A is the stoichiometric time (min) P_s is the C/C_o ratio at the stoichiometric center of the breakthrough curve B is related to A and inversely proportional to the rate coefficient at the stoichiometric center G is fitting parameter H is a fitting parameter
Yoon-Nelson [26]	$t_b = \tau + \frac{1}{k'} ln\left(\frac{C}{C_o - C}\right)$	τ is the time required for 50%breakthrough $k'$is a rate constant (min^{-1})
Linear- Driving Force [95][96]	$\frac{\partial q}{\partial t} = k_q(q^* - q)$	q^* is the surface concentration q is the average adsorbed phase concentration k_q is the intraparticle mass transfer coefficient

2.10 Factors Affecting Cartridge Service life

The accuracy of all the predictions models for estimating the service life or organic respirator cartridges are influenced by the environmental conditions such as temperature, airflow (breathing similar), and the presence of other contaminants. However, no physical properties such as boiling point and the vapor presure of the contaminant or the sorbent have shown to correlate with the adsorption capacity and service life [39]. Information about cartridge service life regarding real industrial hygiene conditions is limited. By far, the study of Nelson et al. where 121 organic vapors were tested in breakthrough experiments for respirator cartridges in the 1970s, is the most extensive study which resulted in a series of papers [18,98–100]. In these series, Nelson and co-workers studied the effects of the environmental conditions on the respirator cartridge service life. A brief account of this study will be discussed along with some of the most current studies.

2.10.1 Effect of Granule Size/Packed Bed Density

The amount and packing density as well as the granule size are all important factors in the prediction of cartridge service life. Rehrmann and Jonas [101] showed that the adorption capacity was very little affected by the size diameter whereas the rate coefficient decreased with carbon granule size. In other words, adsorption is faster for smaller carbon granules, but the resistance to airflow may increase. Also, Trout et al. [102] studied the variation of packed bed density of organic vapor respirator cartridges on breakthrough time.

2.10.2 Effect of Cartridge Geometry

The evaluation of the configuration of the cartridge or the channel geometry on the performance of respirator cartridge has hardly been investigated. The study by Nelson et al. [18] found that cartridge configuration out of the 2000 cartridges tested had no effect in cartridge efficiency with the exception of thin beds. A wall effect in activated carbon was also reported by Leonard et al. [103] and Lodewyckx [104] by examination with X-ray microtomography for cylindrical configuration. In their work, X-ray microtomography was used to visualize the wall effect during dynamic adsorption of CH_3I. This non-invasive technique proved to be beneficial in identifying radial adsorbate concentration profiles at different activated carbon bed thickness.

This phenomenon may be important to consider since most prediction models use linear velocity for vapors gases and neglect radial velocity profiles within the carbon beds.

2.10.3 Effect of Temperature

Few studies on the effect of temperature on respirator cartridge performance and efficiency have been reported. Even if respirators are expected to be used in normal temperature conditions, the adsorption process is exothermic. Jonas et al.[97] evaluated the effect of the temperature might have on the breakthrough time of a chemical warfare simulant, dimethyl methylphosphonate (DMMP) using the Wheeler-Jonas predictive equation in combination with the DR equation. It follows that an increase in temperature will have a detrimental effect and will favor the desorption rate due to the evaporation of the vapor molecules, which will leave the active sites and consequently lower the concentration and adsorption capacity. Furthermore, the Nelson et al. [99] study established a general rule that breakthrough times diminish from 1-10% for each 10°C increase in temperature. This rule of thumb was based solely on adsorption isotherms obtained from experimental data ranging from temperature of 20-25°C. In another study, Wood [105] performed breakthrough tests in humid conditions (50-70% RH) and varied the temperature (25-38°C) for CH_3I for different types of activated carbon respirator cartridges, which showed that penetration increased and that cartridge service life diminished significantly from 4-15% per °C for this substance.

2.10.4 Effect of Rate of Flow and Flow type

Typically, the dynamic adsorption of toxic vapors on activated carbon cartridge is often studied using steady flow rates. Nelson et al. [98] conducted breakthrough measurements with both fixed and pulsating flow rates, for which the former was obtained by means of a breathing simulator. Nelson's study found no significant difference between breakthrough time values obtained at steady flow and under pulsating flow patterns at 1000 ppm, even at flows representing the highest work rates (71.4 L/min) and high relative humidity (85% RH) [98]. This result is in agreement with the adsorption equilibrium theory, which assumes that the amount of vapor adsorbed at a given temperature, relative humidity, and concentration is independent of the flow rate [39]. Therefore, assuming negligible desorption, the breakthrough

time is affected by the *average flow rate* rather than uniformity of the flow and consequently steady flow rates is acceptable in respirator cartridge breakthrough tests; and is inversely proportional to the flow rate [98].

This approach has been criticized for being too simplistic and it appears that it may lead to an overestimation of the respirator cartridge service time, and pulsation flow may provide a more realistic assessment. Tanaka et al. [108] considered the effect of a pulsating sine wave flow on low boiling point organic vapors for respirator cartridge and demonstrated that the breakthrough time was shorter with pulsating flow than with steady flow rates. A possible explanation for the shortened breakthrough time for a pulsed airflow of the same average value to the steady state flow, is due to an enlargement of the critical bed depth, whereas the dynamic adsorption capacity (W_e) does not depend on the flow pattern [19,89]. Tanaka et al. [108] showed that the breakthrough time for the workers' respiratory pattern was the shortest between the steady flow rate and equivalent pulsating flow rates (rectangle, sine and triangle waves) for tetrachloride in shallow carbon bed (see Figure 2.6) due to the molecules being unable to achieve the adsorption equilibrium.

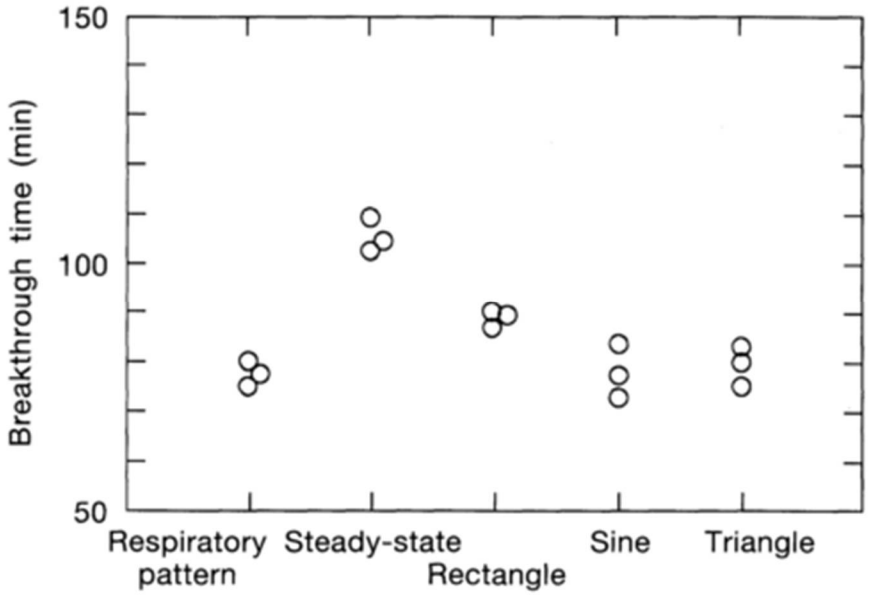

Figure 2.6 Effect of different flow patterns on the breakthrough time for tetrachloride at 300 ppm for round shape respirator cartridges with dimension of 13 mm bed height and 78 mm inner diameter. Taken from [106].

However, increasing the breathing rate (air flow) will have a direct effect on the cartridge service life. With the flow rate being inversely proportional to the service life, any increase in the air flow rate to adjust for heavier breathing rates due to greater workloads while wearing a respirator, will reduce the service life [19,106].

2.10.5 Effect of Contaminant Concentration

The effect of contaminant concentration on respirator cartridge service life has been well investigated especially at high concentrations [100,109,110]. The study of Nelson et al. [18] found that the service life is inversely proportional to the log of the concentration. They described a general relation, for which a decreased in the concentration by a factor of 10 corresponds to an increase in service time by a factor of 4 or 5. In other terms, an increase in concentration will shorten the respirator cartridge service life. This is in agreement with the adsorption theory, which predicts that less solvent is adsorbed at lower concentrations. To date, very few studies have been done at low concentration (< 50 ppm) and it may be important to consider such studies for contaminants with low threshold limit values (TLVs) and in the presence of other contaminants. Breakthrough tests at low concentrations are not easy; the lower the concentration is, the longer it will take for the cartridge to reach its breakthrough time. Thus, maintaining constant control over experimental conditions may be difficult.

2.10.6 Effect of Relative Humidity (RH)

By far, the effect of moisture on the adsorption of organic vapor for activated carbon used in respirator cartridge has been the most studied. Nelson et al. [99] found that RH values between 0 - 50 % had no significant effect on the breakthrough time at 10% saturation for high concentration of organic vapors at 1,000 ppm, whereas above 60% RH, the dependence of the humidity became quite significant and was more important at lower concentration. They also concluded that the RH of the challenge concentration had a greater effect on the adsorption than preconditioning the cartridge. These results are in agreement with the observation that water adsorption isotherm on activated carbon increased sharply at about 50% RH [68]. In another study, Jonas et al. [111] investigated the effect of preconditioning the test carbon and exposing it to different RH from 13-95% in the air stream for chloroform vapours at low concentration.

They observed that below 40% RH for prehumidified carbon beds, it produced no change in the 1% breakthrough time for chloroform and no RH effect on the adsorption of chloroform was observed for dry carbon beds. However, contradicting results have been reported by Werner [112] who observed marked effect on breakthrough times below 50% RH for trichloroethylene vapor at a concentrations range of 300-1,000 ppm.

The loss of efficiency at high RH and low concentration is probably due to competition between contaminant vapor and water vapor for the same sorbent active sites or "space". More recently Lodewyckx and Vansant [113] showed that the loss of adsorption capacity could be modeled by volume exclusion. The more volatile the compound is, the more it will be influenced by water adsorption as it is unable to replace the more strongly adsorbed water molecules. The water adsorbed on the carbon will also affect the adsorption kinetics by slowing down the mass transfer kinetics [113]. This effect is more pronounced for volatile hydrophobic compounds, which will compete with water for active sites, whereas hydrophilic compounds will tend to dissolve in water.

2.10.7 Effect of Mixtures

Early works investigated the effects of binary mixtures on respirator cartridge service life and presented qualitative observations [18,25,114] but they lack thorough understanding of multivapor adsorption mechanism. It was only until the 90-mid 90s that Lara, Yoon and collaborators [20,115,116] developed a mathematical approach for binary mixtures and multivapors. Their descriptive model relied on fitting parameters that have to be obtained from experimental data. They showed that breakthrough might occur earlier for a contaminant in the presence of mixtures than as a single vapor. For example, when they exposed a respirator cartridge to a binary mixture composed of acetone (97 ppm) and styrene (892 ppm) as shown in Figure 2.7, the concentration of acetone continued to increase rapidly and exceeding the acetone inlet concentration of about 3.5 times its initial concentration. In other words, in this binary system, if the initial exposure concentration of acetone is 100 ppm, it can reach up to 350 ppm inside the mask when the concentration of styrene is 900 ppm. This means that the mask wearer can be more exposed to the contaminant inside the mask than if he had no mask! The interpretation of these results can be explained by the weak adsorption of the volatile

contaminants on the surface of the carbon. For this reason, the more volatile contaminant, which is less adsorbed, can be displaced by the less volatile contaminant. This is referred as the displacement phenomenon with translates to a transition period where the concentration of the most volatile contaminant in the mask is higher than the exposure concentration [20]. Therefore, when estimating the cartridge service life for mixtures, the cartridge should be replaced more frequently. The next section will describe in further details the adsorption process and the kinetics for mixtures.

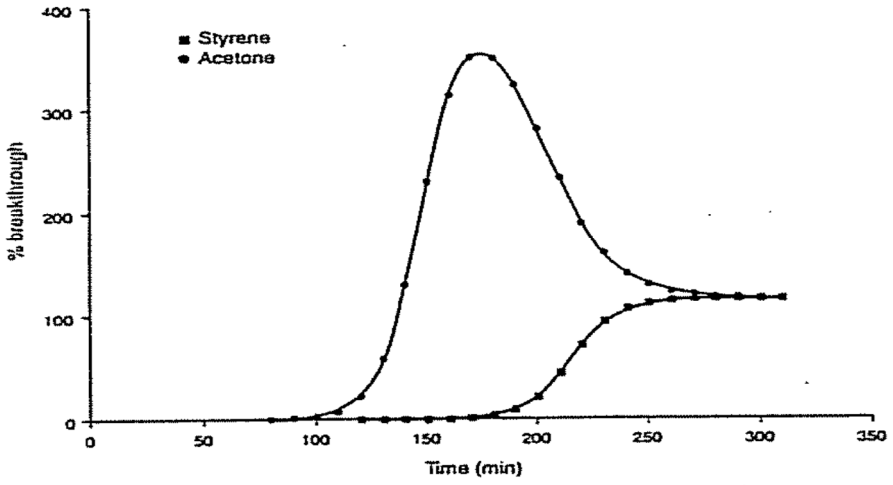

Figure 2.7 Breakthrough curves for the mixture containing 97 ppm acetone and 892 ppm styrene [26].

2.11 Adsorption Process in Mixtures

Exposure to a single pure vapor may occur in the laboratory and may be useful in developing adsorption and predictive models, but in practice, the air is contaminated with more than one contaminant. The effect of mixtures on the adsorption of vapors on activated carbon respirator cartridge can be treated like in the case of single contaminant; first the adsorption equilibrium theory is discussed followed by a predictive model and consideration of mixtures toxicity.

2.11.1 Adsorption Equilibrium Theory for Mixtures

The prediction of mixed-gas adsorption equilibrium from pure single component adsorption isotherms is preferred because experimental data on mixed-gas is laborious and time consuming [117]. In 1965 Myers and Prausnitz [118] proposed the ideal adsorbed solution theory (IAST) to thermodynamically describe the adsorption of multi-vapors onto activated carbon. The IAST theory is based on the assumption that adsorbed phase behaves like an ideal solution and is analogous to Raoult's law for vapor-liquid equilibrium. It stipulates that the partial vapor pressure of each component of an ideal mixture of liquids is equal to the vapor pressure of the pure component multiplied by its mole fraction in the mixture and the pressure it would exert if it were a pure component at the temperature and spreading pressure of the mixture [119]. In fact, the concept of spreading pressure is central to the IAST theory. The spreading pressure is calculated from Gibbs adsorption isotherm equation using single gas component [81,120]:

$$\Pi_i = \frac{RT}{A}\int_0^{p_i^o} \frac{n_i^o}{p_i}\, dp_i \tag{2.10}$$

where Π_i is the spreading pressure for each component i, A is the specific area of the adsorbent, R is the ideal gas constant, T is the temperature in Kelvin, n_i^o is the number of moles of the pure component adsorbed obtained from a pure component isotherm for vapor pressure p_i and p_i^o is the pressure corresponding to spreading pressure. The solution to the integration requires iterative solutions [117], which may be seen as a disadvantage.

2.11.2 Dynamic Adsorption Models for Multicomponent Mixtures

Currently, there are no official accepted methods for the estimation of cartridge service life for contaminant mixtures. However, OSHA compliance directive *CPL 2-0.120*, *Inspection procedures for the Respiratory Protection Standard*, states in section 4 [121]:

> The change schedule for a mixture should be based on reasonable assumptions that include a margin of safety for the worker wearing the respirator. Where the individual compounds in the mixture have similar breakthrough times (i.e. within one order of magnitude), service life of the cartridge should be established assuming the mixture stream behaves as a pure system of the most rapidly migrating component or compound with the shortest breakthrough time (i.e., sum up the concentration of the components). Where the individual compounds in the mixture vary by 2 orders of magnitude or greater, the service

life may be based on the contaminant with the shortest breakthrough time. OSHA believes that an approach such as this reflects good health and safety practice where neither objective or experimental data is available for the mixture.

This directive is valid in both cases even if the concentration of the more volatile contaminant is infinitely small and poses no health effect. These recommendations upon which prediction models are based for mixtures are lacking in significant in mixtures toxicity. The notion that the dose required to produce a given effect is constant under all concentration-time conditions does not apply for breakthrough contaminant mixtures where the observation of the displacement phenomenon occurs.

As mentioned in the previous section, Yoon, Nelson, and Lara [20,115] used a descriptive model based on the Wheeler-Jonas equation to account for breakthrough curves of binary and multi contaminants. Good fit to experimental data was obtained, and they showed that the adsorption capacity and breakthrough time of the less volatile contaminant was decreased by exposure to mixtures. However, deviation from the ideal sigmoidal shape was observed at breakthrough fractions > 50% especially at high humidity and low concentrations. Furthermore, this model requires prior identification of parameters from experimental data and it is only applicable for the specified system (e.g. cartridge type, contaminants, and environmental conditions).

Vahdat et al. [122,123] have proposed a predictive model for multicomponent systems that is also based on the Wheeler-Jonas equation and the IAST model combined with the Langmuir equation to obtain adsorption isotherms for each component. This model was successfully applied to binary mixtures of acetone-m-xylene, acetone-styrene, and carbon dioxide-water. This method considers a binary system in bed for which the breakthrough curve behavior is shown in Figure 2.8. Component 1 ($C1$) is more volatile or less adsorbed than component 2 ($C2$). The breakthrough curve concentration is divided in four distinct zones [122]:

- Zone I: Contaminant 1, which is the more volatile contaminant and has lower adsorption capacity breaks through.
- Zone II: Contaminant 1 reaches its maximum concentration (C1MAX), which is higher than its initial inlet concentration (C01).

- Zone III: Contaminant 2, which is strongly adsorbed breaks through and reaches its maximum value while contaminant 1 concentration decreases.
- Zone IV: Saturation of carbon bed with both Contaminant 1 and Contaminant 2 and breakthrough concentrations are equal to the inlet concentrations (C01 and C02).

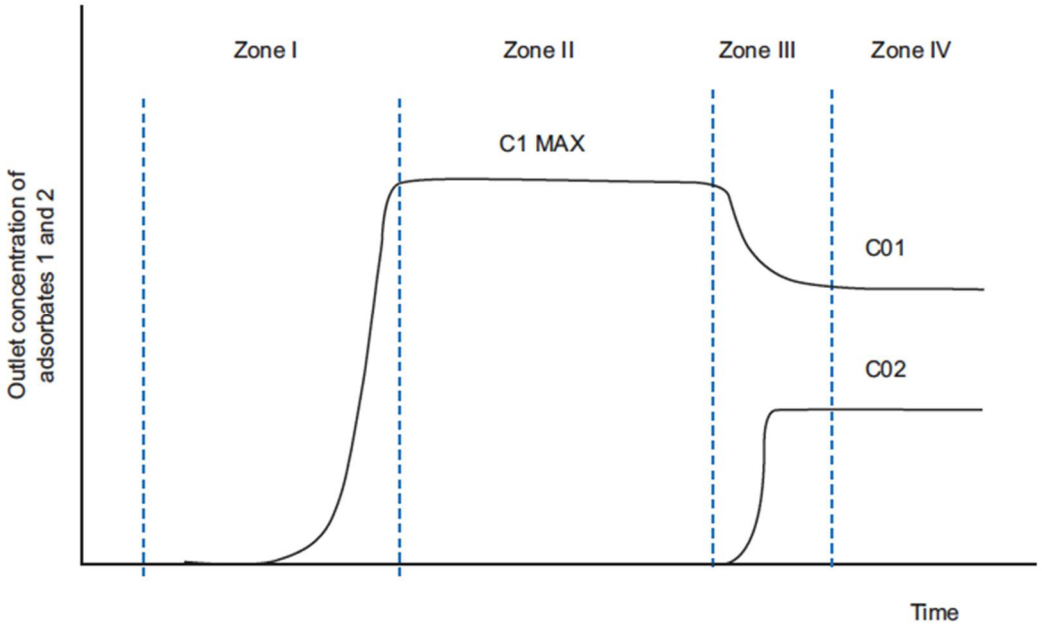

Figure 2.8 Binary breakthrough curve of component 1 (*C1*) and component 2(*C2*) for inlet concentration *C01*, and *C02, and C1* Max is the maximum concentration of component 1 during the desorption phenomenon. Adapted from [124].

Breakthrough curves for each effluent corresponds to concentrations that will eventually be inside the worker's mask, especially in the case of the of a volatile contaminant where contribution to overall risk is considered fairly high [125]. To further evaluate the toxicity effect of breakthrough contaminant mixtures and evaluate the potential health risks to workers, it is important to understand the basic concepts of combined action and interaction of mixtures.

2.12 Mixtures Toxicity and Risk Assessment

It is a well known concept in toxicology, that when exposed to several chemicals, several interactions can occur such as additivity, synergistic, potentiation, and antagonism [126]. The additivity effect is simply the sum of each individual effect and it is the most commonly observed effect (e.g. 2 + 3 = 5). A synergistic effect arises when the combined effect of each component is greater than the individual sum (e.g. 2 + 3 = 10) and the potentiation effect occurs when a non-toxic chemical enhances the toxicity of another chemical (e.g. (0 + 2 = 3) while the antagonism is when the combined effect is less than the sum of the effect of each component (e.g. 2 + 3 = 3) [127]. Also, it is possible that two or more substances when they come together exhibit independent effect because they target different organs or have dissimilar modes of action.

Figure 2.9 illustrates the different approaches for evaluating chemical mixtures in toxicology. Essentially, there are three types of 'component based approach' where the toxicity of a known mixture is assessed based on the properties of a single contaminant. The first type embodies the assumption of similar modes of action, known as concentration addition (CA) or similar mode of action, and the other type is on the basis of dissimilar modes of action referred to as independent action (IA) or response action, and the last one is a mixture of both [128]. Thus, depending on the concept adopted, if CA is applied, it would mean that that all components participate in the toxicity even when below the no effect at dose or concentration. Whereas the concept of IA implies that only concentration above the reference dose or concentration should be considered.

Guidelines for chemical mixtures risk assessment have been proposed by U.S. EPA [129]. The preferred approach is to use data available from the mixtures of interest without identifying the mode of action between each component. However, mixtures can change over time and vary in composition [130]. The second best approach is to use data from one or more mixture similar to the mixture of concern such as "mixture having the same components but in slightly different ratios, or having several common components but lacking one or more components, or having one or more additional components" [129]. The challenge of this method is to assess how similar the mixture of interest is to that of the available data. Because limited data are

available, the next best approach to evaluate the risk assessment of chemical mixtures is the combined based action, which is frequently used.

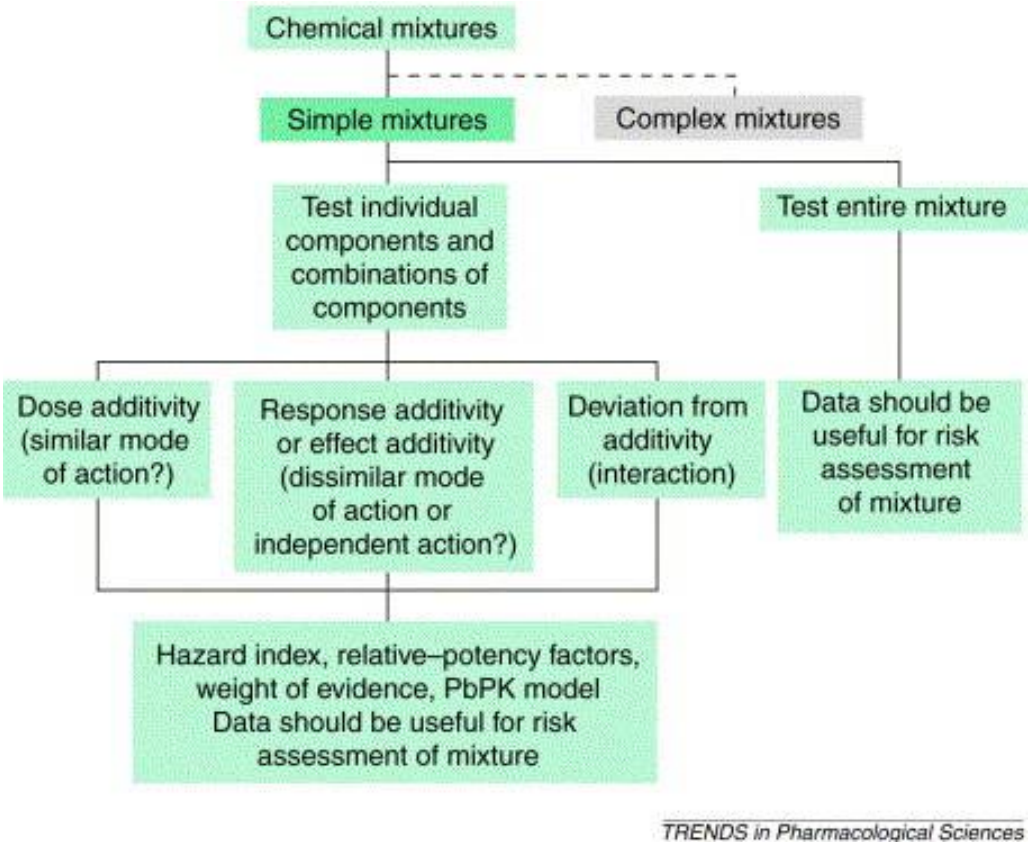

Figure 2.9. Flow chart of the best approach to mixture toxicity. Adapted from [130].

2.12.1 Hazard Index (HI)

The risk assessment based on the combined action of each component in the chemical mixture may be characterized by using the Hazard index (HI) approach, which was originally proposed by the US Environmental Protection Agency (EPA) mixture guidelines [129]. The assumptions of this approach are that the components of the mixture have the same toxic effect, in the same organ via the same mode of action. This approach assumes that there is an additivity of doses (*or concentrations)* of the components of a mixture and a hazard quotient is calculated for each component and the quotient of each mixture is added. The HI an be calculated with:

$$HI = \sum_{i=1}^{n} \frac{D_i}{RfD_i} \quad (2.11)$$

where the exposure doses (or concentrations) of each component of the mixture (Di) are normalized by the threshold dose (DRi) (or concentration) considered acceptable (e.g., reference dose [RfD], reference concentration [RfC], average daily intake [ADI], threshold limit value [TLV], etc). When the hazard index exceeds unity, there may be concern for potential health effects. While any single chemical with an exposure level greater than the toxicity value will cause the hazard index to exceed unity, for multiple chemical exposures, the hazard index can also exceed unity even if no single chemical exposure exceeds its threshold. If HI equals is less than 1, then it will pose no risk to calculate the breakthrough time of a mixture.

A modification of the standard Hazard index principle has been proposed by the Subcommittee on Mixtures of the National Research Council Safe Drinking Water [131] who recommended to use an uncertainty factor (UF) ranging from 1 to 100 to protect for unforeseen potential synergistic interactions. An uncertainty factor of 1 would indicate that synergistic effect is unlikely or that the concentration of the contaminants is low whereas an uncertainty factor of 10 would be used when little information about the potential of interactions of the mixture is known or if relatively high concentrations of the mixture compounds are present [131]. The hazard index, which incorporates an uncertainty factor, is calculated with:

$$HI = (UF) \sum_{i=1}^{n} \frac{D_i}{DR_i} \quad (2.12)$$

CHAPTER 3: RESEARCH METHODOLOGY

To optimize prediction models valid for organic vapor respirator cartridges, it is first necessary to accurately obtain information about the micropore structure (surface area, micropore volume, and pore size distribution) of the activated carbons of respirator cartridges. First equilibrium adsorption isotherms were obtained with the standard method on the basis of comparison with the novel approach, which consists of using organic vapors of different boiling points to characterize the microstructure of activated carbons. Second, a specifically designed miniaturized cartridge device reproducing a small area of a respirator cartridge was utilized with the purpose of obtaining accurate and reliable breakthrough data from dynamic breakthrough experiments under controlled environmental conditions. Then, the static and dynamic adsorption isotherms were analyzed to allow a suitable adsorption isotherm approach for micropore characterization of activated carbon using organic vapors of substances of different vapor pressures.

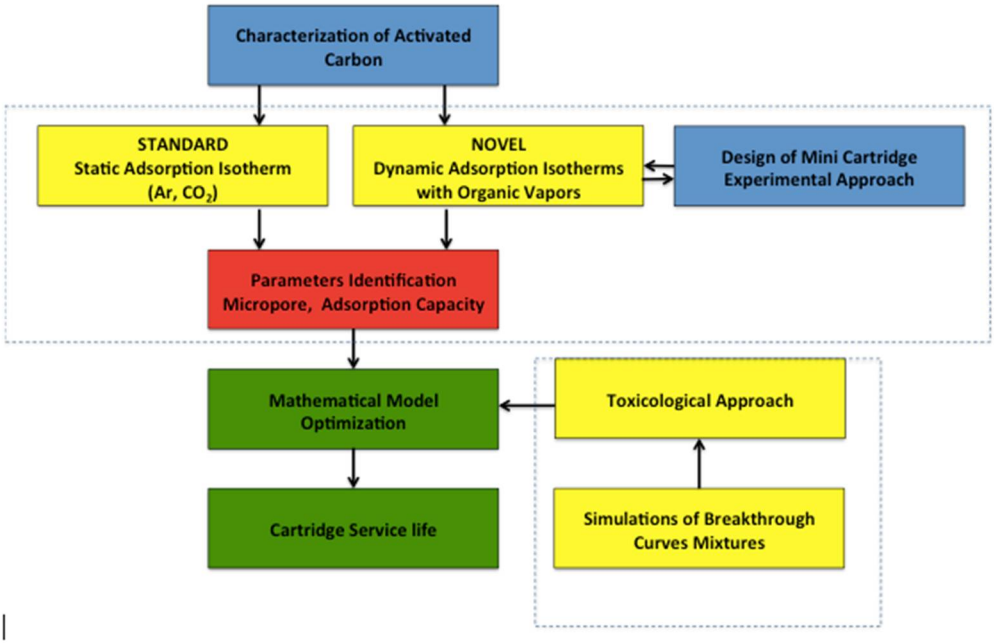

Figure 3.1 Flow chart of methodology.

From the organic vapors breakthrough data, a mathematical model was developed to incorporate a more representative micropore volume and adsorption capacity estimates into cartridge service life prediction models. Finally, a toxicological approach for chemical mixtures was introduced by integrating the hazard index in the prediction of breakthrough time with the final goal to provide further protection to workers without miscalculating the cartridge service life. Figure 3.1 depicts the necessary methodology steps to achieve the optimization of cartridge service life model for organic vapors.

3.1 Selection of Respirator Cartridges

A survey of all the available manufacturers of respirator cartridge used in Quebec for the adsorption of organic vapors was conducted by consulting with different manufacturers and distributors. Approved NIOSH organic vapor (OV) respirator cartridges were used in this study and are listed in Table 3.1.

Table 3.1 List of all the NIOSH approved cartridges used in this study.

#	Cartridges	Manufacturer	Part Number	Approval #
1	3M™ Organic Vapor Cartridge 6001	3M Company	6001	1062
2	Dräger-OV	Dräger Safety AG& Co KGaA	68 38 024	2203
3	North N75001L	Honeywell International Inc.	N75001	**2051**
4	Sperian Survirvair 100100	Honeywell International Inc.	B100100	1782
5	Moldex 7100	Moldex-Metric Inc.	7100	2520
6	Moldex 8100	Moldex-Metric Inc.	8100	1223
7	MSA (GMA) OV Advantage	Mine Safety Appliances Company	815 5355	2693
8	MSA Comfo	Mine Safety Appliances Company	464031	2694
9	Scott 7422-BA1 OV	Scott Health & Safety	7422-BA1	2111
10	Scott 7422-BC1 OV Plus	Scott Health & Safety	7422-BC1	2128
11	Sundström- SR 218-6 OV	Sundström Safety AB	SR 218-6 OV	1881

Approval # from the Certified Equipment List of the National Personal Protective Technology Laboratory (NPPTL) of NIOSH 42 CFR Part 84 [132].

3.2 Selection of Organic Vapors

In working environments, workers are exposed to a variety of solvents. It would be time consuming to test all the solvents found in the workplace to assess the breakthrough time of all the respirator cartridges. Therefore, for practical reasons, preselected solvents were chosen to obtain a ratio of relative vapor pressure (p/p_o $0 \leq 0.1$), within the micropore size distribution to reproduce a *Type I* adsorption isotherm.

Table 3.2 Physicochemical properties of organic solvents used as adsorbates taken from ref. [133–135].

Adsorbates	Molecular weight (g/mol)	Boiling point (ºC)	ρ (g/cm^3)	Water solubility (g/L)	P_o (mm Hg)	P_e (cm^3/mol)	Kinetic diameter Å
Dichloromethane (DCM)	84.93	39.75	1.3260	13	372.8	16.34	3.3 [136]
Mehtyl Isobutyl Ketone (MIBK)	100.16	116.50	0.7970	19	16.5	30.06	7.35 [120]
m-Xylene	106.16	139.12	0.8842	0.146	6.24	35.97	6.8 [137]
n-Hexane	86.18	68.73	0.6593	0.0098	147.6	29.70	4.3 [138]
Toluene	92.14	110.63	0.8669	0.530	28.9	31.12	5.85 [137]

ρ is the liquid density at 20°C.

P_o is the saturated vapor pressure at 20 or 21°C.

P_e is the molar polarization from ref. [26].

The selected hydrophobic solvents for this study were dichloromethane (DCM), n-hexane, toluene, methyl isobutyl ketone (MIBK), and m-xylene and their physical and chemical properties are listed in Table 3.2. These organic solvents are commonly found in the printing, painting, surface coating, degreasing, and adhesive industries. A survey conducted in Kyoto, Japan between 2004 – 2005, which collected 1,010 air samples in 156 enterprises, revealed that toluene (42%) was the most common used solvent and xylene was found in 27% of the samples, MIBK was present in 17% of the cases, and n-hexane in 12% of the total samples [139]. These

selected solvents not only exhibit a wide variety of vapor pressures but are also representative of what is found in the workplace.

3.3 Characterization with Argon and CO_2

The static equilibrium adsorption isotherms were carried out with Argon at 87.3 K, and CO_2 at 273 K using ASAP 2020 (Micromeritics Ins. Corp., Norcross, GA). All samples were degassed before the adsorption measurements at 300°C for 24 hours in the physiosorption analyzer. From the resulting equilibrium adsorption isotherm data, the Brunauer- Emmett-Teller (BET) equation was applied to calculate the specific surface areas (S_{BET}) in the relative pressure (P/P_o) range of 0.009−0.1. The total pore volume, V_{total}, was determined from the amount of Ar adsorbed at $P/P_o \approx 0.99$. The Barrett-Joyner-Halenda (BJH) and the Dubinin-Radushkevich (DR) equations were used to determine the mesopore and micropore volumes, respectively. The microporosity and the mesoporosity percentages were assessed by dividing the micropore volume obtained with Argon by the total pore volume. The DR equation was also used with the CO_2 adsorption data to calculate the narrow micropore volume, V_n ($w < 7$ Å). The pore size distributions (PSD) were analyzed by the Density Functional Theory (DFT) for each sample using the adsorption isotherm of Ar at 87.3 K and CO_2 at 273 K with the software provided by Micromeritics. The DFT slit pore model was used with the non-negative regulation method and confirmed goodness of fit.

3.4 Breakthrough Measurements with Organic Vapors

A series of single and parallel breakthrough experiments were performed to assess the suitability of the Mini approach described in Chapter 5. A single experiment is defined as a breakthrough measurement performed with only one filter device (Mini or OV cartridge), whereas in the parallel experiment, both devices (Mini and OV cartridges) are exposed simultaneously to the same contaminated airstream. The advantages of using the latter method are: sustainability, timesaving, and that it removes the experimental variables because both carbon beds are exposed at once to the same conditions. Thus, for this study, the parallel experiments are the preferred testing method. However, initial single experiments were performed to verify the repeatability and reproducibility of the test system.

3.4.1 Experimental Set-Up

A schematic diagram of the atmosphere generation system used for exposing the Mini and the OV cartridge is illustrated in Figure 3.2. A MNR (Miller-Nelson, HCS-501, Miller-Nelson Research, Inc., Dublin, Calif.) flow controller was used in this set-up. The vapor introduced in the mixing chamber was generated with a syringe pump (KDS Legato 210, Holliston, Ma). All solvents were HPLC grade from Sigma-Aldrich: dichloromethane (DCM), methyl isobutyl ketone (MIBK), n-hexane, m-xylene, and toluene. The mixing chamber contained a fan, which allowed a uniform distribution of the airstream into the exposing chamber. The feeding rate of the exposure chamber was set to 30 L/min to generate a concentration of ~ 500 ppm with an overall ± 3% coefficient of variation for the organic vapor at 21 ± 1ºC and 40 ± 1% RH. Using five concentration points, a calibration curve for each chemical substance was obtained. The temperature and humidity were controlled and monitored by means of a direct-reading hygrometer. The OV cartridge and the Mini were either ran in single or parallel experiments and were connected to separate vacuum pump lines, operating at 24 L/min for the cartridge and at the equivalent flow rate between 1.30 – 2.40 L/min for the Mini depending on the cartridge (see Table 3.3) and they were measured with a TSI Mass Flow meter 4040 (Shoreview, MN). The airstream was monitored by flow meters throughout the experiments. The inlet and the outlet vapor concentrations of the Mini and the OV cartridge were measured at 30 second intervals with a gas chromatograph (HP, 5890 Series II, Alto Palo, CA, USA) equipped with a flame ionization detector (FID) and a selection valve (Model A60, VICI, Houston, TX, USA). A deactivated silica column (40 cm x 0.32 mm I.D.) was attached to the injection port with a loop of 250 µL. The carrier (helium) flow rate was 4.6 mL/min, the detector makeup gas (nitrogen) flow rate was 30 mL/min, and the hydrogen and airflow rates were 30 and 400 mL/min, respectively. The oven temperature was set at 200 °C and the FID temperature was at 250 °C.

The experimental activated carbon adsorption capacities (We_{exp}) were measured gravimetrically after the downstream concentration (C_x) had reached ~100% of the upstream concentration (C_o). Prior to experimentation, empty OV cartridges and Mini were weighed and removed from cartridge total weight to determine the initial activated carbon weight. A blank experiment (without solvent vapor) of the OV cartridge was run for 8 hours at 40% RH, at 24

L/min, and showed that only 0.7 % of water was adsorbed, which was judged negligible. The calculated adsorption capacity (We_{calc}) was approximated by using the midpoint of the breakthrough time at 50% saturation ($tb_{50\%}$) with Eq. 2.7:

.

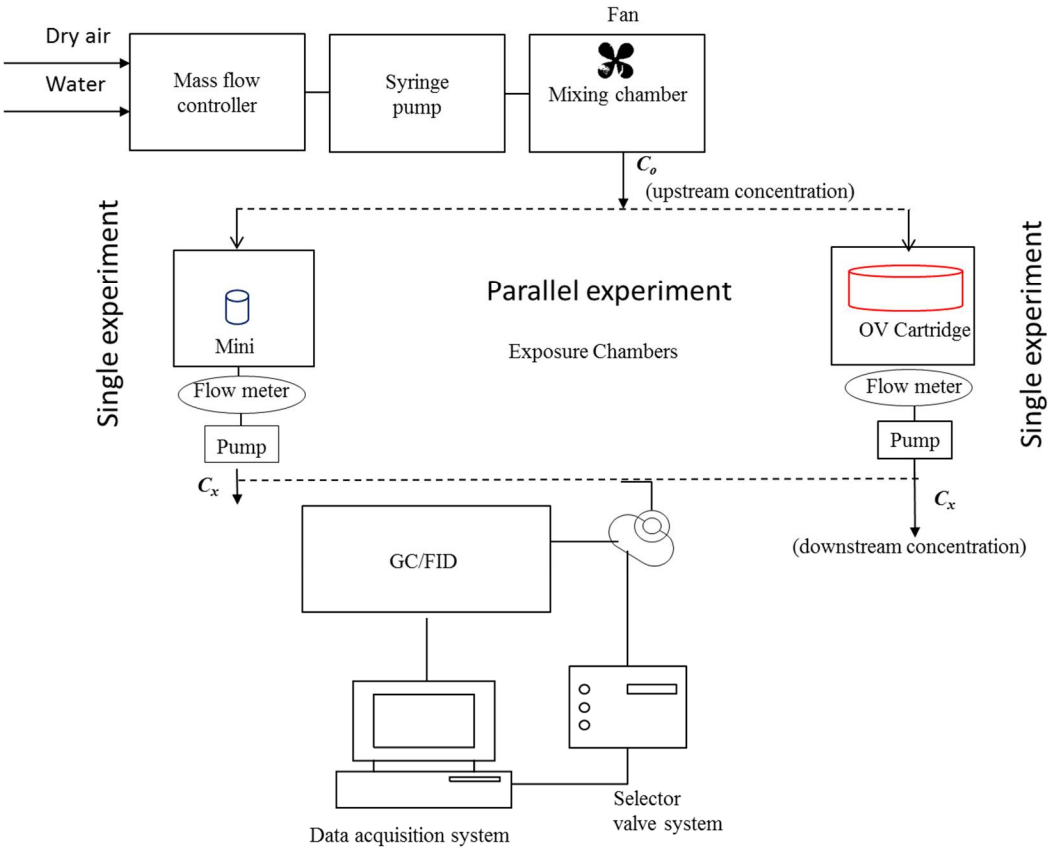

Figure 3.2 Schematic diagram of the experimental set-up for Mini and OV cartridge breakthrough experiment.

The breakthrough tests were performed at 40% RH and the adsorption of water vapor at this RH is considered insignificant [10], [11]. A concentration of 500 ppm was chosen as a reasonable level to achieve 100% saturation in a controllable time manner for all the tested vapors.

Commonly, the time at 10% saturation ($t_{b10\%}$) is used to define the cartridge service life and it was also obtained from the breakthrough curve measurements of the Mini and OV cartridge.

The carbon bed length, which corresponds to the thickness of the respiratory cartridge was measured by using a caliper. Both values ($t_{b10\%}$ and We) were used to compare Mini versus OV cartridge filtering capacity.

3.4.2 Miniaturized (Mini) Cartridge Device

Figure 3.3 illustrates the Mini device and the vertical fall tube specially designed in house for this study. The Mini is made of stainless steel with a cylindrical collection container with an inside radius of 1.14 cm and a length of 5.00 cm. The packed carbon was kept in place by two wired meshed screens and filters (Texel, TRIBO 60 HJ, St-Elzéar-de-Beauce, QC) tightly screwed in at each end. These dimensions for a packed bed activated carbon filter ensure a linear flow throughout the Mini cartridge.

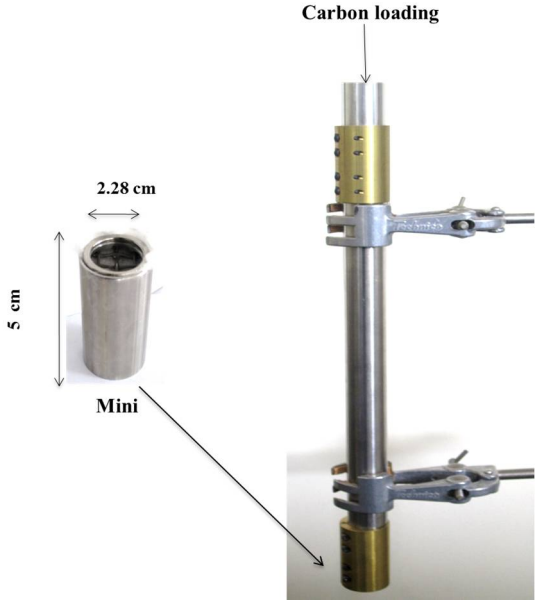

Figure 3.3 Photograph of the miniaturized (Mini) cartridge used in this study and the vertical fall tube.

Assumptions of the Mini

The approach of the Mini relies on two fundamental assumptions: (1) identical carbon bed density and (2) equivalent linear air through velocity to the OV Cartridge. To fulfill the first assumption, an equivalent amount of carbon obtained from the respiratory cartridge must be added to the Mini device. By considering that for a given area of the Mini, it should have the same carbon thickness and bed density as the OV cartridge, an equivalent amount (W) in grams

of activated carbon was calculated. Thus, equation 3.1 was used to calculate and the carbon loading is illustrated in Figure 3.3.

$$W\ of\ Mini = \pi r^2 l \rho_{\boldsymbol{B}} \qquad (3.1)$$

$$= \pi\ (1.14\ cm\ )^2 \cdot 1.65\ cm \cdot 0.42 \frac{g}{cm^3}$$

$$= 2.83\ g$$

where ρ_B is the carbon bed density and l thickness of the OV cartridge, and r is the radius of the Mini.

The second requirement was fulfilled by the estimation of an equivalent flow rate (Q) to the 24 L/min, which passes through the OV cartridge bed area. By assuming that for a given area of the Mini that the throughout linear air velocity for a plug flow through the bed is identical to OV cartridge, the corresponding flow rate (Q) of the Mini was calculated with the following equation using the 3M6001 cartridge as an example cartridge:

$$Q\ of\ Mini = \frac{Area\ of\ OV\ cartridge}{Area\ of\ Mini} \times\ Q\ of\ OV\ cartridge \qquad (3.2)$$

$$= \frac{63.18\ (cm^2\ )}{4.09\ (cm^2\ )} \times 24 \frac{L}{min} = 1.55\ L/min.$$

The equivalent flow rates and equivalent weights for the Mini are listed in Table 3.3 along with the characteristics of the cartridges studied.

Table 3.3 **Characteristics of the organic vapor respirators and mini cartridges used in this study.**

Organic vapor respirator cartridges								Mini Cartridge *	
Manufacturer	Weight(g)	Humidity Content (%)	Packed Bed Density (g/cm^3)	Thickness (cm)	Surface Area (cm^2)	PS¥ (mm)	Flow Rate (L/min)	Equivalent. Weight (g)	Equivalent. Flow Rate (L/min)
3M6001	45.76	2.4	0.42	1.67	63	1.15	24	2.83	1.55
Dräger-OV	47.98	3.2	0.41	2	54*	1.15	24	3.38	1.82
North N75001L	41.84	0.2	0.43	2.2	44	1.1	24	4.3	2.23
Survirvair 100100	50.84	2.1	0.46	2.1	50	1.15	24	4.02	1.94
Moldex 7100	48.45	3.9	0.44	2.2	46	1.15	24	3.96	2.13
Moldex 8100	37.87	4	0.39	2	45	1.15	24	3.21	2.16
MSA Advantage	50.49	3.9	0.44	2.2	53*	1.1	24	3.83	1.84
MSA Comfo	42.39	4.3	0.43	2.5	41	1.05	24	4.39	2.37
Scott 7422-BA1	33.44	3.3	0.41	1.25	60*	1.1	24	2.1	1.63
Scott 7422-BC1	54.82	3.8	0.42	2	60*	1.05	24	3.47	1.63
Sundström- SR							24	5.01	1.34

* Area of mini 4.079

* Bed area for none cylindrical respirator cartridges were determined with millimeter paper.

¥ PS is Particle size determined at 70% cumulative mass fraction.

3.4.3 Experimental Design Studies

This work consisted of four investigations. The first two, involved corroborating the assumptions in the design of the Mini in terms of the equivalent weight and flow rate. The third investigation was a reproducibility and repeatability study with selected solvents in single experiments, and the last one consolidated all the results in parallel experiments. The four experiments are listed below:

a) reproducibility of the carbon bed thickness of the Mini;

b) flow rate experiments from 1.30 L/min to 1.55 L/min of the Mini with dichloromethane (DCM);

c) single experiments of the Mini and OV cartridge tested in triplicate with n-hexane and DCM;

d) parallel experiments (Mini and OV cartridge) conducted with DCM, n-hexane, methyl isobutyl ketone (MIBK), toluene, and m-xylene.

3.4.4 Predictive Model

Analysis of breakthrough of the OV cartridge and the Mini were performed using the Wheeler-Jonas equation [28].

3.5 Calculation of Binary Breakthrough Curves

Using the ideal adsorbed solution theory (IAST) with Langmuir constants from pure component systems, the adsorption capacity of the mixture was calculated.

The adsorption capacity for single contaminants may be expressed using the Langmuir equation with the following form [123]:

$$We = \frac{m_i k_i C}{1+k_i C} \tag{3.3}$$

where m and k are Langmuir constants, and C is the concentration of the single contaminant i.

Calculation of binary breakthrough curves of acetone (10-700 ppm) and the other contaminants of lower volatility (toluene, xylene, styrene) were simulated using the Vahdat et al. model [122]. The chemical and physical properties of the selected solvents are shown in Table 3.4. The flow rate (24 L/min), temperature (25°C), weight of carbon (50 g), adsorption capacity (0.44 g/cm$^{3)}$ remained fixed while several scenarios of various concentrations were simulated.

Table 3.4 Properties of contaminants studied [140].

Solvent	Density (g/cm^3)	Boiling point (°C)	Vapor Pressure (mm Hg)	Odor Threshold (ppm)	TLV (CSST) (ppm)
Acetone	0.784	56.29	185	50	500
Toluene	0.866	110.6	22	6.7	50
o-xylene	0.88	144.4	4.97	5.4	100
m-xylene	0.864	139.1	5.9	0.6	100
Styrene	0.906	145	5	0.14	50

The Vahdat model describes the pressure for a single contaminant, which will reduce the Gibbs adsorption isotherm in Eq.2.10 to

$$\frac{\Pi_i A}{RT} m_i \ln(1 + k_i p_i^0) \tag{3.4}$$

where The IAST model describes the spreading pressure of each contaminant being equal at the adsorption equilibrium, which yields [122]

$$m_1 \ln(1 + k_1 p_1^0) = m_2 \ln(1 + k_2 p_2^0) \tag{3.5}$$

Additionally, the mole fraction X_1 is calculated from the following equation

$$X_1 = \frac{P_{y1}}{P_{1^o}} \tag{3.6}$$

where $y1$ is the mole fraction of component 1, P is the pressure of component 1 and P_{1^o} the pure component pressure of component 1 at the spreading pressure of the mixture. A similar

equation can be written for component 2. The P_{1^o} was obtained by solving the following two equations by using the quadratic equation:

$$\frac{1+K_1P_1^o}{1+K_2P_2^o} = exp\left(\frac{m_2}{m_1}\right) \tag{3.7}$$

$$X_1 + X_2 = 1 \tag{3.8}$$

The model was validated with previously published data [20]. The Microsoft Excel program was used for the calculations using the quadratic equation to solve for the unknown parameters.

The exposure concentration inside the mask was obtained by integrating the breakthrough curve from time zero to a defined point in the curve judged safe for the worker based on the chosen reference concentration. Using the concentration time dependent, a Hazard index was calculated as a function of time to predict theoretically the service life for the safe use of a given respirator cartridge. Other parameters or thresholds such as the IDLH were considered. Finally, in the last step, the risk characterization was evaluated to see if the risk was acceptable.

CHAPTER 4: Micropore characterization of activated carbons of respirator cartridges with argon, carbon dioxide, and organic vapors of different vapor pressures[1]

4.1 Abstract

Activated carbon is the preferred adsorbent to remove organic vapor (OV) because of its micropore structure. For ten activated carbons of commercially available respirator cartridges, the microstructure was characterized using argon at 87.3 K, carbon dioxide at 273 K, and five organic vapors having different vapor pressures (dichloromethane, n-hexane, methyl isobutyl ketone (MIBK), m-xylene, and toluene) at 500 ppm, 294 K, and 40% relative humidity. The corresponding OV adsorption isotherm at relative vapor pressures ranging from 9 x 10^{-4} to 0.1 exhibited the characteristic Type I isotherm as verified by the Langmuir model. The Dubinin Radushkevish (DR) equation was applied to the argon and OV data to extrapolate the micropore volumes and the specific relative structural constants, *B*. The micropore volumes obtained with the OV experimental data were within 0 - 19 % of the values of the argon data. Comparison between the DR predicted and experimental adsorption capacities showed that the OV approach could successfully predict the adsorption capacity for the tested OV. The complementary characterization with carbon dioxide showed that narrow micropores might play an important role in the adsorption.

[1] The modified version of this chapter has been published as : Janvier, Florence, Ludovic Tuduri, Daniel Cossement, Daniel Drolet, and Jaime Lara. "Micropore characterization of activated carbons of respirator cartridges with argon, carbon dioxide, and organic vapors of different vapor pressures." *Carbon* 94 (2015): 781-791.
.

4.2 Introduction

Activated carbon is the preferred adsorbent material for the removal of toxic organic vapors given its low cost, high specific surface area, extensive pore volume, and tunable pore size distribution depending on the activation process used [1-4]. Particularly, activated carbon is widely used in the removal of toxic vapors from the ambient air by a process known as physical adsorption [5-8]. This adsorption process relies on the physical and chemical properties of the adsorbent (activated carbon) and of the adsorbate (organic vapor) as well as on the environmental conditions [7, 8]. Knowledge of the pore structure and the physicochemical properties of activated carbon are important for industrial adsorption process and for the prediction of adsorption capacity, which is the most important factor governing the service life of the device [9] such as in respirator cartridges [10].

Characterization of the porous structure of activated carbon in respirator cartridges and other applications is typically achieved with N_2 at 77 K. However, relying only on N_2 may be misleading and can provide limited information [8, 11] about the micropore (pore width [w] < 20 Å) structure where most of the organic vapor adsorption takes place [12]. Therefore, for a more reliable and detailed characterization of the micropore structure of activated carbons, other molecular probes such as Ar at 87.3 K have been suggested [13, 14]. This molecule is less reactive (i.e., monatomic, no multipolar moments) than N_2 at 77 K and its micropore filling occurs at higher relative pressures. Both characteristics are advantageous to reduce some of the kinetic restrictions usually associated with N_2 at 77.4 K [15, 16]. In addition, a complimentary characterization of the narrow micropores (w < 7 Å) can be achieved in combination with CO_2 at 273 K. The initial part of the CO_2 adsorption isotherm describes more accurately than is normally possible with other probing gas because its maximum relative vapor pressure occurs at 0.03 [15]. However, standard molecular probes (N_2, Ar or CO_2) rely on indirect measurements for which the interpretation of the resulting adsorption isotherm is based on molecular models with their own assumptions and limitations [7, 9]. Because adsorption isotherms for organic vapors (OVs) are important for assessing their suitability and application, ideally the best molecular probe to characterize the activated carbon is that to be utilized in the final use, under conditions that mimic their real environment conditions [7, 17].

Micropore analysis of activated carbons based on adsorption isotherm of OV has been proposed as an alternative method [18]. Typically an isotherm of an OV at various concentrations is used in combination with a reference adsorbate or by using quantitative structure activity relationship (QSAR) to characterize the micropore structure [18-20]. Others have used the adsorption of molecular probes with various molecules of different sizes and shapes to assess the effective size of the pore entrance by heats of adsorption with immersion calorimetry for the estimation of the micropore size distribution [9, 15, 21]. However, the molecular probes technique is tedious and time-consuming in terms of the experimental procedure [12]. Despite several studies describing adsorption of OV onto activated carbon [3, 18-20, 22, 23] and using only one type of OV and a reference compound to characterize the pore structure, this approach may not be suitable for all compounds.

Classical methods for characterization of micropore structure are limited to ultra-dry conditions. However, removal of OV by adsorption in filtering applications is concerned with air streams with humidity. Our current understanding is that adsorption capacity is usually the main determinant of the service life in OV adsorption of respiratory cartridges. Consequently, it is crucial to characterize the micropore structure of activated carbon where OV adsorption occurs in environmental conditions (e.g. not ultra- dry) for predictive adsorption capacity equations intended for use in humid air. Accuracy in the prediction of the adsorption capacity is crucial because errors as small as 5% will affect the service life prediction [24] .

In this study, a novel approach is proposed to characterize commercially available activated carbons of respiratory cartridges with an adsorption isotherm obtained using five organic vapors: dichloromethane, n-hexane, methyl isobutyl ketone (MIBK), m-xylene, and toluene having different vapor pressures and at the same targeted concentration. The micropore volumes and adsorption capacities of the activated carbon tested with the organic vapors were compared with Argon at 87.3 K. A complementary analysis of narrow micropores with CO_2 at 273 K was performed.

4.3 Background

4.3.1 Adsorption isotherms models

The Dubinin Radushkevish (DR) equation is derived from the Polanyi's adsorption potential theory and relates the adsorption capacity of organic vapors to the micropore volume of activated carbon [18, 25]:

$$We = W_o \rho \exp - \left[\frac{K}{\beta^2} W_o R^2 T^2 \ln^2 \left(\frac{P_o}{P} \right) \right] \tag{4.1}$$

where We is the adsorption capacity (g/g of carbon), W_o represents the micropore volume usually obtained from standard adsorption isotherm (N_2 or Ar) (cm^3/g) , ρ is the liquid density of the organic solvent (g/cm^3), K is the carbon structural constant, β is the affinity coefficient for the target adsorbate, R is the ideal gas constant, T is the temperature (K), P is the partial pressure (mm Hg), and P_o is the saturation vapor pressure of the adsorbate (mm Hg).

To apply the DR equation to the prediction of adsorption capacity for cartridge service life, Wood has related the term β to the molar polarization P_e of the adsorbate ($\beta^2 \cong P_e^{1.8}$), and correlated a universal relative structural constant $b = 3.56 \times 10^{-5}$ mol^2cal^{-2} $(cm^3/mol)^{1.8}$ for which the micropore volume and the structural parameters are expressed in the form of [26, 27]:

$$We = W_o \rho \exp - \left[b W_o P_e^{-1.8} RT \ \ln \left(\frac{P_o}{P} \right) \right]^2 \tag{4.2}$$

Wood's universal relative structural constant b is derived from selected vapor adsorbates from various studies and reports and replaces the structural constant K and the affinity coefficient β from the DR equation [26]. Thus, b relies on over generalization concepts that all adsorbent-adsorbate systems have the same physicochermical properties and interactions. This approximation may prove to be an arbitrary choice, and it may not be suitable for all activated carbons and organic vapors systems.

In this study, the Wood approach was adapted such that a descriptive micropore volume (W_{ov}) may be obtained from an isotherm of the adsorption of OVs at the same concentration but of different vapor pressures [28]. Thus, applying the linear form of DR equation to the adsorption capacity facilitates determination of its parameters with:

$$\ln\left(\frac{We}{\rho}\right) = \ln W_{ov} - \left[\left(\frac{RT}{BP_e^{-1.8}}\right)\ln\left(\frac{P_o}{P}\right)\right]^2 \tag{4.3}$$

where $B = bW_{ov}$ is the unique relative structural constant and depends only on the micropore volume.

The plot of $\ln\left(\frac{We}{\rho}\right)$ versus $\left[\ln\left(\frac{P_o}{P}\right)\right]^2$ yields W_{ov} from the intercept, whereas the slope provides B for a given carbon. The derived parameter W_{ov} is independent of the experimental temperature and of the nature of the adsorbate vapor, hence, it can be used for other adsorbates and adsorption conditions [29].

The Langmuir equation describes Type I equilibrium adsorption isotherms in activated carbons and it can also be used to fit the adsorption data [30]. The Langmuir equation postulates that the adsorption of molecules on a solid surface forms a monolayer and that the concentration is proportional to the adsorbate concentration in the gas phase and can be expressed as follows:

$$V = \frac{A \cdot P/P_o}{1 + B \cdot P/P_o} \tag{4.4}$$

where V is the volume (cm^3/g), A (g/cm^3) and B (cm^3/g) are Langmuir constants related to the adsorption capacity and the rate of adsorption. The Langmuir equation can be rearranged in the form of:

$$\frac{P/P_o}{V} = \frac{1}{A} + \frac{B}{A} \times P/P_o \tag{4.5}$$

where $P/P_o/V$ versus P/P_o leads to a linear form from which parameters A and B can be obtained.

4.4 Experimental

4.4.1 Adsorbents and Adsorbates

The activated carbons used in this study were obtained from commercially available organic vapor (OV) respirator cartridges and are listed in Table 4.1 with the characterization of their physical properties. The moisture content was assessed by weight difference after the sample had been put in the oven for 24 hours at 125°C.

Five organic vapors listed in Table 4.2 were selected from our previous report [31] on the basis of their hydrophobicity, and on their ability to cover a broad range of partial pressure in the desired range of $P/P_o < 0.1$ where adsorption of OV occurs. All solvents were HPLC grade from Sigma-Aldrich. For this study, the targeted concentration was set to 500 ppm so that 100% breakthrough concentration could be reached for all OVs under controlled experimental condition and in a timely matter. Though the temperature is known to have an effect on OV adsorption [32], it was out of the scope of this study.

Table 4.1 - **Characterization of commercial activated carbon organic vapor cartridges used in this study.**

Cartridges	Weight (g)	Water content (%)	Apparent density (g/cm^3)	Thickness (cm)	Carbon bed area (cm^2)
3M6001	45.76	2.4	0.42	1.67	63
Dräger-OV	47.98	3.2	0.41	2.0	54*
Moldex 7100	48.45	3.9	0.44	2.2	46
Moldex 8100	37.87	4.0	0.39	2.0	45
MSA Advantage	50.49	3.9	0.44	2.2	53*
MSA Comfo	42.39	4.3	0.43	2.5	41
North N75001L	41.84	0.2	0.43	2.2	44
Scott 7422-BA1	33.44	3.3	0.41	1.25	60*
Scott 7422-BC1	54.82	3.8	0.42	2.0	60*
Survivair 100100	50.84	2.1	0.46	2.1	50

* Bed areas for none cylindrical cartridge were determined with millimeter paper

Table 4.2 – Physicochemical properties of organic solvents used as adsorbates from ref. [33-35].

Adsorbates	Molecular weight (g/mol)	Boiling point (ºC)	ρ (g/cm^3)	Water solubility (g/L)	P_o (mm Hg)	P_e (cm^3/mol)	Kinetic diameter Å
dichloromethane (DCM)	84.93	39.75	1.3260	13	372.8	16.34	3.3 [36]
MIBK	100.16	116.50	0.7970	19	16.5	30.06	7.35 [37]
m-xylene	106.16	139.12	0.8842	0.146	6.24	35.97	6.8 [38]
n-hexane	86.18	68.73	0.6593	0.0098	147.6	29.70	4.3 [39]
toluene	92.14	110.63	0.8669	0.530	28.9	31.12	5.85 [38]

ρ is the liquid density at 20°C.
P_o is the saturated vapor pressure at 20 or 21°C.
P_e is the molar polarization from ref. [26].

4.4.2 Adsorption Measurements with OV

The adsorption capacity of the five OVs was characterized by equilibrating the activated carbon with an airstream of vapor at controlled flow rate, concentration, and temperature for each respirator cartridge [27]. The schematic diagram of the breakthrough experimental set-up is illustrated in Figure 4.1. The experimental tests were performed at 21 ± 1°C at a targeted OV concentration of 500 ppm with ± 3% coefficient variation, and at a relative humidity (RH) of 40 ± 1%. The in-house air was dried in line and the inlet airflow was controlled from 15 to 35 L/min. A syringe pump (KDS Legato 210, Holliston, MA) injected the liquid vapor at a predetermined rate for each OV used in this study. Adjusting the syringe pump feed rate and the inlet flow rate generated the specified concentration within ± 20 ppm. A mixing chamber was added to the system to reduce the fluctuations in the inlet concentration. An air flow-humidity-temperature system was also added in line (Miller-Nelson, HCS-501, Miller-Nelson Research, Inc., Dublin, Calif.). The injected vapor airstream passed through the exposure chamber containing the activated carbon respirator cartridge. The inlet and outlet vapor concentrations of the exposure chamber were continuously monitored by a flame ionization detector (FID) by using a gas chromatograph (HP, 5890 Series II, Wilmington, DE) equipped with deactivated silica gel column (40 cm x 0.32 mm) and an injection loop of 250 µL. The carrier gas was Helium at 4.6 mL/min. The other detector gas flow rates were set to 400 mL/min for air, 30 mL/min for nitrogen, and 30 mL/min for hydrogen. The oven temperature was set at 200 °C and the FID temperature at 250 °C. The inlet and outlet concentrations were calibrated every week or each time a new OV was tested and were controlled every day at one standard gas concentration. The data was further analyzed by custom-built software that allowed the plotting of breakthrough curves as a function of time. The experiment was stopped when the equilibrium of the breakthrough concentration was reached (see Figure. 4.2). The amount of OV adsorbed onto activated carbon is referred here as the experimental adsorption capacity (We_{exp}) and was measured by dynamic saturation by simply weighing the cartridge before and after 100% saturation of the vapor breakthrough concentration was reached as illustrated in Figure 4.2. Prior to experimentation, empty cartridges were weighed and extracted of the cartridge total weight to ascertain the initial activated carbon weight.

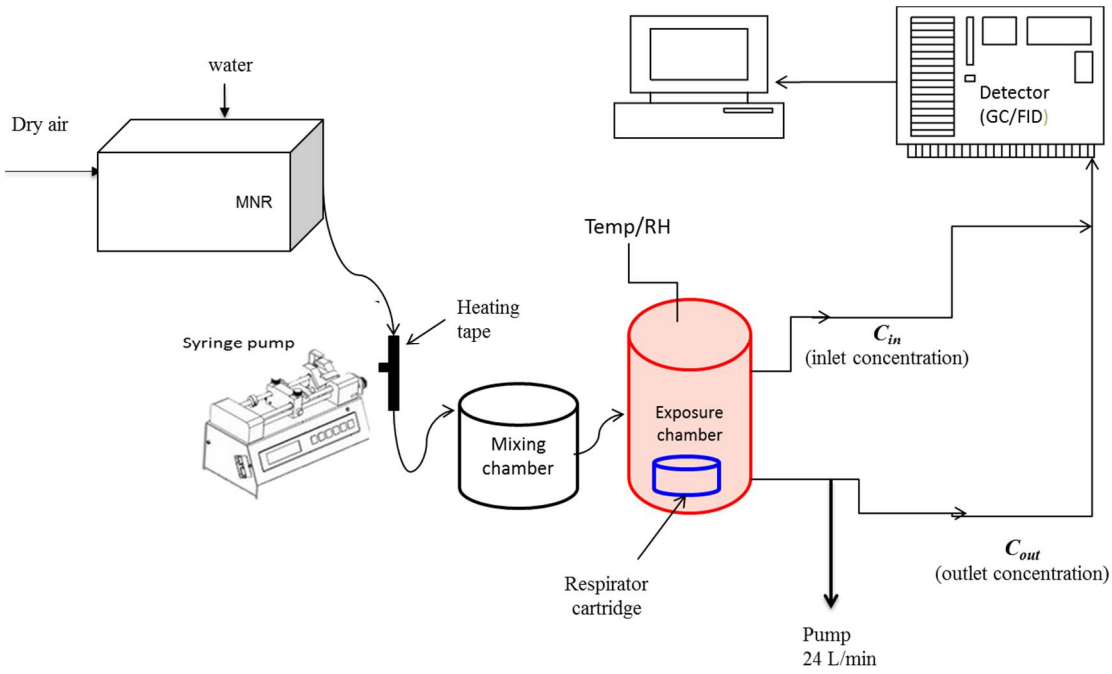

Figure 4.1 Schematic diagram of the experimental set-up for breakthrough experiments.

The calculated adsorption capacities, (We_{calc}) in cm^3/g of carbon of each sample for a given vapor were also computed by integration of the breakthrough curve at 50% breakthrough time ($t_{b50\%}$). Because $t_{b50\%}$ was a good approximation of the integration of the breakthrough curve as shown in Figure 4.2, the integration of the breakthrough curve was estimated with:

$$We_{calc} = \frac{C_o \cdot Q \cdot t_{b50\%}}{w \cdot \rho} \tag{4.6}$$

where C_o is the challenge concentration in g/cm^3, Q is the flow rate in cm^3/min, w is the weight of activated carbon in g, ρ is the liquid density of the solvent in g/cm^3, and $t_{b50\%}$ is the breakthrough time at 50% saturation in minutes, which is a good approximation of the stoichiometric point of the breakthrough curve [27]. By using We_{calc} it removes the influence of the humidity (water adsorption or desorption). A blank experiment (without solvent) was run for 8 hours to evaluate the extent of water adsorption at 40% RH on the activated carbons studied.

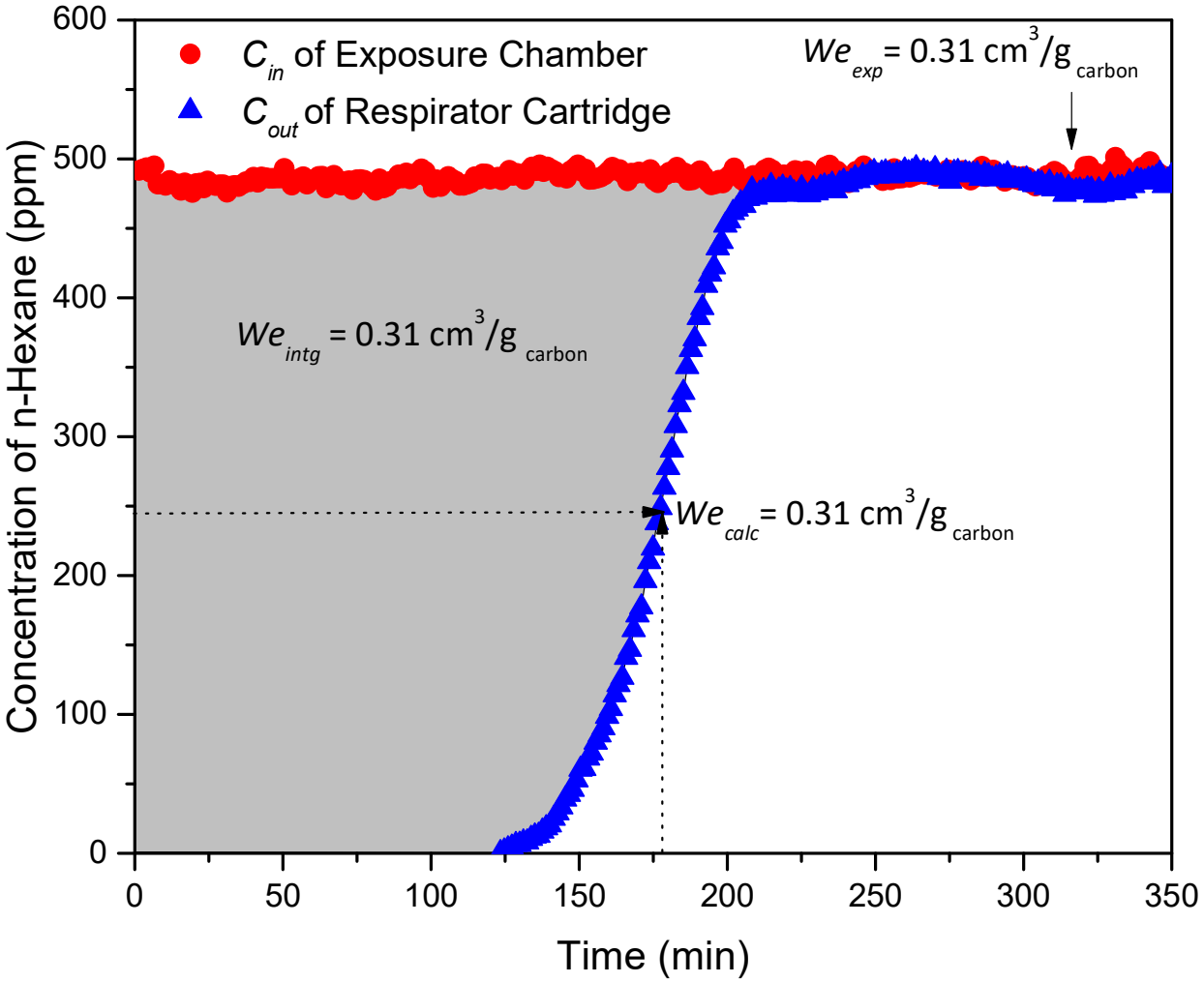

Figure 4.2 -A typical example of a breakthrough curve of activated carbon in respirator cartridge. The experimental adsorption capacity (We_{exp}) is measured gravimetrically at equilibrium conditions when the outlet concentration (C_{out}) equals that of the inlet concentration (C_{in}) of the exposure chamber. The calculated adsorption capacity (We_{calc}) is obtained from the integration of the breakthrough curve (We_{intg}) or it can be approximated from the midpoint of the curve at 50% saturation time.

4.4.3 Adsorption Isotherm Measurements with Argon and CO_2

The static equilibrium adsorption isotherms were carried out with Argon at 87.3 K, and CO_2 at 273 K using ASAP 2020 (Micromeritics Ins. Corp., Norcross, GA). All samples were degassed before the adsorption measurements at 300°C for 24 hours in the physiosorption analyzer. From the resulting equilibrium adsorption isotherm data, the Brunauer- Emmett-

Teller (BET) equation was applied to calculate the specific surface areas (S_{BET}) in the relative pressure (P/P_o) range of 0.009−0.1. The total pore volume, V_{total}, was determined from the amount of Ar adsorbed at $P/P_o \approx 0.99$. The Barrett-Joyner-Halenda (BJH) and the Dubinin-Radushkevich (DR) equations were used to determine the mesopore and micropore volume, respectively. The microporosity and the mesoporosity percentages were assessed by dividing the micropore volume obtained with Argon by the total pore volume. The DR equation was also used with the CO_2 adsorption data to calculate the narrow micropore volume, V_n ($w < 7$ Å). The pore size distributions (PSD) were analyzed by the Density Functional Theory (DFT) for each sample using the adsorption isotherm of Ar at 87.3 K and CO_2 at 273 K with the software provided by Micromeritics. The DFT slit pore model was used with the non-negative regulation method and conformed goodness-of-fit.

4.5 Results and Discussion

4.5.1 Micropore Characterization with OV

Breakthrough experiments were conducted to obtain experimental (We_{exp}) and calculated adsorption (We_{calc}) capacities for each activated carbon of the respirator cartridge. Figure 4.3 shows a good linear relationship between We_{exp} and We_{calc} for all the adsorbate-adsorbent systems, which indicates that Eq. 4.6 is a good approximation of the experimental data.

The We_{exp} and We_{calc} values of the activated carbons of respirator cartridges are presented in Table 4.3 listed in cm^3/g of activated carbon using the liquid densities of the solvents. Table 4.3 shows that there is a trend for the experimental and calculated adsorption capacities, which displayed the following order: DCM < n-hexane < MIBK ≤ toluene < m-xylene and agrees well with their descending order of their vapor pressures (see Table 4.2). Thus in general, the more volatile the contaminant is, the less it is adsorbed onto activated carbon. This characteristic is in agreement with the micropores ($w < 20$ Å) being described as having a 3D-ordered structure with graphene layers forming most hydrophobic parts of the carbon structures and thus adsorbing more easily non-polar solvents unlike the mesopores (20Å < w < 500 Å), which consist most of hydrophilic sites where lies most of the surface polar functional groups [7]. Moreover, the difference in the liquid adsorption capacities between We_{exp} and We_{calc}

increased with the following order: DCM > n-hexane > MIBK > toluene > m-xylene where the calculated values were greater than the experimental adsorption data.

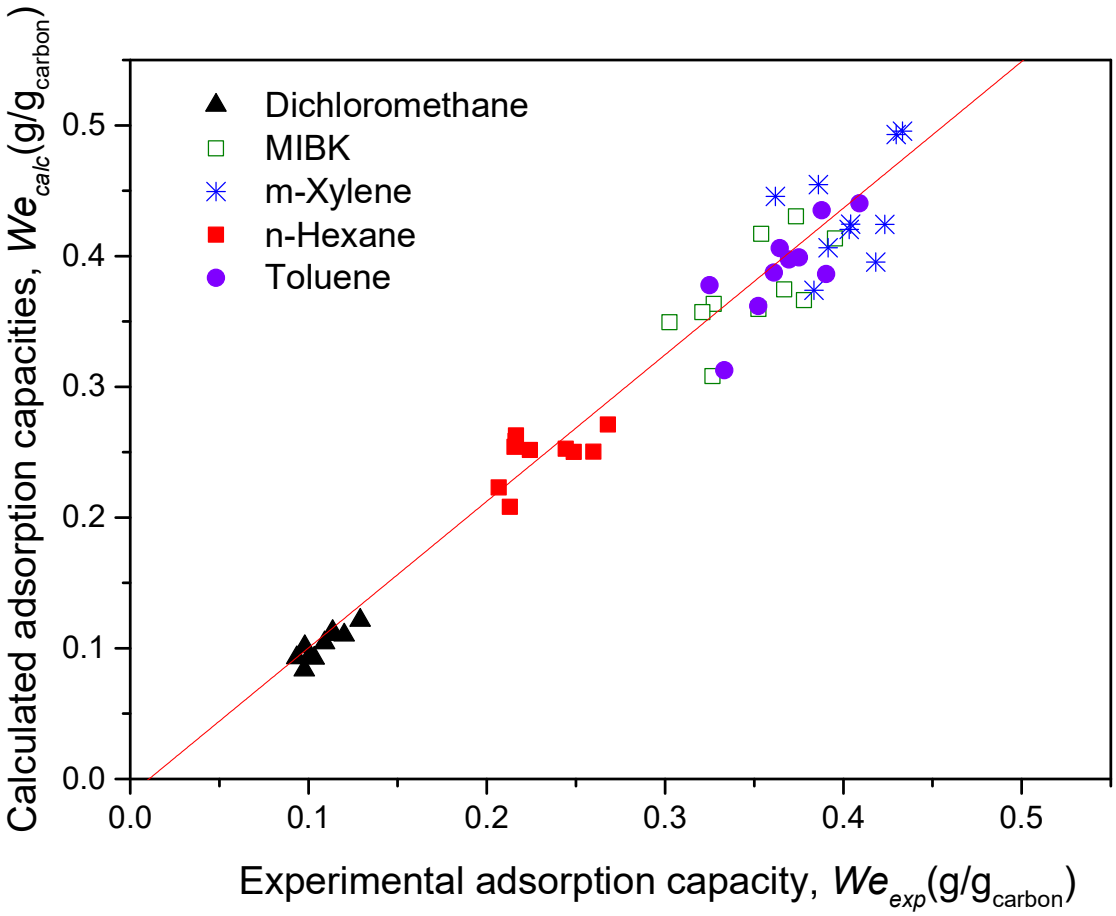

Figure 4.3 Linear relationship of experimental adsorption capacities and calculated adsorption capacities for all of organic solvents for all activated carbons used in the study with y = -0.0118 + 1.121x R^2= 0.961.

The differences observed between the We_{exp} and We_{calc} values especially for less volatile solvents may come from non-homogenous flows of the contaminated air stream on the carbon bed (the respirator cartridge). The lower boiling point OVs migrate inside the carbon bed more rapidly than the higher boiling point solvents, thus reaching equilibrium faster.

Blank experiments performed at the same experimental conditions as the breakthrough tests (24 L/min air flow rate at 21°C) without contaminant, showed that only 0.7% of water was

adsorbed onto activated carbon at 40% RH. This amount was judged negligible. Nelson et al. have shown that RH values between 0–50 % had no significant effect on the breakthrough time for 121 organic vapors, whereas above 60% RH, the dependence of the humidity became quite significant and was more important at lower concentrations [40]. These results are in agreement with another study that showed that water adsorption isotherm on activated carbon had increased sharply at about 50% RH [41]. But, contradicting results have been reported by Werner [42] who observed marked effect on breakthrough times below 50% RH for trichloroethylene vapor at low concentrations. The loss of efficiency at high RH and low concentration is probably a result of the competition between contaminant vapor and water vapor for the same sorbent active sites or "space". More recently, Lodewyckx and Vansant [43] showed that the loss of adsorption capacity could be modeled by volume exclusion. The more volatile the compound is, the more it will be influenced by water adsorption because it is unable to replace the more strongly adsorbed water molecules. Furthermore, at $P/P_o < 0.3$ material with mid width 7–12 Å adsorbed little water because carbons are free of primary polar oxygen sites as revealed by xps analysis [7]. The $We_{exp} < We_{calc}$ results presented in Figure 4.3 and in Table 4.3 suggests that these differences are more pronounced for the hydrophobic OVs with higher boiling points (MIBK, toluene, and m-xylene) in comparison with the lower boiling solvents (DCM and n-hexane). A possible explanation could be due to desorption of water with the high boiling points hydrophic solvents causing a decreased in the experimental adsorption capacity (We_{exp}) compared with the integrated value.

To assess the volume of micropore occupied by an OV, the ratio of the calculated liquid volume of OV (cm^3/g) to that of the micropore volume (cm^3/g) with the Argon data was determined and is shown in Table 4.3. Unlike the adsorption capacity, the results revealed that the volume occupied by an adsorbed vapor increased in the following order: DCM > n-hexane > toluene > MIBK > m-xylene. Other adsorbate properties such as size exclusion effect must be considered when describing the adsorption capacity [13, 44]. For example, MIBK shows the greatest discrepancies (0.74 - 1.03 cm^3 OV/ cm^3 Ar) and has the highest kinetic diameter of 7.35 Å (see Table 4.2) compared with DCM (0.13 - 0.18 cm^3 OV/ cm^3 Ar), which has a small kinetic diameter of 3.3 Å comparable to that of CO_2 and Argon. Thus size exclusion effect is less pronounced for smaller molecules and may play a role in the adsorption of larger molecules for

microporous activated carbon [41]. Moreover, the pore size distribution is another important contributor to the adsorption of OV onto activated carbon. For example, the activated carbon from MSA Comfo, which has the highest micropore volume (0.59 cm^3/g) following the Ar data presented in Table 4.5 also has the widest micropore size distribution and overall, had the least micropore volume used. The activated carbon from North N75001L, which has the highest micropore content (93%), had overall the most micropore volume occupied by an OV. Thus, optimization of the micropore size distribution may be critical for improving adsorption of OVs.

***Table 4. 3* - Comparison of liquid adsorption capacities and ratio of the micropore volume occupied by an organic vapor at 24 L/min, 294 K, ~ 500 ppm, and 40% RH per adsorbate-adsorbent systems.**

Adsorbate	Adsorbent	P/P_o	We_{exp} (cm^3/g_{carbon})	We_{calc} (cm^3/g_{carbon})	cm^3 liq OV/cm^3 Ar micropores
Dichloromethane	3M 6001	0.0010	0.09	0.09	0.15
	Dräger-OV	0.0009	0.09	0.08	0.15
	Moldex 7100	0.0010	0.10	0.09	0.18
	Moldex 8100	0.0010	0.07	0.06	0.13
	MSA Advantage	0.0009	0.09	0.08	0.16
	MSA Comfo	0.0010	0.08	0.08	0.13
	North 75001L	0.0009	0.08	0.07	0.13
	Scott 7422-BA1	0.0010	0.08	0.07	0.13
	Scott 7422-BC1	0.0010	0.07	0.08	0.14
	Survivair 100100	0.0010	0.07	0.07	0.16
n-Hexane	3M 6001	0.0030	0.41	0.41	0.73
	Dräger-OV	0.0029	0.39	0.39	0.73
	Moldex 7100	0.0029	0.37	0.37	0.71
	Moldex 8100	0.0029	0.31	0.31	0.65
	MSA Advantage	0.0029	0.34	0.34	0.64
	MSA Comfo	0.0029	0.33	0.33	0.55
	North 75001L	0.0030	0.33	0.33	0.63
	Scott 7422-BA1	0.0031	0.33	0.33	0.62
	Scott 7422-BC1	0.0029	0.38	0.38	0.70
	Survivair 100100	0.0030	0.32	0.32	0.72
MIBK	3M 6001	0.025	0.49	0.51	0.92
	Dräger-OV	0.024	0.47	0.46	0.84
	Moldex 7100	0.023	0.44	0.45	0.86
	Moldex 8100	0.024	0.41	0.45	0.94
	MSA Advantage	0.023	0.40	0.44	0.84
	MSA Comfo	0.023	0.38	0.43	0.74
	North 75001L	0.024	0.46	0.54	1.03
	Scott 7422-BA1	0.024	0.44	0.52	0.98
	Scott 7422-BC1	0.024	0.46	0.47	0.86
	Survivair 100100	0.024	0.41	0.38	0.85
Toluene	3M 6001	0.016	0.47	0.51	0.91
	Dräger-OV	0.015	0.37	0.44	0.81
	Moldex 7100	0.015	0.43	0.46	0.88
	Moldex 8100	0.015	0.41	0.42	0.87
	MSA Advantage	0.015	0.42	0.45	0.84
	MSA Comfo	0.015	0.43	0.46	0.78

	North 75001L	0.016	0.45	0.50	0.97
	Scott 7422-BA1	0.015	0.42	0.47	0.88
	Scott 7422-BC1	0.015	0.45	0.45	0.82
	Survivair 100100	0.015	0.38	0.36	0.80
m-Xylene	3M 6001	0.074	0.49	0.57	1.01
	Dräger-OV	0.067	0.49	0.49	0.90
	Moldex 7100	0.068	0.46	0.48	0.93
	Moldex 8100	0.069	0.47	0.49	1.02
	MSA Advantage	0.069	0.45	0.47	0.88
	MSA Comfo	0.069	0.42	0.51	0.87
	North 75001L	0.072	0.50	0.57	1.10
	Scott 7422-BA1	0.073	0.44	0.52	0.99
	Scott 7422-BC1	0.066	0.48	0.46	0.84
	Survivair 100100	0.071	0.44	0.43	0.96

P/P_o is the partial pressure.
We_{exp} is the liquid experimental adsorption capacity.
We_{calc} is the liquid calculated adsorption capacity used to calculate the micropore volume ratio to Ar.

4.5.2 Predicted Langmuir isotherms

The Langmuir model (Eq. 4.5) is frequently used to describe the adsorption behavior of organic vapors on activated carbon and it was fitted to the experimental liquid adsorption capacities data. The fitted Langmuir parameters and the *R*-squared are listed in Table 4.4. As shown in Table 4.4. the Langmuir isotherm fitted well with the experimental data, indicating that the Langmuir isotherm is appropriate for describing the adsorption of organic solvents of different vapor pressures onto activated carbons. Furthermore, to verify the validity of the Langmuir model, it is important to simulate isotherm curves determined with the Langmuir constants listed in Table 4.4 and to compare them to the experimental data. Figure 4.4 shows the superposition of the experimental (closed) and calculated (open) adsorption capacity data with their respective predicted Langmuir fit. The shape of the isotherms curves shows that all samples exhibited the Type 1 characteristic adsorption isotherm as described by the micropore adsorption occurring at $P/P_o < 0.1$, however, at these relative vapor pressures, the micropores may not have all been completely saturated. The predicted Langmuir isotherms of the experimental and calculated adsorption data were similar especially for samples Survivair 100100, Dräger-OV, Moldex 7100, Moldex 8100, and North N75001L. In addition, it is well known that the Langmuir isotherm reduces to a linear form at lower pressure, which is in accordance with Henry's law, unlike the DR equation. Thus, with this type of approach, a predictive isotherm over a wide range of relative pressures may be obtained. However,

additional test vapors on the OV adsorption isotherm between DCM and n-hexane and MIBK and m-xylene could have provided more accuracy (see Figure 4.4).

Table 4.4- **Langmuir parameters for organic vapors adsorption isotherms at 294 K for activated carbon from respirator cartridges.**

Adsorbents	Langmuir Parameters					
	Experimental			Calculated		
	A (g/cm^3)	B (cm^3/g)	R^2	A (g/cm^3)	B (cm^3/g)	R^2
3M6001	235	458	0.997	172	289	0.999
Dräger-OV	163	319	0.996	181	356	0.997
Moldex 7100	217	452	0.999	211	420	0.998
Moldex 8100	133	272	0.997	129	249	0.995
MSA Advantage	170	364	0.998	214	441	0.997
MSA Comfo	208	485	0.996	148	275	0.995
North N7001L	176	348	0.995	234	493	0.995
Scott 7422 BA1	159	304	0.998	154	255	0.995
Scott 7422 BC1	196	424	0.997	174	315	0.995
Survivair 100100	137	296	0.997	123	271	0.997

Experimental values from experimental adsorption capacity, We_{exp}
Calculated values from calculated adsorption capacity, We_{calc}

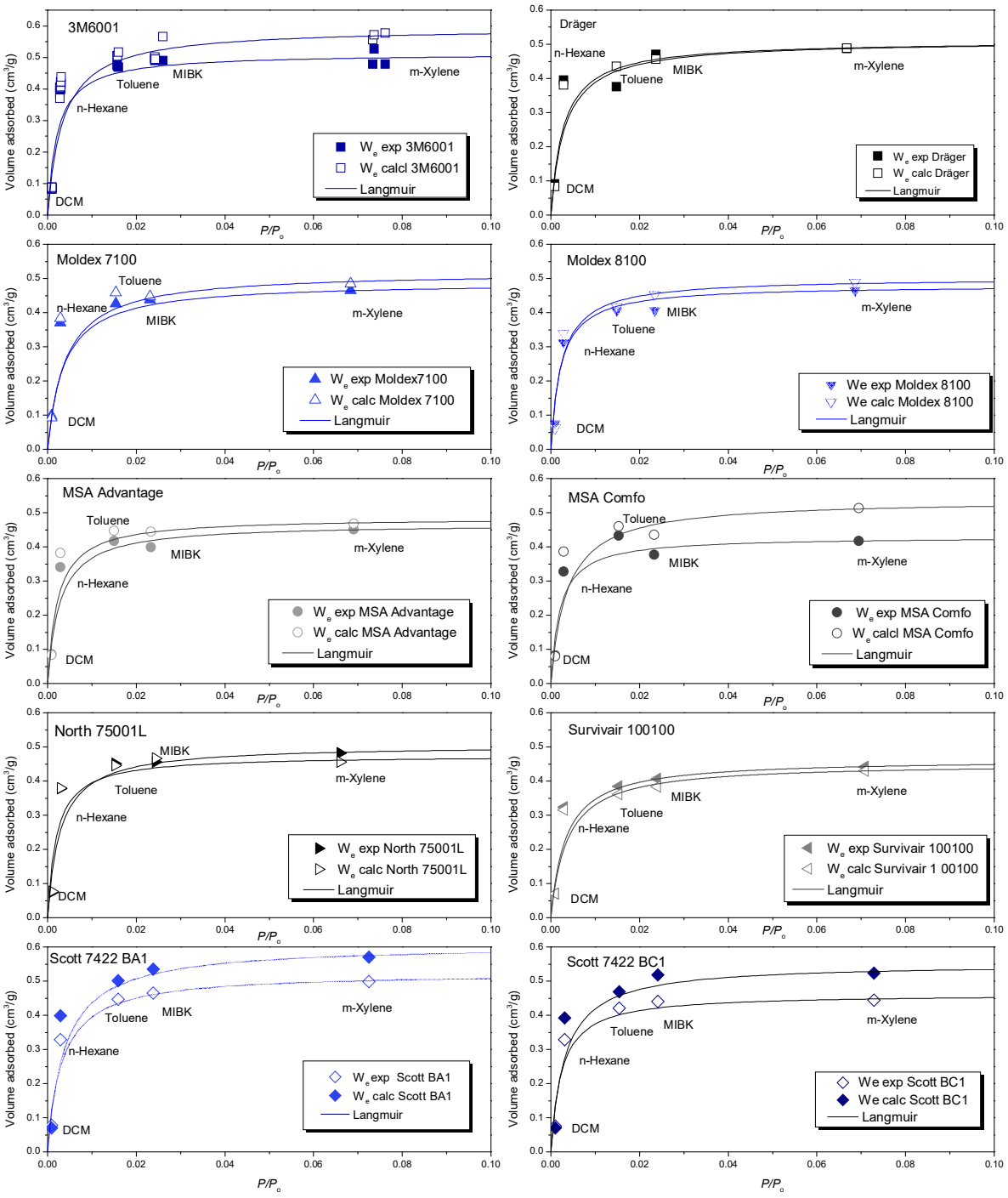

Figure 4.4 Experimental (closed symbols) and calculated (open symbols) adsorption data points versus predicted Langmuir isotherms curves of the five organic vapors with different vapor pressures at ~500 ppm onto activated carbon of respirator cartridges.

4.5.3 Comparison of the DR Prediction Approaches

The adsorption isotherm obtained with OVs of different vapor pressures at the same concentration may provide a more complete and accurate description of the adsorption mechanism of organic vapors onto activated carbon during filtration than the traditional methods with N_2 or Ar at equilibrium conditions because it is obtained at environmental conditions (flow rate, humidity, OV, and temperature) similar to that of real filtration situations. Comparable to the Langmuir model, the DR equation is able to predict the adsorption capacity for any other solvent for a given carbon and relative vapor pressure. The liquid and calculated experimental data for the OVs of different boiling points onto activated carbons of respirator cartridges were further analyzed by applying the linearized form of the DR in Eq. 4.3. Figure 4.5 shows an example of a good linear fit of the DR equation. All samples exhibited a good coefficient of determination.

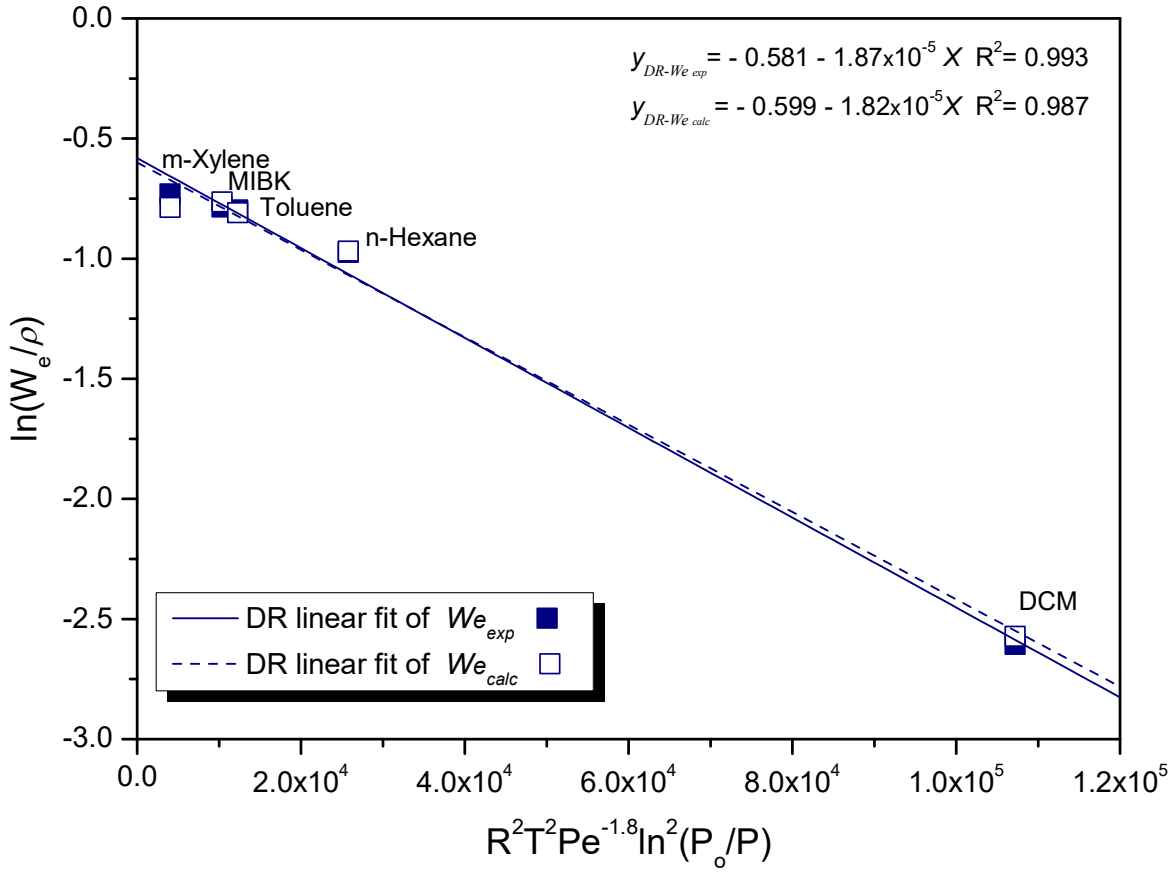

Figure 4.5 Example of a DR linear fit for activated carbon of 3M6001.

Table 4.5 -Summary of pore characteristics of activated carbons of respirator cartridges obtained with adsorption isotherms of Ar at 87.3 K, CO_2 at 273.2 K, and organic vapors of different vapor pressures at 294 K..

	Ar and CO_2 adsorption data					*OV adsorption data*			
Cartridges	S_{BET} (m^2/g)	W_o (cm^3/g)	V_{meso} (cm^3/g)	V_n (cm^3/g)	V_{total} (cm^3/g)	$W_{ov-DR\ exp}$ (cm^3/g)	$W_{ov-DR\ calc}$ (cm^3/g)	B_{exp} $x10^{-5}$	B_{calc} $x10^{-5}$
Survivair 100100	*1242*	*0.45 (71%)*	*0.36 (57%)*	*0.20*	*0.63*	*0.49*	*0.46*	*1.81*	*1.77*
Moldex 8100	*1311*	*0.48 (86%)*	*0.19 (34%)*	*0.14*	*0.56*	*0.50*	*0.55*	*1.77*	*1.99*
North 75001L	*1376*	*0.52 (93%)*	*0.14 (25%)*	*0.18*	*0.56*	*0.56*	*0.55*	*1.87*	*1.82*
Moldex 7100	*1414*	*0.52 (88%)*	*0.17 (29%)*	*0.19*	*0.59*	*0.52*	*0.55*	*1.53*	*1.64*
MSA Advantage	*1430*	*0.53 (90%)*	*0.15 (25%)*	*0.22*	*0.59*	*0.49*	*0.54*	*1.60*	*1.70*
Dräger-OV	*1440*	*0.54 (84%)*	*0.22 (34%)*	*0.19*	*0.64*	*0.53*	*0.55*	*1.61*	*1.72*
Scott 7422 BC1	*1455*	*0.54 (90%)*	*0.16 (27%)*	*0.17*	*0.60*	*0.51*	*0.61*	*1.76*	*1.99*
Scott 7422 BA1	*1466*	*0.53 (85%)*	*0.19 (31%)*	*0.17*	*0.62*	*0.54*	*0.65*	*1.79*	*2.04*
3M6001	*1515*	*0.56 (88%)*	*0.19 (30%)*	*0.26*	*0.64*	*0.58*	*0.63*	*1.77*	*1.85*
MSA Comfo	*1602*	*0.59 (85%)*	*0.25 (36%)*	*0.17*	*0.69*	*0.48*	*0.56*	*1.62*	*1.82*

S_{BET} : specific surface area using the BET method.

V_{total}: total pore volume at $P/P_o = 0.9$.

V_n: narrow micropore volume obtained with Dubinin-Radushkevich (DR) equation using CO_2 at 273 K.

V_{meso}: mesopore volume obtained with Barrett-Joyner-Halenda method, % mesopore content (V_{meso}/ V_{total}).

W_o : micropore volume obtained with DR equation with Ar at 87.3 K, % micropore content (W_o /V_{total}).

W_{ov-DR} : micropore volume obtained with DR equation with organic vapors at 298K for experimental or calculated data

B : specific structural constant obtained from experimental or calculated data.

The extrapolated micropore volumes and the specific structural constant B for the experimental and calculated values are summarized in Table 4.5 with the Ar and CO_2 data. Discrepancies up to 57% difference are observed between the universal and the specific relative structural constants for the B_{exp} and B_{calc} which are greater than the difference observed in the micropore volumes. The experimental pore volume values derived from the OV adsorption isotherm with different boiling points at the same concentration using the DR equation were within 0 - 19% for $W_{ov\text{-}DR\ exp}$ and 2 – 23% for $W_{ov\text{-}DR\ calc}$ from the micropore volume derived from the Ar data, thus reiterating the importance of having a specific structural constant which takes into account the differences in the micropore structure [41]. With the exception of MSA Comfo, which has the widest pore size distribution and the largest specific surface area, in general, the micropore volume values obtained with OV adsorption isotherm were greater than those of Ar, especially for $W_{ov\text{-}DR\ calc}$. A possible explanation for smaller values obtained with Ar compared with the OVs is because of the hindrance in the diffusion within the micropores especially for the narrow micropores because of low temperature and low kinetic energy [7].

The corresponding micropore volumes and the specific relative structural constants B for the experimental and calculated data were incorporated into the DR equation to predict the adsorption capacity. These values were compared with those obtained with Ar at 87.3 K and with the universal relative structural constant ($b = 3.56 \times 10^{-5}$ mol^2cal^{-2} $(cm^3/mol)^{1.8}$). Figure 4.6 shows that the predicted adsorption capacities using the micropore volume obtained from OV data and their relative structural constants B for the experimental and calculated data ($\boldsymbol{W_{OV\text{-}DR\ exp}}$ and $\boldsymbol{W_{ov\text{-}DR\ calc}}$) are in good agreement with the experimental data because the average discrepancy is only 0 % - 16% and 0 – 26 % for the latter. For the standard approach with Ar and the universal relative structural constant, the model seems to underestimate the adsorption capacities onto activated carbons with differences ranging from 1 % to 89%, being much larger for the lower boiling point solvents (DCM and n-hexane). Although these deviations seem high, the model does capture the trend of the adsorption behavior. Thus, more precise characterization can be achieved with the OV adsorption isotherm and a specific relative structural constant which are important for the understanding of the activated carbon pore structure for a given application [11].

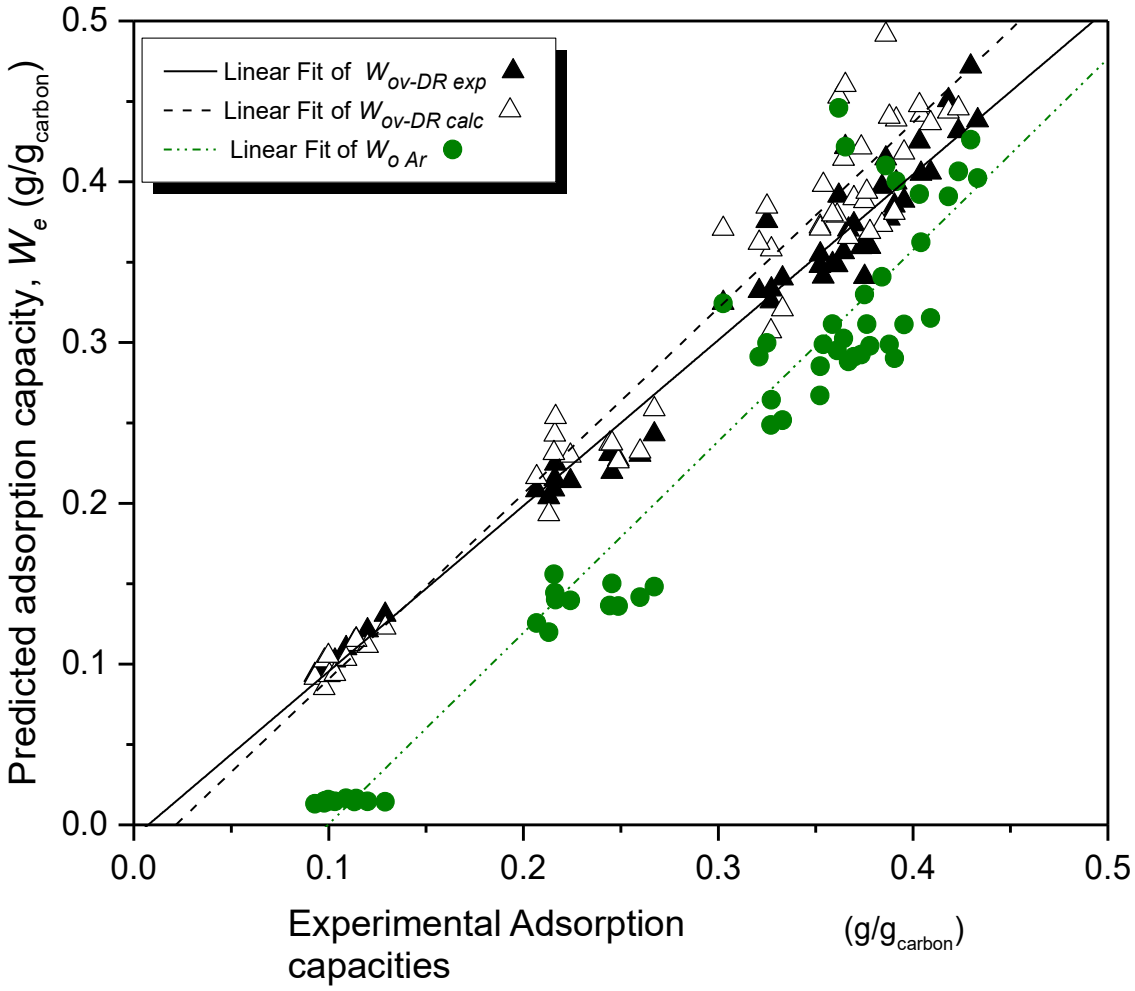

Figure 4.6 Comparison between the experimental adsorption data with the DR predicted experimental or calculated adsorption capacities micropore volumes ($W_{OV\text{-}DR\ exp}$ *and* $W_{ov\text{-}DR\ calc}$) and the corresponding specific relative structural constants (B) obtained from OV of different vapor pressures at~ 500 ppm, the Argon's micropore volume ($W_{o\text{-}Ar}$) and the universal structural constant (b) with $y_{exp} = -0.00758 + 1.0346x$ $R^2 = 0.976$, $y_{calc} = -0.02478 + 1.15408$ $R^2 = 0.955$, and $y_{Ar} = -0.11851 + 1.19029x$ $R^2 = 0.924$ respectively.

4.5.4 Micropore Characterization with Ar at 87.3K and CO_2 at 273K

Figure 4.7 shows the equilibrium adsorption/desorption isotherms for Ar at 87.3 K for the activated carbons of the ten commercially available respirator cartridges used in this study. With the exception of Survivair 100100 activated carbon, all samples exhibit Type I isotherms features with micropore filling occurring at low relative pressures (i.e., $P/P_o < 0.1$) and with a sharp knee followed by the characteristic plateau indicative of the predominant presence of micropores where most of the adsorption takes place. Hysteresis are observed toward $P/P_o >$ 0.9 especially for activated carbon samples of Survivair100100, which indicates the presence of mesoporous structure. However, the sample North 75001L seems to have a sharp knee and less hysteresis suggesting a narrow micropore distribution and stronger adsorbate-adsorbent interactions in the carbon's microporosity [45]. Among all the samples, activated carbon from MSA Comfo exhibits the highest uptake of Ar and the activated carbon of Survivair100100 shows the lowest uptake. The other samples show an uptake of Ar ranging from 400–500 cm^3/g. It is also observed that within the same manufacturers, carbon from MSA Comfo has a wider knee compared with that of MSA Advantage suggesting a higher activation time and burn-off, which may have resulted in the broadening of microporosity while creating more micropores [15].

The total micropore volumes (V_{total}), the Dubinin Radushkevish (DR) micropore volumes (W_o), and the mesopore volumes (V_{meso}) and specific BET surface areas obtained from Ar adsorption data are presented in Table 4.5. Overall the samples cover a wide range of specific BET surface area from 1242 m^2/g to 1602 m^2/g and the micropore content varies from 71 % to 93 %. In general, the specific BET specific area increased with the micropore volume (W_o) and not the total pore volume, reflecting the importance of the micropore size distribution. The micropore and mesopore contents do not add to unity because they were obtained by different method analysis as explained in the experimental section.

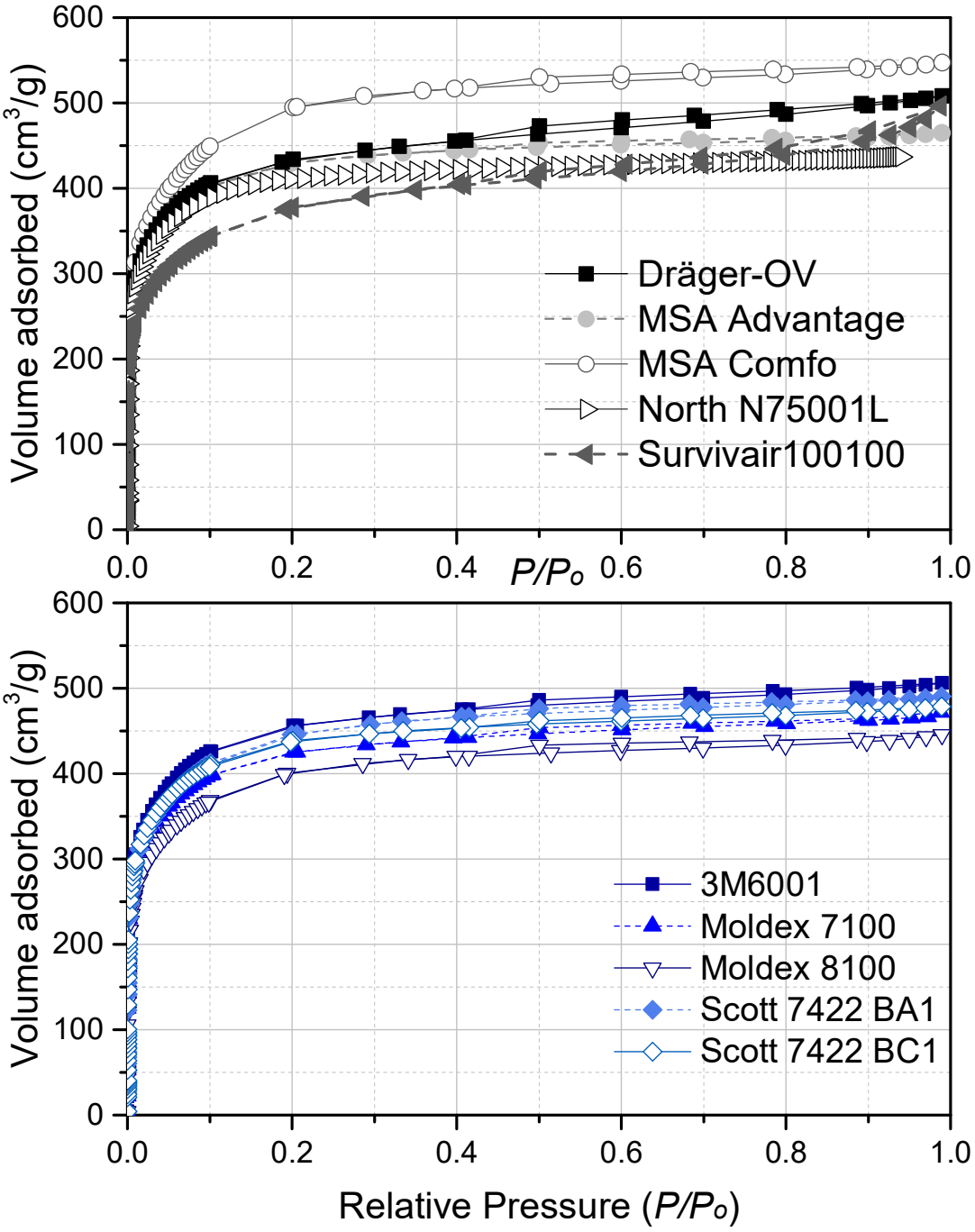

Figure 4.7 Adsorption/desorption isotherms with Ar at 87.3 K for all activated carbons of respirator cartridges studied.

The pore size distribution (PSD) with Ar and CO_2 data of the activated carbons respirator cartridge are presented in Figure 4.8. A common feature of the obtained Ar PSD is that they all exhibit five distinct peaks, around the mean pore size of 5, 8.5, 11.5, 14.5, and 17 Å but of varying maxima for the first and the second peak. The first peak of Ar data is sharp compared with the PSD results of CO_2 at 273 K, which may suggest late pore filling because of slow diffusion [14]. The minima observed at 10 Å is an artifact of the DFT method as a result of the simplification of the numerical solution [11]. Most of the pores of the activated carbon samples fall into the micropore range (< 20 Å). The samples Survivair 100100 and Dräger-OV have the greatest content of mesopores as evidenced by the broad peak in the 20-30 Å range and consequently have large mesopore volume (V_{meso}) ranging of 0.36 and 0.22 cm^3/g, respectively. The difference between the micropore volumes obtained with N_2 and the narrow micropore volumes measured with CO_2 has been used to describe the difference in the micropore size distribution in activated carbons [24]. Similarly, the difference between Ar micropore values and CO_2 narrow micropore values can indicate the micropore size distribution. The sample MSA Comfo exhibits the greatest difference between Ar and CO_2 micropore volumes (0.42 cm^3/g), which suggest a wider micropore distribution than the other samples (see Figure 4.8). Despite this difference, the PSD data calculated with CO_2 is more sensitive to the narrow microporosity because CO_2 at 273 K can easily access narrow micropores (i.e., pores of widths < 4.5 Å) than Ar at 87.3 K because it has less restricted diffusion at low pressure even if they have similar molecular dimensions [46, 47]. In particular, Sample 3M6001 shows a marked difference with the highest value of narrow micropore volume of 0.26 cm^3/g and also exhibits the highest peak at 5 Å and has narrow micropore size distribution (0.30 cm^3/g).

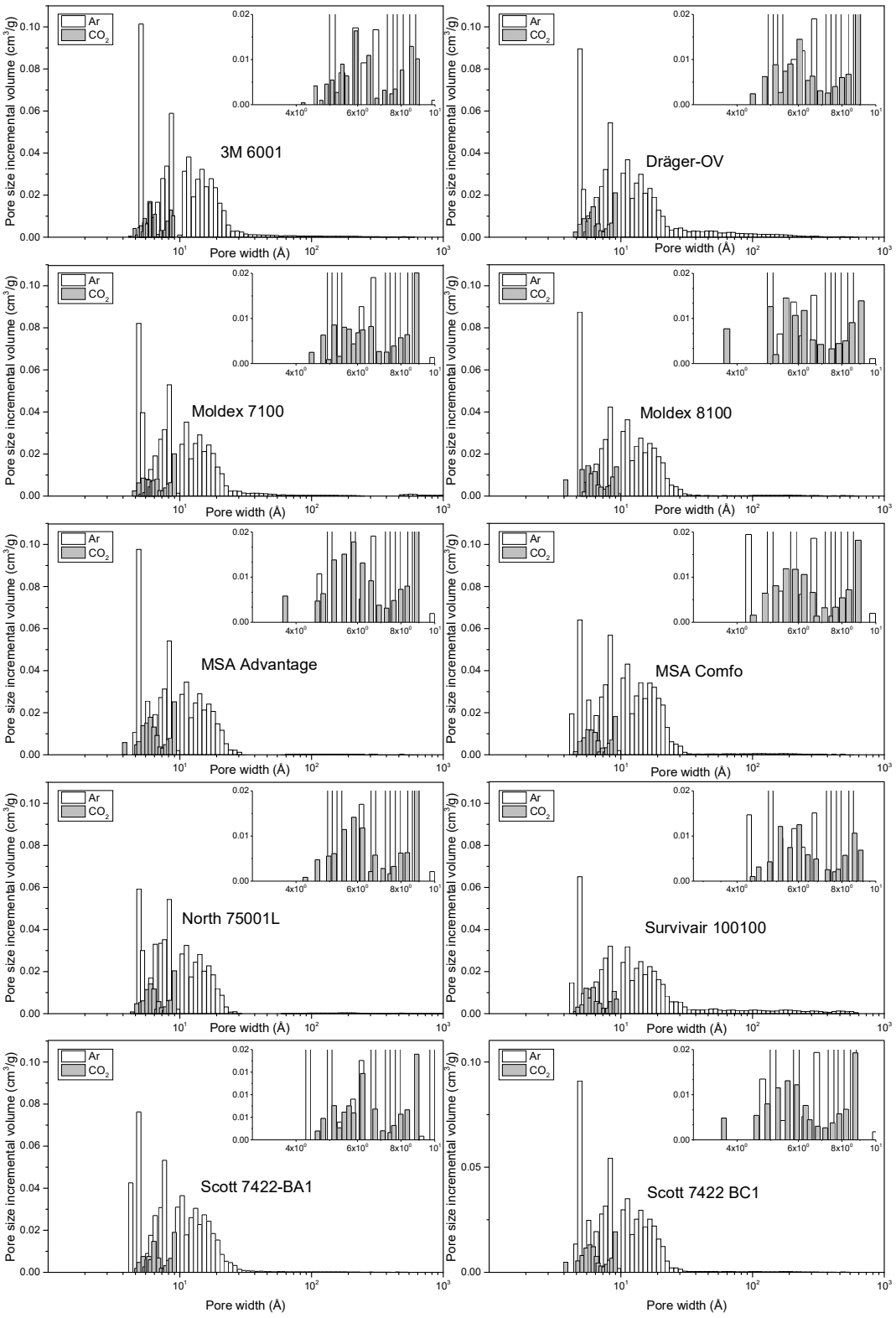

Figure 4.8 Pore size distribution of the activated carbons respirator cartridges obtained from Ar adsorption data at 87.3 K and CO_2 at 273 K.

4.6 Conclusion

An adsorption characteristic curve with five OVs at 500 pm with different vapor pressures of activated carbon of respirator cartridges was established for predicting the OV adsorption capacity. The organic vapor adsorption isotherm exhibited the characteristic Type I adsorption isotherm for $P/P_o < 0.1$ and was suitable for the linearization of the Langmuir and DR equations. This method, which is utilizing humid conditions to characterize the micropore structure of activated carbons of respirator cartridge, gave pore volume consistent with those obtained from equilibrium adsorption isotherm with Argon at 87.3 K in dried conditions. Moreover, this study showed that a good agreement between the experimental and predicted adsorption capacity values using the micropore values obtained with the OV adsorption isotherm and the specific structural constant could be achieved in comparison with the Argon adsorption data and the universal relative structural constant. The pore size characterization with argon showed that the series of activated carbon studied displayed mostly microporosity content whereas the narrow micropore size distribution (CO_2 at 273 K) may have an effect on the adsorption of organic vapor. It is recommended that the micropore characterization of activated carbons of respirator cartridge be done in similar conditions to its application with OV adsorption isotherm of different vapor pressures because it provides a simple and accurate method to predict pore volume, a specific relative structural constant, and adsorption capacity for organic vapors. These parameters in turn, can be used to predict service life and provide unique information about carbon structure. Further study of the effect of water on the adsorption and characterization of OV was beyond the scope of this study but does merit further investigation.

Acknowledgements

Authors acknowledge grant from IRSST (Institut de recherche Robert-Sauvé en santé et en sécurité du travail) project grant (0099-5080). F.J acknowledges financial support from IRSST, FRSQ (Fonds de recherche du Québec-Santé), and ÉSPUM (École de santé publique de l'Université de Montréal).

4.7 References

[1] Fletcher AJ, Kennedy MJ, Zhao XB, Bell JB, Thomas KM. Adsorption of Organic Vapour Pollutants on Activated Carbon. In: Mota JP, Lyubchik S, eds. Recent Advances in Adsorption Processes for Environmental Protection and Security: Springer Netherlands 2008, p. 29-54.

[2] Nguyen C, Do DD. A New Method for the Characterization Of Porous Materials. Langmuir. 1999;15(10):3608-15.

[3] Abiko H, Furuse M, Takano T. Reduction of Adsorption Capacity of Coconut Shell Activated Carbon for Organic Vapors Due to Moisture Contents. Industrial Health. 2010;48(4):427-37.

[4] Branton P, Bradley R. Effects of active carbon pore size distributions on adsorption of toxic organic compounds. Adsorption. 2011;17(2):293-301.

[5] Haghighat F, Lee C-S, Pant B, Bolourani G, Lakdawala N, Bastani A. Evaluation of various activated carbons for air cleaning – Towards design of immune and sustainable buildings. Atmospheric Environment. 2008;42(35):8176-84.

[6] Wood GO. Estimating service lives of air-purifying respirator cartridges for reactive gas removal. Journal of Occupational and Environmental Hygiene. 2005;2(8):414-23.

[7] Bradley R. Recent Developments in the Physical Adsorption of Toxic Organic Vapours by Activated Carbons. Adsorption Science & Technology. 2011;29(1):1-28.

[8] Fletcher AJ, Kennedy MJ, Zhao XB, Bell JB, Thomas KM. Adsorption of Organic Vapour Pollutants on Activated Carbon Recent Advances in Adsorption Processes for Environmental Protection and Security. In: Mota JP, Lyubchik S, eds.: Springer Netherlands 2008, p. 29-54.

[9] Helmich M, Luckas M, Pasel C, Bathen D. Characterization of microporous activated carbons using molecular probe method. Carbon. 2014;74:22-31.

[10] Wood GO, Stampfer JF. Adsorption rate coefficients for gases and vapors on activated carbons. Carbon. 1993;31(1):195-200.

[11] Rios RVRA, Silvestre-Albero J, Sepúlveda-Escribano A, Molina-Sabio M, Rodríguez-Reinoso F. Kinetic Restrictions in the Characterization of Narrow Microporosity in Carbon Materials. The Journal of Physical Chemistry C. 2007;111(10):3803-5.

[12] Rodríguez-Reinoso F, Molina-Sabio M. Textural and chemical characterization of microporous carbons. Advances in Colloid and Interface Science. 1998;76–77(0):271-94.

[13] Nguyen TX, Bhatia SK. Determination of Pore Accessibility in Disordered Nanoporous Materials. The Journal of Physical Chemistry C. 2007;111(5):2212-22.

[14] Nguyen TX, Bhatia SK. Kinetic Restriction of Simple Gases in Porous Carbons: Transition-State Theory Study. Langmuir. 2008;24(1):146-54.

[15] Silvestre-Albero J, Silvestre-Albero A, Rodríguez-Reinoso F, Thommes M. Physical characterization of activated carbons with narrow microporosity by nitrogen (77.4 K), carbon dioxide (273 K) and argon (87.3 K) adsorption in combination with immersion calorimetry. Carbon. 2012;50(9):3128-33.

[16] Gauden PA, Terzyk AP, Rychlicki G, Kowalczyk P, Ćwiertnia MS, Garbacz JK. Estimating the pore size distribution of activated carbons from adsorption data of different adsorbates by various methods. Journal of Colloid and Interface Science. 2004;273(1):39-63.

[17] Bradley RH, Rand B. Activated carbon adsorbents for organic vapours. Fuel. 1993;72(3):389-93.

[18] Urano K, Omori S, Yamamoto E. Prediction method for adsorption capacities of commercial activated carbons in removal of organic vapors. Environmental Science & Technology. 1982;16(1):10-4.

[19] Noll KE, Wang D, Shen t. Comparison of three methods to predict adsorption isotherms for organic vapors from similar polarity and nonsimilar polarity reference vapors. Carbon. 1989;27(2):239-45.

[20] Prakash J, Nirmalakhandan N, Speece RE. Prediction of Activated Carbon Adsorption Isotherms for Organic Vapors. Environmental Science & Technology. 1994;28(8):1403-9.

[21] Sing KSW, Williams RT. The Use of Molecular Probes for the Characterization of Nanoporous Adsorbents. Particle & Particle Systems Characterization. 2004;21(2):71-9.

[22] Reucroft PJ, Simpson WH, Jonas LA. Sorption properties of activated carbon. The Journal of Physical Chemistry. 1971;75(23):3526-31.

[23] Lu X, Jaroniec M, Madey R. Use of adsorption isotherms of light normal alkanes for characterizing microporous activated carbons. Langmuir. 1991;7(1):173-7.

[24] Wu J. Modeling adsorption of organic compounds on activated carbon: A multivariate approach. 2004.

[25] Dubinin M. The Potential Theory of Adsorption of Gases and Vapors for Adsorbents with Energetically Nonuniform Surfaces. Chemical Reviews 1960;60(2):235-41.

[26] Wood GO. Activated Carbon Adsorption Capacities for Vapors. Carbon. 1992;30(4):593-9.

[27] Wood GO. D-R Plots and Typical Parameters for Several OV and Multigas Cartridges and Canisters. Journal of the International Society for Respiratory Protection. 2009;26:71-81.

[28] Cossement DB, Iheb; Dubois, Patrick-Daniel; Bose, Tapan K.; Lara, Jaime; Drolet, Daniel; Lemay, François; Fortin, Zélie. Mise au point et validation d'un outil de calcul du temps de service des cartouches filtrantes pour vapeurs organiques. Montréal: IRSST; 2008.

[29] Keener T, Zhou D. Prediction of activated carbon adsorption performance under high relative humidity conditions. Environmental Progress. 1990;9(1):40-6.

[30] Wood GO, Moyer ES. A review and comparison of adsorption isotherm equations used to correlate and predict organiv vapor cartridge capacities American Industrial Hygiene Association Journal. 1991;52(6):235-42.

[31] Cossement D, Bellasfar, I., Dubois, P.-D., Bosse, T.K., Lara, J., Drolet, D., Lemay, F. et Fortain, Z. Mise au point et validation d'un outil de calcul du temps de service des cartouches chimiques. Montreal: IRSST; 2008.

[32] Chiang Y-C, Chiang P-C, Huang C-P. Effects of pore structure and temperature on VOC adsorption on activated carbon. Carbon. 2001;39(4):523-34.

[33] Donald M, Wan Ying S, Kuo-Ching M, Sum Chi L. Aliphatic and Cyclic Hydrocarbons. Handbook of Physical-Chemical Properties and Environmental Fate for Organic Chemicals, Second Edition. Boca Raton: CRC Press 2006, p. 61-404.

[34] Donald M, Wan Ying S, Kuo-Ching M, Sum Chi L. Halogenated Aliphatic Hydrocarbons. Handbook of Physical-Chemical Properties and Environmental Fate for Organic Chemicals, Second Edition. Boca Raton: CRC Press 2006, p. 921-1256.

[35] Donald M, Wan Ying S, Kuo-Ching M, Sum Chi L. Aldehydes and Ketones. Handbook of Physical-Chemical Properties and Environmental Fate for Organic Chemicals, Second Edition: CRC Press 2006, p. 2583-686.

[36] Silvestre-Albero A, Rico-Francés S, Rodríguez-Reinoso F, Kern AM, Klumpp M, Etzold BJM, et al. High selectivity of TiC-CDC for CO2/N2 separation. Carbon. 2013;59(0):221-8.

[37] Kim D, Cai Z, Sorial GA. Determination of gas phase adsorption isotherms—a simple constant volume method. Chemosphere. 2006;64(8):1362-8.

[38] Baertsch CD, Funke HH, Falconer JL, Noble RD. Permeation of Aromatic Hydrocarbon Vapors through Silicalite−Zeolite Membranes. The Journal of Physical Chemistry. 1996;100(18):7676-9.

[39] Ferreira AF, Mittelmeijer-Hazeleger MC, Granato MA, Martins VFD, Rodrigues AE, Rothenberg G. Sieving di-branched from mono-branched and linear alkanes using ZIF-8: experimental proof and theoretical explanation. Physical Chemistry Chemical Physics. 2013;15(22):8795-804.

[40] Nelson GO, Correia AN, Harder CA. Respirator cartridge efficiency studies: VII. effect of relative humidity and temperature. American Industrial Hygiene Association Journal. 1976;37(5):280-8.

[41] Werner MD, Winters NL, Moyer ES. A review of models developed to predict gaseous phase activated carbon adsorption of organic compounds. Critical Reviews in Environmental Control. 1986;16(4):327-56.

[42] Werner MD. The Effects of Relative Humidity on the Vapor Phase Adsorption of Trichloroethylene by Activated Carbon. American Industrial Hygiene Association Journal. 1985;46(10):585-90.

[43] Lodewyckx P, Vansant EF. Influence of Humidity on Adsorption Capacity from the Wheeler-Jonas Model for Prediction of Breakthrough Times of Water Immiscible Organic Vapors on Activated Carbon Beds. American Industrial Hygiene Association Journal. 1999;60(5):612-7.

[44] Nguyen TX, Bhatia SK. Pore accessibility of N2 and Ar in disordered nanoporous solids: theory and experiment. Adsorption. 2007;13(3-4):307-14.

[45] Lodewyckx P. Adsorption on activated carbon: One underlying mechanism? Recent Advances in Adsorption Processes for Environmental Protection and Security. 2008:19-28.

[46] Jagiello J, Thommes M. Comparison of DFT characterization methods based on N2, Ar, CO2, and H2 adsorption applied to carbons with various pore size distributions. Carbon. 2004;42(7):1227-32.

[47] Thommes M. Physical Adsorption Characterization of Nanoporous Materials. Chemie Ingenieur Technik. 2010;82(7):1059-73.

CHAPTER 5: Systematic Evaluation of the Adsorption of Organic Vapors onto a Miniaturized Cartridge Device Using Breakthrough Tests in Parallel Experiment with a Full Size Respirator Cartridge[†]

5.1 Abstract

Breakthrough experiments are essential for the characterization of the adsorption capacity and micropore volume of activated carbon respiratory cartridges and for the validation and determination of cartridge service life models. In an effort to gain better control over environmental conditions in breakthrough tests and to obtain reliable data, a novel experimental approach using a miniaturized (Mini) cartridge was designed to replicate a small section of a respiratory cartridge. The Mini device and the organic vapor (OV) respiratory cartridge were tested in single and parallel experiments where in the former, one filter was tested one at a time and in the latter both devices were exposed simultaneously to the same conditions. The Mini device gave results comparable to the 10% breakthrough times and adsorption capacities of the OV cartridges. The reproducibility of the packed carbon bed of the Mini provided strong support for using the Mini in breakthrough experiments for the characterization of the activated carbon adsorption capacity and estimation of cartridge service life.

5.2 Introduction

Respirators are commonly used to protect workers against the toxic inhalation of dust, fumes, and organic vapors [1]. Among all the respirator masks, air-purifying respirators are the

[†] The modified version of this chapter was published as : Janvier, F., Tuduri, L., Cossement, D., Drolet, D., & Lara, J. (2016). Systematic evaluation of the adsorption of organic vapors onto a miniaturized cartridge device using breakthrough tests in parallel experiment with a full size respirator cartridge. *Adsorption Science & Technology*, *34*(4-5), 287-306.

most widely used. The National Institute for Occupational Safety and Health (NIOSH) and the Bureau of Labor Statistics reported that air purifying respirators were used in 95% of all the establishments requiring respirators used in the United States following the 2001 survey [2]. Typically, the preferred sorbent material for organic vapor (OV) respirator cartridge is activated carbon due to its high porosity, low cost, and good adsorption capacity for many vapors [3, 4]. Because activated carbon cartridge filters and end of service life indicators (ESLIs) are limited for organic vapors [5], determining cartridge service life is a complex task.

Therefore, mathematical models are recommended to estimate the time at which the cartridge reaches the saturation point or is no longer able to filter out the contaminant [6]. To use such prediction models, knowledge of both the sorbent capacity and breakthrough behavior are essential for the prediction of their performance [7, 8]. This information can be obtained by characterizing the vapor concentration (or relative concentration) versus time profile of the effluent, termed ‘‘breakthrough curve’’ [9, 10]. Even so, breakthrough curve experiments are laborious, time consuming, and the control of the environmental conditions can be challenging. Furthermore, these breakthrough curves depend simultaneously on the physical and chemical characteristics of the sorbent material (activated carbon) [10, 11] and the adsorbate vapor [12-14], presence of other contaminants [15], and the environmental conditions such as temperature, air flow, relative humidity (RH), and vapor contaminant concentration [13, 16-18]. Hence, controlling the environmental conditions to obtain reliable breakthrough curve data is essential to assess the cartridge service life model validity and to estimate its parameters within a range of the expected working conditions [19].

Most cartridge service life predictive models assume that each contaminant breakthrough curve is a symmetric sigmoidal curve. Yet, some studies have shown that for some contaminants, at high breakthrough fraction above 50%, the experimental data deviates from symmetry particular at low concentrations and at high humidity [7, 20]. Thus, obtaining reliable and accurate data from breakthrough experiments in controlled environmental conditions that closely match the working settings is desired.

Early works from Cohen et al. have described in a series of papers the use of a filter device, which they termed “small respirator carbon tubes (RCT)” with the aim to estimate cartridge service life in work place conditions [21-24]. The RCT was filled with the same sorbent

material contained in the respirator cartridge and was connected to a pump for laboratory testing and to a small personal pump for field-testing. The breakthrough time and the bed-residence model method [25] were applied and compared favorably with the cartridge data for CCl_4 at dry and humid conditions and for multiple exposures with n-hexane and pyrimidine. However, only a fraction of the breakthrough profile was measured (up to the 10% breakthrough fraction) rather than the entire breakthrough curve. This limits the applicability of the RCT method by missing important information, which is needed to assess the validity of their device throughout the entire filtration process.

In our previous paper [26], the micropore structure of activated carbons of ten commercially available respirator cartridges were characterized. It was demonstrated that breakthrough experiments, which were used to obtain adsorption isotherms from five organic vapor substances of different vapor pressures at a concentration of 500 ppm and 40% of relative humidity (RH) could be used to obtain the micropore volume of activated carbons. Using the organic vapor approach, the adsorption capacity was successfully predicted.

To improve control over environmental conditions in breakthrough tests and to obtain reliable data, a novel experimental approach utilizing a miniaturized (Mini) cartridge was designed to replicate a small section of a respiratory cartridge. To evaluate whether the breakthrough curves obtained with the Mini were a suitable representation of the full size respirator cartridge, repeatability and reproducibility studies were conducted in single experiments (Mini and OV cartridge separately) and in parallel experiments (Mini and OV cartridge at the same time).

5.3 Material and Methods

5.3.1 Miniaturized (Mini) and OV Cartridges

Figure 5.1 illustrates the Mini device and the vertical fall tube specially designed in house for this study. The Mini is made of stainless steel with a cylindrical collection container with an inside radius of 1.14 cm and a length of 5.00 cm. The packed carbon was kept in place by two wired meshed screens and filters (Texel, TRIBO 60 HJ, St-Elzéar-de-Beauce, QC)

tightly screwed in at each end. These dimensions for a packed bed activated carbon filter ensured a linear flow throughout the Mini device.

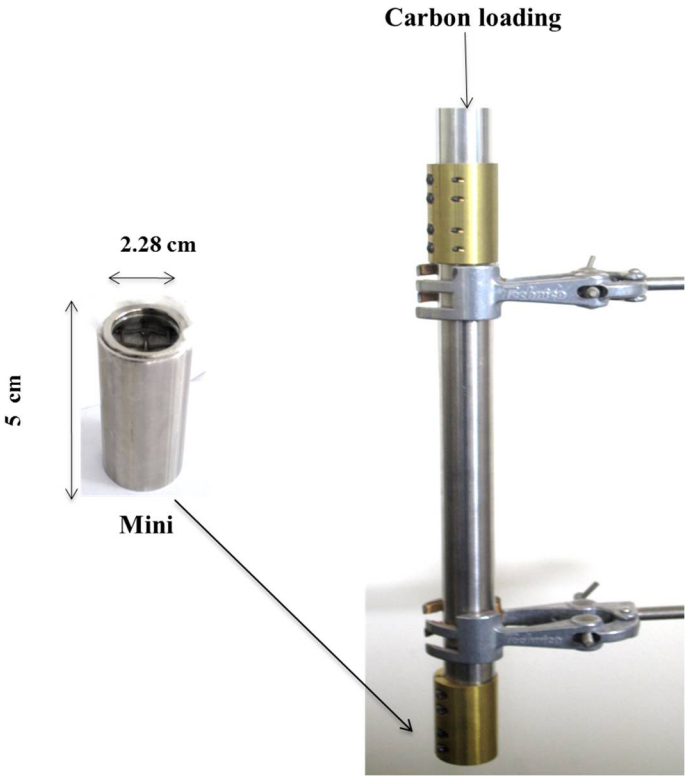

Figure 5.1 Photograph of the miniaturized (Mini) cartridge used in this study and the vertical fall tube.

.

Table 5.1

Structural properties of the activated carbon characteristics of the media and the experimental conditions.

	OV Cartridge	Mini

Amount of carbon (g)	45.76	2.83
Packed bed density (g/cm^3)	0.42	0.42
Water content (%)	2.4	2.4
Carbon bed thickness (cm)	1.65	1.65
Surface area of media (cm^2)	63.180	4.079
Cartridge configuration	Trapeze	Round
Relative humidity (%)	40	40
Targeted concentration (ppm)	500	500
Targeted flow rate (L/min)	24	1.55
OV micropore volume* (cm^3/g)	0.58	0.56
B, structural Constant*	1.77 x10^{-5}	1.82 x10 $^{-5}$

*OV micropore volume and *B* are derived from the Dubinin-Radushkevich equation using breakthrough experiments as described in ref [26].

A fresh OV respirator cartridge and activated carbon filled in the Mini were used for each experiment and were from 3M6001 (3M Company, Saint-Paul, MN). The physical properties of the OV cartridge and the Mini are both presented in **Table 5.1.** The characterization of the micropore volume and the structural constant *B* were performed using a previously described method with organic vapors [26]. The flow rate of 24 L/min through the OV cartridge was chosen as the equivalent breathing rate for moderate work. The breakthrough tests were performed at 40% RH and the adsorption of water vapor at this RH is considered insignificant [16, 27]. A

concentration of 500 ppm was chosen as a reasonable amount to achieve 100% saturation in a controllable time manner for all the tested vapors

5.3.2 Assumptions of the Mini

The approach of the Mini relies on two fundamental assumptions: (1) identical carbon bed density and (2) equivalent linear air through velocity to the OV Cartridge. To fulfill the first assumption, an equivalent amount of carbon obtained from the respiratory cartridge must be added to the Mini device. By considering that for a given area, the Mini should have the same carbon thickness and bed density as the OV cartridge, an equivalent amount (W) in grams of activated carbon was calculated using **Eq. (5.1)** and was transferred to the Mini device using the following equation:

$$W\ of\ Mini = \pi r^2 l \rho_{\boldsymbol{B}} \tag{5.1}$$

$$= \pi\,(1.14\ cm)^2 \cdot 1.65\ cm \cdot 0.42\,\frac{g}{cm^3}$$

$$= 2.83\ g$$

where ρ_B is the carbon bed density and l thickness of the OV cartridge, and r is the radius of the Mini.

The second requirement is fulfilled by the estimation of an equivalent flow rate (Q) to the 24 L/min, which passes through the OV cartridge bed area. By assuming that for a given area of the Mini that the throughout linear air velocity for a plug flow through the bed is identical to that of the OV cartridge, the corresponding flow rate (Q) of the Mini was calculated with the following equation:

$$Q\ of\ Mini = \frac{Area\ of\ OV\ cartridge}{Area\ of\ Mini} \times\ Q\ of\ OV\ cartdrige \tag{5.2}$$

$$= \frac{63.18\ (cm^2)}{4.09\ (cm^2)} \times 24\frac{L}{min} = 1.55\ L/min.$$

5.3.3 Design of Breakthrough Experiments

Complete breakthrough experiments of the Mini and the OV cartridge were conducted in single (Mini **or** OV Cartridge) and parallel experiments (Mini **and** OV Cartridge) to compare breakthrough data useful for the prediction of cartridge service life. A single experiment is defined as a breakthrough measurement performed with only one filter device, whereas in the parallel experiment, both devices (Mini and OV cartridges) are exposed simultaneously to the same contaminated airstream. The advantages of using the latter method are: sustainability, timesaving, and that it removes the experimental variables because both carbon beds are exposed at once to the same conditions. Thus, for this study, the parallel experiments are the preferred testing method. However, single initial experiments were performed to verify the repeatability and reproducibility of the test system.

This work consisted of four investigations: The first two, involved corroborating the assumptions in the design of the Mini in terms of the equivalent weight and flow rate. The third investigation was reproducibility and repeatability study with selected solvents in single experiments, and the last one consolidated all the results in parallel experiments. The four experiments are listed below:

(1) Reproducibility of the carbon bed thickness of the Mini;
(2) Flow rate experiments from 1.30 L/min to 1.55 L/min for the Mini with Dichloromethane (DCM);
(3) Single experiments of the Mini and OV cartridge tested in triplicate with n-hexane and DCM;
(4) Parallel experiments (Mini and OV cartridge simultaneously) conducted with DCM, n-hexane, methyl isobutyl ketone (MIBK), toluene, and m-xylene.

5.3.4 Experimental Set-Up

A schematic diagram of the atmosphere generation system used for exposing the Mini and the OV cartridge is illustrated in **Figure 5.2.** A MNR (Miller-Nelson, HCS-501, Miller-Nelson Research, Inc., Dublin, Calif.) flow controller was used in this set-up. The vapor gas introduced

in the mixing chamber was generated with a syringe pump (KDS Legato 210, Holliston, Ma). All solvents were HPLC grade from Sigma-Aldrich: dichloromethane (DCM), methyl isobutyl ketone (MIBK), n-hexane, m-xylene, and toluene. The mixing chamber contained a fan, which allowed a uniform distribution of the airstream into the exposing chamber. The feeding rate of the exposure chamber was set to 30 L/min to generate a targeted concentration of ~ 500 ppm with an overall ± 3% coefficient of variation for the organic vapor at 21 ± 1ºC and 40 ± 1% RH. The calibration of the generated vapor was performed by using calibration curves obtained with five concentrations points for each tested vapor. The temperature and humidity were controlled and monitored by means of a direct reading of a hygrometer. The OV cartridge and the Mini were either run in single or parallel experiments and were connected to separate vacuum pump lines, operating at 24 L/min for the cartridge and at the equivalent flow rate of 1.55 L/min for the Mini and were measured with TSI Mass Flow meter (4040, Shoreview, MN). The airstream was monitored by flow meters throughout the experiments. The inlet and the outlet vapor concentrations of the Mini and the OV cartridge were measured at 30-second intervals with a gas chromatograph (HP, 5890 Series II, Alto Palo, CA, USA) equipped with a flame ionization detector (FID) and a selection valve (Model A60, VICI, Houston, TX, USA). A deactivated silica column (40 cm x 0.32 mm I.D.) was attached to the injection port with a loop of 250 µL. The carrier (helium) flow rate was 4.6 mL/min, the detector makeup gas (nitrogen) flow rate was 30 mL/min, the hydrogen and airflow rates were 30 and 400 mL/min, respectively. The oven temperature was set at 200 °C and the FID temperature was at 250 °C.

The experimental activated carbon adsorption capacities (We_{exp}) were measured gravimetrically after the downstream concentration (C_x) had reached ~100% of the upstream concentration (C_o). Prior to experimentation, empty OV cartridges and Mini were weighed and removed from cartridge total weight to determine the initial activated carbon weight. A blank experiment (no vapor) of the OV cartridge was run for 8 hours at 40% RH, at 24 L/min, and showed that only 0.7 % of water was adsorbed, which was judged negligible.

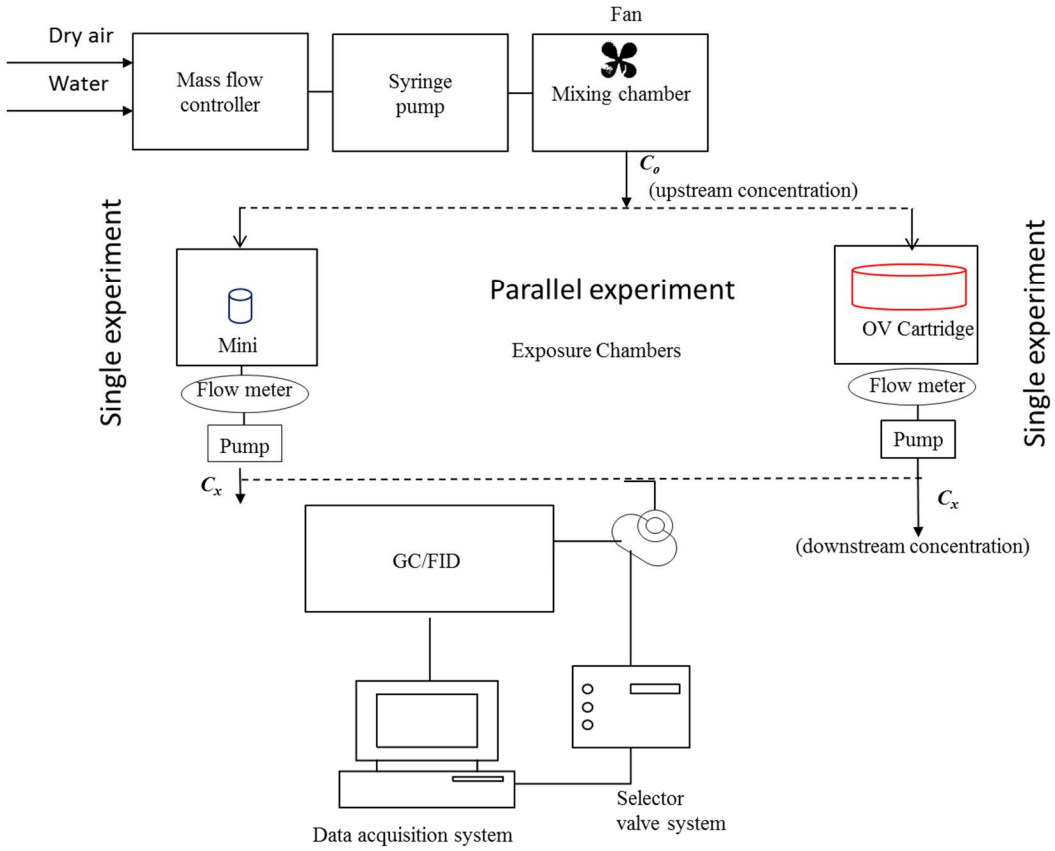

Figure 5.2 Schematic diagram of atmosphere generation system for the single and parallel experimental set-up of Mini and OV cartridge.

The calculated adsorption capacity (We_{calc}) was approximated by using the midpoint of the breakthrough time at 50% saturation ($t_{b50\%}$) with [8]:

$$We = \frac{Q \cdot t_{b50\%} \cdot C_o}{W} \tag{5.3}$$

Commonly, the time at 10% saturation ($t_{b10\%}$) is used to define the cartridge service life and it was also obtained from the breakthrough curve measurements of the Mini and OV cartridge. The carbon bed length, which corresponds to the thickness of the respiratory cartridge, was measured by using a caliper. Both values ($t_{b10\%}$ and We) were used to compare Mini versus OV cartridge filtering capacity.

5.3.5 Predictive Model

Analysis of breakthrough curves of the OV cartridge and the Mini were performed using a simple semi-empirical model, the Wheeler-Jonas equation [28], which relates the breakthrough time t_b in minutes with:

$$t_b = \left(\frac{We \cdot W}{C_o Q}\right) - \left(\frac{We \rho_B}{C_o k_v}\right)\left[ln\left(\frac{C_o - C_x}{C_x}\right)\right] \quad (5.4)$$

where C_x (g/cm^3) is the downstream concentration and C_o (g/cm^3) is the upstream concentration, Q (cm^3/min) is the flow rate, We is the adsorption capacity (g/g of carbon), W (g) is the weight of the adsorbent, and k_v is the adsorption rate constant (min^{-1}). The Wheeler-Jonas and the Wood approach have been used in the prediction of cartridge service life [8, 29, 30]. For simplicity purposes, **Eq. (5.4)** may be rewritten as:

$$t_b = A - Bln\left(\frac{C_o - C_x}{C_x}\right) \quad (5.5)$$

where $A = \frac{We \cdot W}{C_o Q}$ and $B = \frac{We \rho_B}{C_o k_v}$.

A plot of t_b versus $ln\left(\frac{C_o - C_x}{C_x}\right)$ results in a straight line with the intercept of A and slope of B. Once A and B have been found, k_v can be calculated with [31]:

$$k_v = \frac{AQ}{BV} \quad (5.6)$$

where V is the volume of the packed bed and $\rho_B = \frac{W}{V}$.

Eqn (5.5) and **eqn (5.6)** were used to simulate breakthrough curves. It is noted that A is equal to $t_{b50\%}$.

5.4 Results and Discussion

5.4.1 Reproducibility of the Carbon Bed Thickness of the Mini

The carbon loading of Mini is shown in **Figure 5.1** and mimics the snow filling method [32], a typical protocol used by manufacturers. This method allows reproducibility of packing density, absence of voids, and even distribution of carbon [32]. The equivalent amount of activated carbon calculated with **Eq. 1.1** was added to the Mini to match the packed bed density of the OV cartridge and resulted in a carbon-bed length thickness of 1.66 ± 0.05 cm for N = 23. This value is in good agreement with the reported thickness of the OV cartridge of 1.65 cm listed in **Table 5.1.** This result indicates that the carbon bed of the Mini is packed uniformly to a maximum density similar to the corresponding cartridge, thus validating the packing method and the carbon bed density assumption. Though, it is well known that a small carbon bed may result in uneven packing due to channel formation [33], this was not observed in the Mini.

5.4.2 Validation of the Flow Rate for the Mini

The equivalent flow rate calculated with **Eq. 5.2** was verified by varying the flow rate of the Mini from 1.30, 1.35, 1.45, and 1.55 L/min in DCM at 500 ppm while the OV cartridge flow rate remained at 24 L/min. As described in the literature [34], the Wheeler-Jonas equation presented in **Eq. 5.4** is essentially flow rate dependent; therefore, a change in the flow rate is expected to affect the breakthrough profile.

Overall, the equivalent flow rate (1.55 L/min) of the Mini provided a good estimation of the breakthrough curve of the respirator cartridge as shown in **Figure 5.3**. In comparison with the smallest flow rates (1.30, 1.35, and 1.45 L/min), the breakthrough profile of the Mini using the equivalent flow rate of 1.55 L/min coincides well with the 10% and 50% breakthrough times of the full-size respirator cartridge. This result indicates that the estimated equivalent flow rate of the Mini is valid within a certain range. The difference in the shape and steepness of the breakthrough curves between the two filtration media is probably due to the difference in the cartridge configuration, which produces distinct adsorption kinetics inside the carbon bed [9].

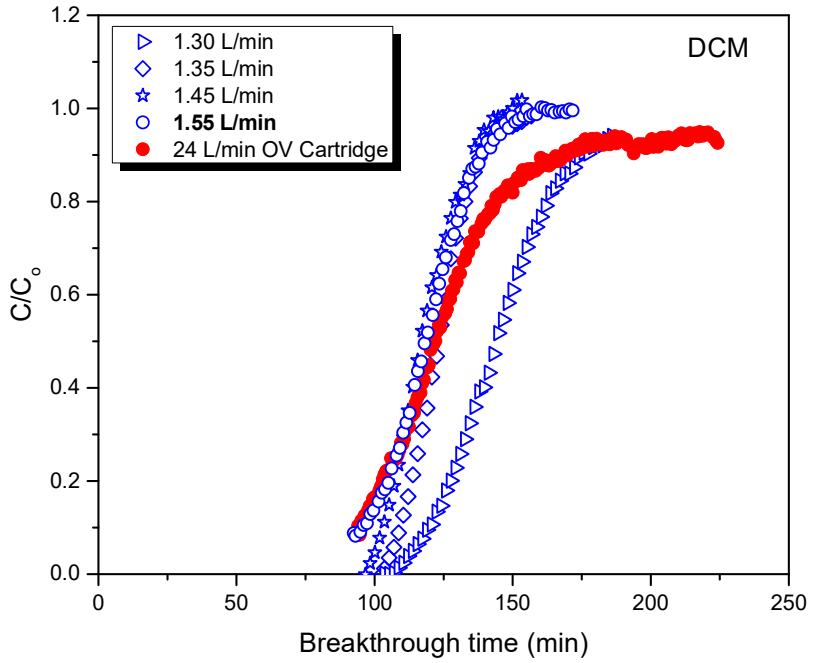

Figure 5.3 Effect of the flow rate on the breakthrough curves of the Mini for DCM. As a reference, the breakthrough curve for the OV cartridge at 24 L/min was included in this figure.

5.4.3 Reproducibility and Repeatability Study

Single triplicate breakthrough experiments were conducted to investigate the reproducibility and repeatability of the Mini using DCM and n-hexane at a concentration of 500 ppm and the results are reported in **Table 5.2**. The individual replicates of the 10% and 50% breakthrough times of the Mini and the OV cartridge differ within less than ± 10 minutes for DCM and n-hexane. Whereas at 100% saturation, the difference among the triplicates is increased but it is still less than 25 min, which is acceptable considering that the concentration generated cannot be replicated exactly in each experiment and has a relative standard deviation of up to 4% in DCM and 1% in n-hexane. **Table 5.2** also shows that $t_{b10\%}$ values of the Mini

are equivalent to the OV cartridge values whereas the $t_{b50\%}$ times are systematically lower than the OV cartridge data.

The resulting breakthrough curves are presented in **Figure 5.4** for the Mini (opened blue symbols) and the OV cartridge (closed red symbols) for DCM and in n-hexane. The superimposition of the triplicate curves of both Mini and OV cartridge using DCM and n-hexane corroborates the stability and reliability of the experimental set-up. The sigmoidal shape of the breakthrough curves in DCM and h-hexane for the Mini confirms the even packing of the carbon bed, which implies that the diffusion of the vapor inside the filter device is uniform. On the other hand, the breakthrough curves of the OV cartridge in **Figure 5.4 (d)** exhibit some spreading in n-hexane and deviate from the sigmoidal shape. The spreading in n-hexane is more pronounced for the respirator cartridge than the Mini, which is probably due to the difference in the cartridge configuration. Moreover, the adsorption rate being more rapid for low boiling points, and volatile compounds than higher boiling-points contaminants may enhance this effect [35].

Table 5. 2

Results of the breakthrough times of the repeatability and reproducibility study of the Mini and OV Cartridge.

Filtering Device	Conc. (ppm)	RSD	$t_{10\%}$ (min)	$tb_{50\%}$ (min)	$tb_{100\%}$ (min)
		Dichloromethane			
Mini	486	0.04	94	118	160
	492	0.04	85	104	142
	493	0.04	88	103	132
OV Cartridge	471	0.04	93	126	221
	482	0.02	94	122	214
	502	0.04	97	128	208
		n-Hexane			
Mini	481	0.01	243	258	317
	500	0.01	244	262	303
	514	0.01	234	255	304
OV Cartridge	485	0.01	248	297	374
	509	0.01	246	295	400
	518	0.01	258	290	386

$tb_{10\%}$ is the 10% breakthrough time

$tb_{50\%}$ is the 50% breakthrough time

$tb_{100\%}$ is the 100% breakthrough time
RSD is the relative standard deviation of the concentration
conc. is the concentration

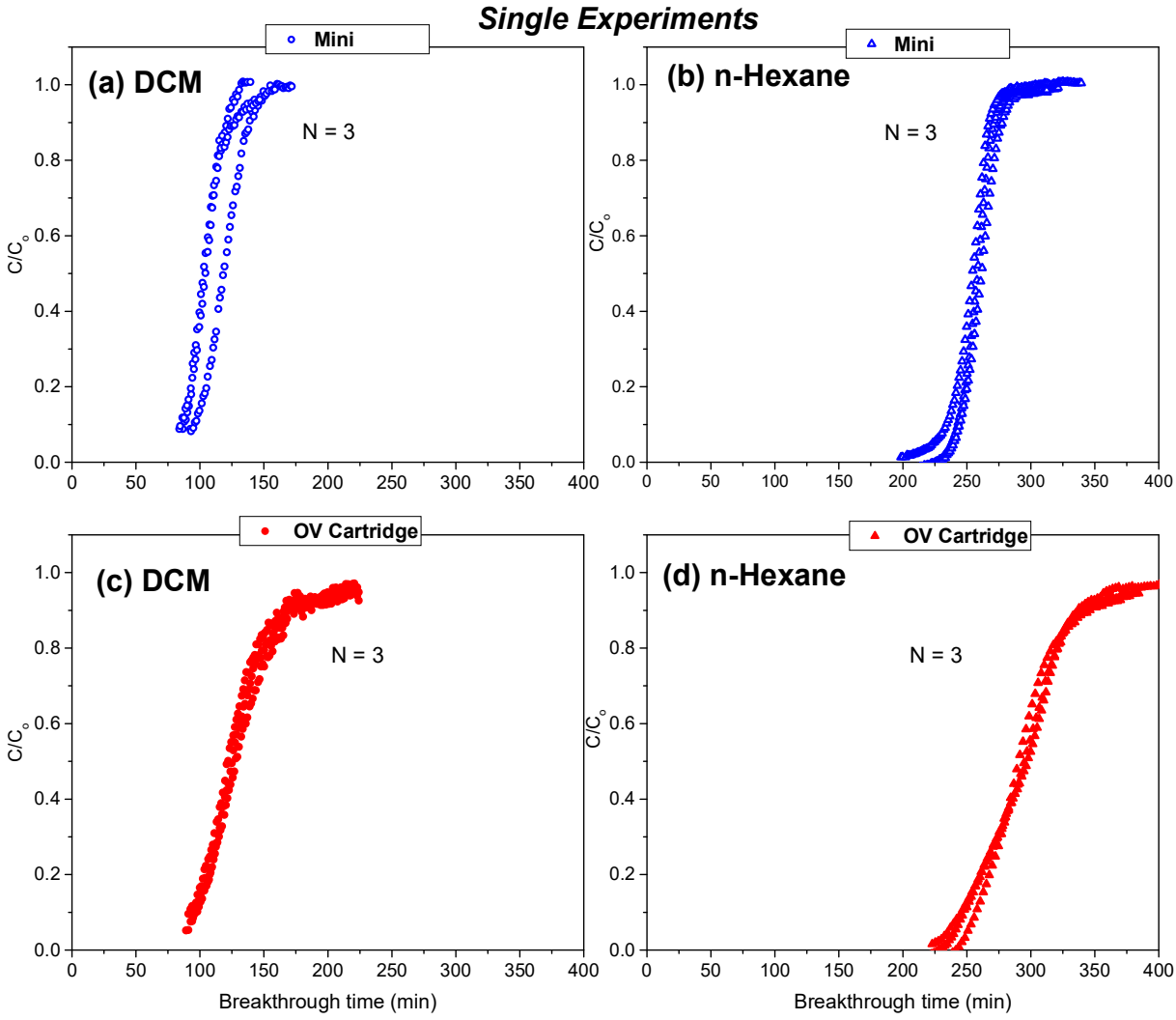

Figure 5.4 Repeatability and reproducibility of the single experiments for Mini and OV cartridges in 500 ppm DCM and n-Hexane at 40% RH and at flow rates of 24 L/min for the cartridge and 1.55 L/min for the Mini.

5.4.4 Breakthrough Curves in Parallel Experiments

Once the reliability of the test system was confirmed, parallel experiments with both the Mini and the OV cartridge were tested. The breakthrough curves of the Mini and OV cartridge

obtained with single and parallel experiments using DCM and n-hexane are compared in **Figure 5.5**. The superposition between the breakthrough curves of the single and parallel experiments of the Mini and the OV cartridge shows that there are no differences between the two experimental approaches. This is an important factor because it ensures that the Mini is exposed to identical conditions as the OV cartridge, therefore allowing an accurate comparison between the Mini and the OV cartridge in real-time.

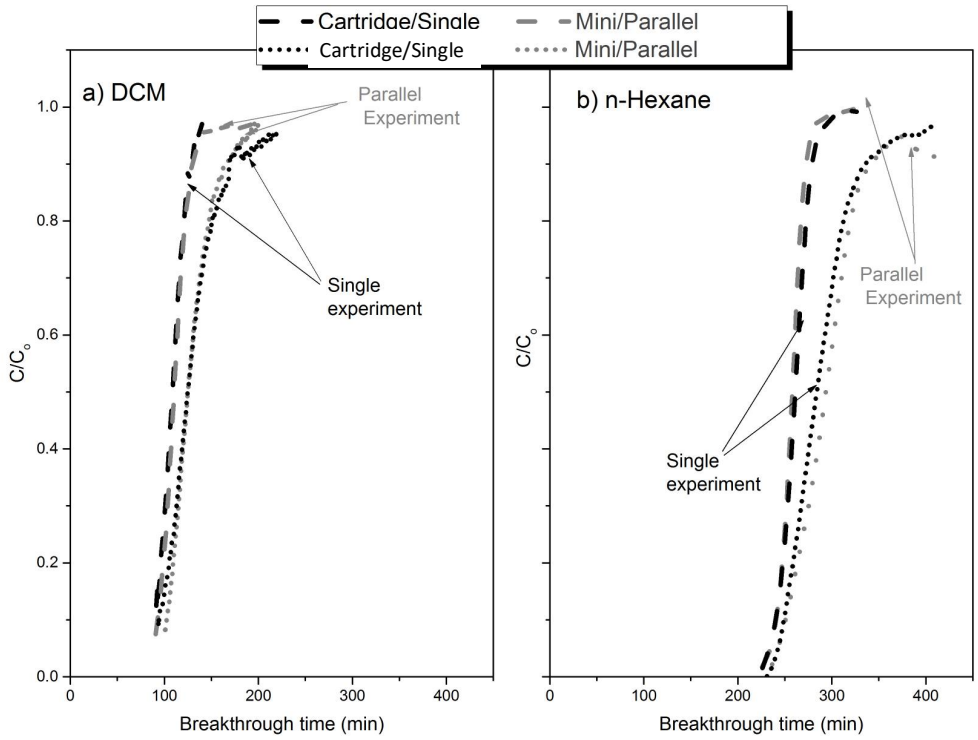

Figure 5.5 Single (black) versus parallel (grey) experiments for the average breakthrough curves in DCM and n-Hexane for the Mini (dotted lines) and the respirator cartridges (dashed lines) at 500 ppm and 40% RH.

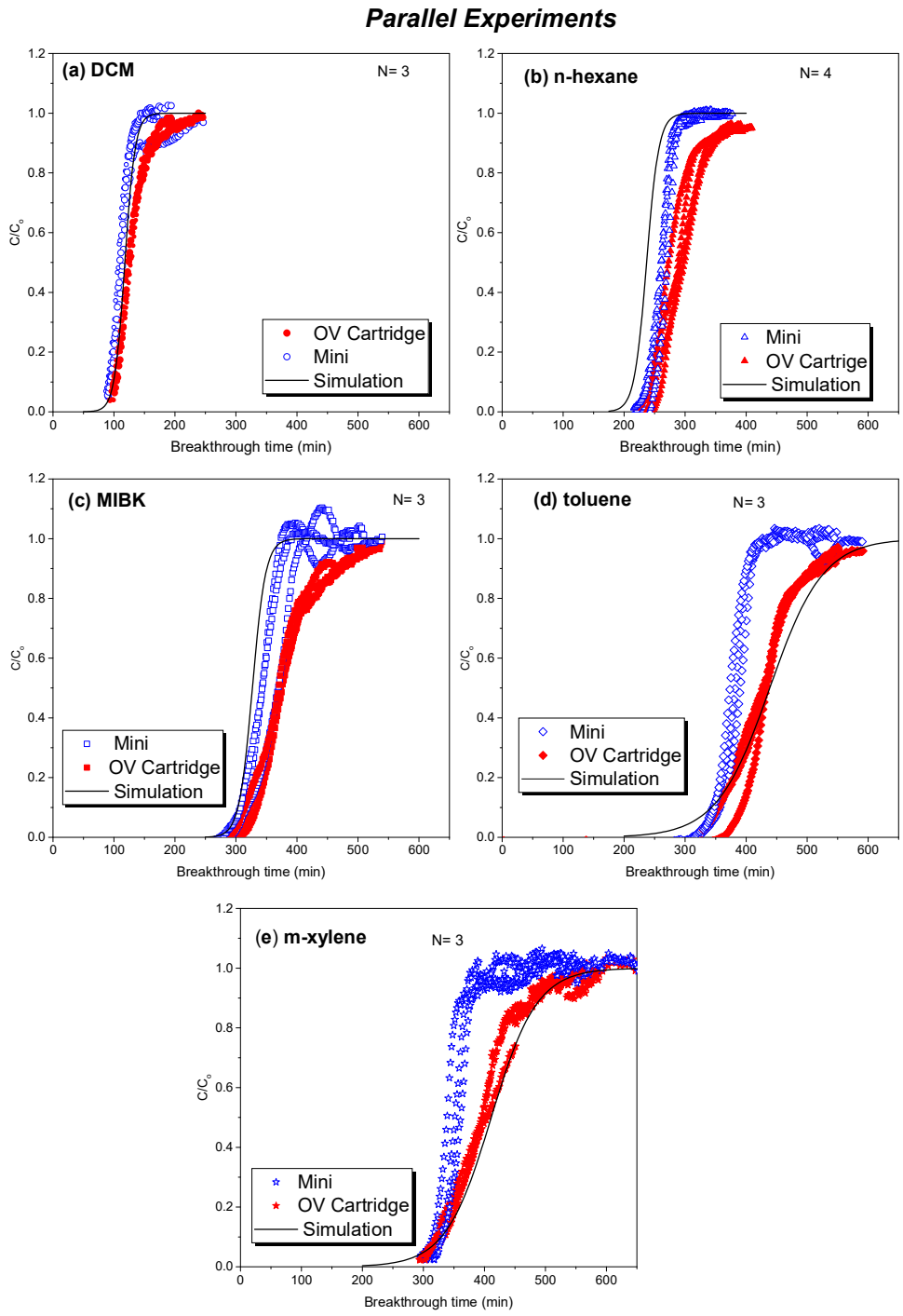

Figure 5.6 Experimental data of parallel experiments with the Mini (blue opened symbols) and the respirator cartridge (red closed symbols) and simulated breakthrough curves for DCM, n-hexane, MIBK, toluene, and m-xylene at ~ 500 ppm and 40% RH.

Figure 5.6 shows all the breakthrough curves of the parallel experiments with the Mini (open blue symbols) and the OV cartridge (closed red symbols) for N = 3. Both Mini and OV cartridge start saturation at the same time and as the saturation fronts advances, the shape of the breakthrough curves of the Mini remains sigmoidal and symmetrical. Overlapping of the curves occurs up to the range of 0.3-0.9 saturation ratio of the upstream concentration. Moreover, as the volatility of the solvent vapor decreased in the order of DCM > n-hexane > toluene > MIBK > m-xylene, the gap between the breakthrough profiles of the Mini and the OV cartridge increased. Similarly to single experiments, skewed breakthrough curves of the OV cartridge in parallel experiments are observed for all the contaminants especially for less volatile contaminants. Conversely, this trend is not observed in the breakthrough profiles of the Mini. The non-symmetry of the breakthrough curve in respirator cartridges has been reported by others [20] and is thought to originate from the heterogeneity of adsorption sites in the micropores of the activated carbon, which results in changes in the adsorption rates and/or mechanisms at the adsorption front of the vapor [20, 36].

The difference in the shape of the breakthrough curve between the Mini and the OV cartridge further challenges the notion that skewed breakthrough curves of respirator cartridge are a result of the kinetics of the adsorber, which is influenced by the volatility of contaminants [7, 20]. Rather, the geometric configuration of the cartridge or the face velocity and the non-linear air through profile throughout the cartridge seem to be the dominant factor affecting skewed breakthrough curves. A study evaluating the adsorption of organic vapors onto activated carbon has shown that surface diffusion or face velocity trumps over pore diffusion [37]. Therefore, as a consequence of the smaller surface of the Mini, the diffusion of the vapor molecule in the pores of the activated carbon is increased and reaches equilibrium faster as shown by the steeper and symmetrical breakthrough curves of the Mini compared to those of the OV cartridge in **Figure 5.6.**

Figure 5.7 illustrates the flow pattern process in the two types of carbon beds; the Mini and OV cartridge. The geometry of the bed diameter of the Mini is cylindrical and exhibits a plug flow for which the face velocity is uniform and is represented by a large arrow. The OV cartridge, which has a trapezoid shape, has an average air-through flow velocity represented with a large arrow in **Figure 5.7**. Although the average flow throughout the cartridges is

considered to be a constant flow across the section of the cartridge (large arrow) like in the Mini, in reality it is not, and the non-linear flow profiles will affect the shape of breakthrough curve. Furthermore, the breakthrough curves of the OV cartridge in **Figure 5.6** show that it becomes increasingly hard to achieve adsorption equilibrium at 100% saturation and consequently it will take a longer time to saturate as evidence by the tailing. Different zones in the carbon bed of the OV cartridge will have different velocities, especially around the wall of the bed. Lodewyck's research team also reported a wall effect in activated carbon by visualization with X-ray microtomography for cylindrical configuration with CH_3I, CCl_4, and water mixtures [38, 39]. A constant wave front was observed for the CCl_4 study and a radial adsorbate concentration profile was observed for different activated carbon bed thickness with the CH_3I study. This phenomenon may be important to consider since most prediction models use linear velocity for vapor gas and neglect radial velocity profiles within the carbon beds. Nonetheless, in terms of characterization of the activated carbon from breakthrough curves, the Mini may prove to be a better choice because it may diminish the influence of the flow pattern.

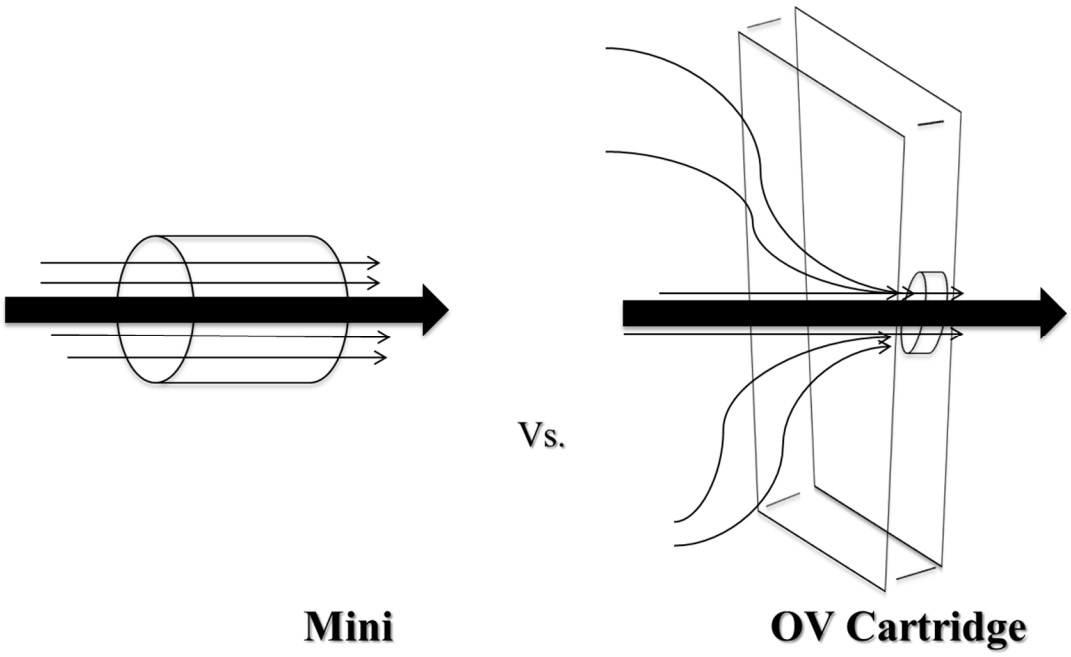

Figure 5.7 Comparison between the flow profiles of the Mini and the OV cartridge. The large arrow is the average flow profile.

5.4.5 Adsorption Capacity

The experimental (We_{exp}) and calculated (We_{calc}) adsorption capacities of the Mini and OV cartridge for the five organic vapors tested are presented in **Figure 5.8**. Overall, the We_{exp} are smaller than the We_{calc} values across the Mini and the OV cartridge. A possible explanation for this discrepancy may be due to the pre-adsorbed water on the activated carbon and in the air stream, which is desorbed by the more strongly adsorbed hydrophobic compound [16, 40] resulting in the appearance of a low We_{exp} compared to the We_{calc}. This is in agreement with another study, which described the breakthrough behaviour difference of low boiling points solvents by stipulating they may have less adsorption affinity, and that they are adsorbed less than contaminants at higher boiling point [35]. Therefore, the calculated adsorption capacity obtained from the midpoint of the breakthrough curve may be more reliable than the gravimetric method because it is not influenced by the presence of water.

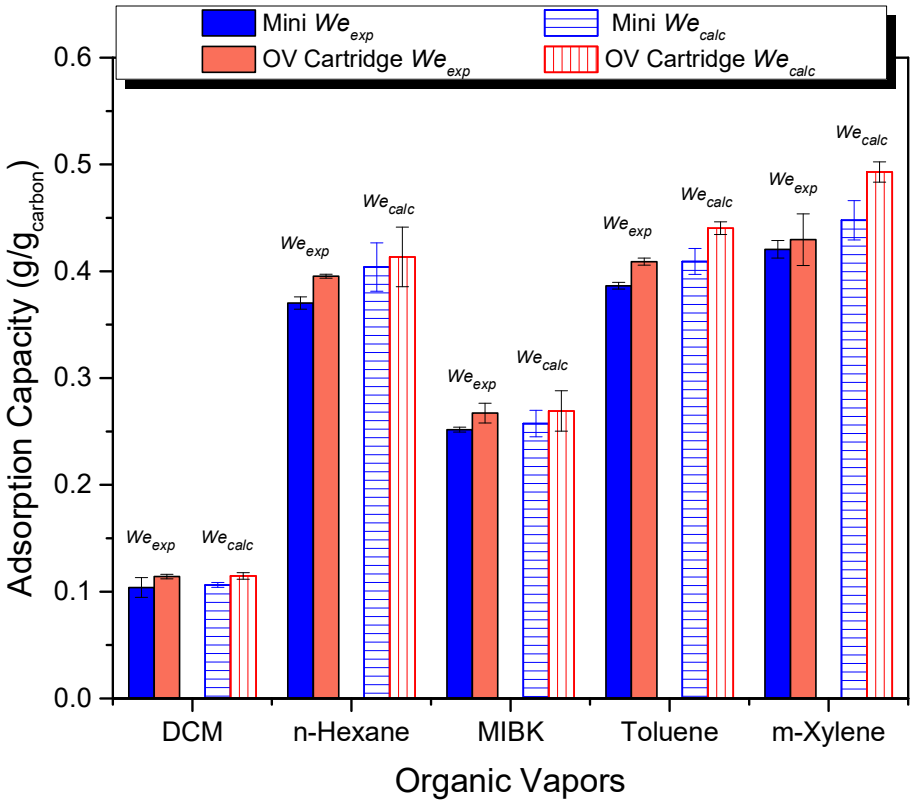

Figure 5.8 Comparison between the Mini and OV cartridge of the experimental and calculated adsorption capacity.

When comparing the Mini vs. OV cartridge, the capacity values of the Mini were slightly lower than that of the OV cartridge but in most cases, the differences were either small or showed no significance difference within experimental errors (see Appendix A).

5.4.6 Breakthrough Time

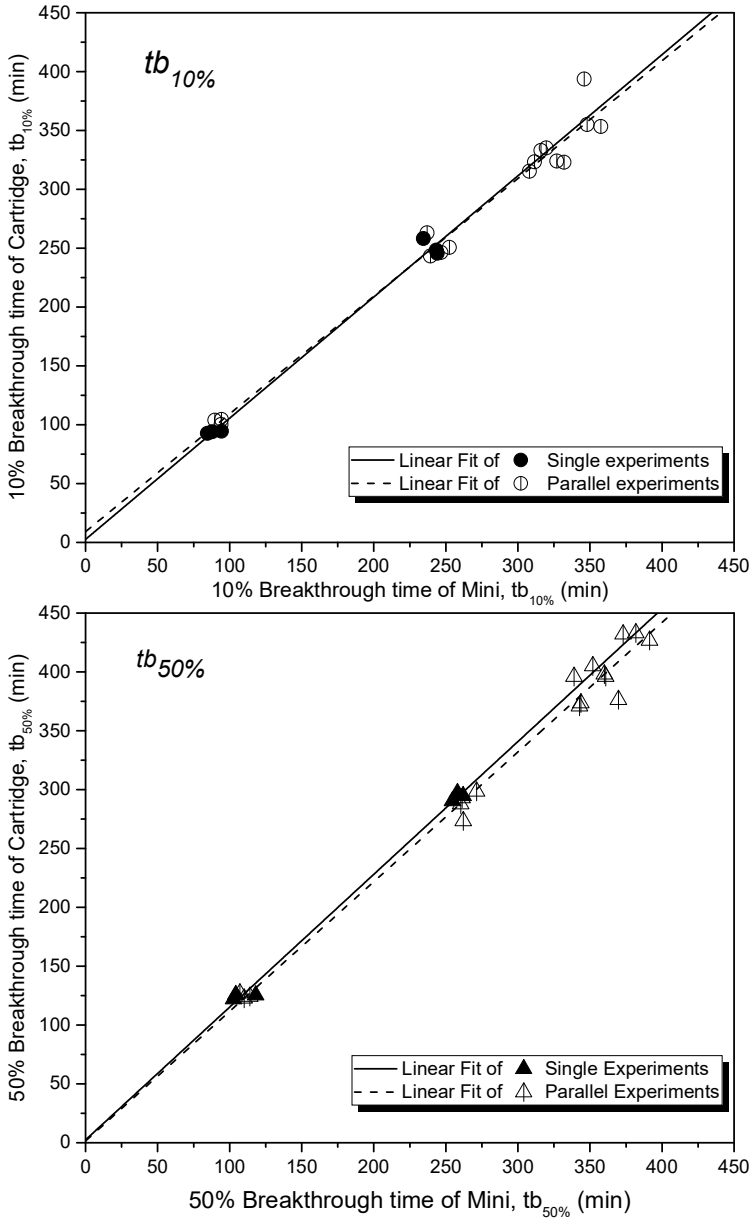

Figure 5.9 Comparison of breakthrough times between the Mini and the OV cartridge at 10% breakthrough time and 50% breakthrough time.

Even with the assumption that the Mini and the OV cartridge exhibit the same linear air through velocity, the difference in the flow rates between the carbons beds did not significantly affect the 10% breakthrough times. **Figure 5.9** compares in (a) 10% breakthrough times and in (b) 50% breakthrough times between the Mini and OV cartridge. Though the 10% breakthrough times of the Mini were slightly smaller than the values of the OV cartridge, they were within experimental errors (less than 10 min difference). Whereas, the 50% breakthrough times of the Mini showed a greater variability than those from the OV cartridge, especially for toluene and m-xylene. This difference in these values is expected because the breakthrough curves of the Mini deviated from the OV cartridge at 0.5 of the saturation fraction (see **Figure 5.6**) and the OV breakthrough curves were asymmetric for the OV cartridge.

The general trend observed both in the single and parallel experiments is that the Mini always reaches complete saturation before the OV cartridge. This implies that the data obtained with the Mini will have a safety factor when estimating the cartridge service life because the $t_{b10\%}$ will always be slightly lower than the ones obtained with the OV cartridge data.

5.4.7 Simulation

Once the performance of the Mini device had been demonstrated, a simulation of the breakthrough time for the OV respiratory cartridge was performed using the mathematical model presented in the section 2.5. **Eq. 5.4** and **Eq. 5.6** have been used to simulate breakthrough curves and are presented as solid lines in **Figure 5.6**. It can be observed that the experimental and theoretical curves calculated according to the Wheeler-Jonas model are very close to each other. Thus, the model utilizing the Mini experimental data provided a good prediction of the organic vapor experimental data at the specified conditions. **Table 5.3** summarizes the parameters used for the simulations. The constant k_v from the OV cartridge was used for the theoretical curves of toluene and m-xylene instead of the Mini in order to get a better fit of the OV cartridge experimental breakthrough due to the asymmetry. The correlation coefficient obtained from the linear fits of parameters A and B were between 0.98-0.99, which revealed that the Wheeler-Jonas equation fits well the experimental data, and is suitable for the prediction of cartridges service life of the OV cartridge.

Table 5. 3

Experimental parameters of the Mini used in the breakthrough curve simulation

Adsorbate	Concentration ($g/cm^3 \cdot 10^{-6}$)	We calc (g/g)	K_v (min^{-1}) Mini	Kv (min^{-1}) Cartridge	A (min)	B (min)	R^2
DCM	1.72	0.106	3055	2321	118	8	0.982
n-Hexane	2.07	0.257	6664	3247	237	10	0.998
MIBK	2.36	0.404	5179	2929	327	11	0.991
Toluene	1.78	0.409	7031	3224	439	44	0.983
m-Xylene	1.95	0.448	6487	2400	411	37	0.992

*Kv is the adsorption rate constants taken from the OV cartridge.

$A = \frac{We \cdot W}{C_o Q}$ and $B = \frac{We\rho_B}{C_o k_v}$ from the Wheeler –Jonas in eqn 5.5.

We calc is the calculated adsorption capacity

5.5 Conclusion

The Mini approach discussed in this work is the first attempt to systemically evaluate the suitability of this novel experimental approach where the Mini represents a section of the full-size respirator cartridge and is tested in parallel breakthrough experiments with the corresponding respirator cartridge. This study demonstrated that assumption of equivalent amount of activated carbon of the Mini on the basis of having the same packing density and bed thickness of the respirator cartridge was justified. Whereas the equivalent flow rate showed some discrepancies in terms of matching breakthrough curves between the Mini and the respirator cartridge due to different flow profiles inside the carbon bed caused by geometric configuration of the cartridge. Nonetheless, the adsorption capacities and 10% breakthrough times of the Mini gave reasonably good estimation of the OV cartridge performance and its applicability may be useful in obtaining data for the model prediction for cartridges service life and characterization of the sorbent capacity.

Further work is in progress to evaluate the Mini with several other respirator cartridges and contaminants to gain a better understanding of the asymmetry of the breakthrough curve observed with OV cartridges and the underlying mechanism of the adsorption of organic vapor onto activated carbon.

Acknowledgements

Authors acknowledge project grant 0099-5080 from IRSST (Institut de recherche Robert-Sauvé en santé et en sécurité du travail) and F.J acknowledges financial support from IRSST, FRSQ (Fonds de recherche du Québec-Santé), and ÉSPUM (École de santé publique de l'Université de Montréal).

5.6 References

1. National Center for Health Statistics. 2010 National Health Interview Survey (NHIS) public use data release. NHIS survey description., Hyattsville, Maryland, 2011.
2. Doney, B.C., Groce, D.W., Campbell, D.L., Greskevitch, M.F., Hoffman, W.A., Middendorf, P.J., Syamlal, G., Bang, K.M., A Survey of Private Sector Respirator Use in the United States: An Overview of Findings. J. Occup. Environ. Hyg. 2005, 2(5), 267-276.
3. Bradley, R., Recent Developments in the Physical Adsorption of Toxic Organic Vapours by Activated Carbons. Adsorpt. Sci. Technol. 2011, 29(1), 1-28.
4. Rodriguez-Reinoso, F., Activated Carbon and Adsorption. In Buschow, K.H.J., Cahn, R.W., Flemings, M.C., Ilschner, B., Kramer, E.J., Mahajan, S., eds.Encyclopedia of Materials - Science and Technology, Volumes 1-11, Elsevier: 2001; Vol. 1-11, pp 22-35.
5. Favas, G., End of Service Life Indicator (ESLI) for Respirator Cartridges. Part 1: Literature Review. In Defence, D.o., ed. Defence Science and Technology Organisaton Victoria (Australia) Human Protection and Performance Div Australian Goverment, 2005; Vol. DSTO-TN-0657, p 49.
6. Occupational Safety and Health Administration (OSHA), D.o.L., Respiratory Protection. In Occupational Safety and Health Administration (OSHA), D.o.L., ed. Occupational Safety and Health Standards, DEPARTMENT OF LABOR: 1998; Vol. 1910.134.
7. Wood, G.O., Organic Vapor Respirator Cartridge Breakthrough Curve Analysis. J. Int. Soc. Respir. Protect. 1993, 10(4), 400-407.
8. Wood, G.O., Estimating service lives of organic vapor cartridges. Am. Ind. Hyg. Assoc. J. 1994, 55(1), 11-15.

9. Wood, G.O., A review of the effects of covapors on adsorption rate coefficients of organic vapors adsorbed onto activated carbon from flowing gases. Carbon 2002, 40(5), 685-694.

10. Wood, G.O., Stampfer, J.F., Adsorption rate coefficients for gases and vapors on activated carbons. Carbon 1993, 31(1), 195-200.

11. Wood, G.O., Activated Carbon Adsorption Capacities for Vapors. Carbon 1992, 30(4), 593-599.

12. Moyer, E.S., Review of Influential Factors Affecting the Performance of Organic Vapor Air-Purifying Respirator Cartridges. Am. Ind. Hyg. Assoc. J. 1983, 44(1), 46-51.

13. Nelson, G.O., Correia, A.N., Respirator cartridge efficiency studies: VIII. summary and conclusions. Am. Ind. Hyg. Assoc. J. 1976, 37(9), 514-525.

14. Freedman, R.W., Ferber, B.I., Hartstein, A.M., Service Lives of Respirator Cartridges versus Several Classes of Organic Vapors. Am. Ind. Hyg. Assoc. J. 1973, 34(2), 55-60.

15. Lara, J., Yoon, Y.H., Nelson, J.H., The Service Life of Respirator Cartridges with Binary Mixtures of Organic Vapors. J. Int. Soc. Respir. Protect. 1995, 13, 7-26.

16. Nelson, G.O., Correia, A.N., Harder, C.A., Respirator cartridge efficiency studies: VII. effect of relative humidity and temperature. Am. Ind. Hyg. Assoc. J. 1976, 37(5), 280-288.

17. Ruch, W.E., Nelson, G.O., Lindeken, C.L., Johnsen, R.G., Hodgkins, D.J., Respirator Cartridge Efficiency Studies. Am. Ind. Hyg. Assoc. J. 1972, 33(2), 105-109.

18. Nelson, G.O., Harder, C.A., Respirator cartridge efficiency studies IV. Effects of steady-state and pulsating flow. American Industrial Hygiene Association Journal 1972, 33(12), 797-805.

19. DeCamp, D.S., Costantino, J., Black, J.E., Estimating Organic Vapor Cartridge S ervice Life. DTIC Document: 2004.

20. Wood, G.O., Quantification and application of skew of breakthrough curves for gases and vapors eluting from activated carbon beds. Carbon 2002, 40(11), 1883-1890.

21. Cohen, H.J., Zellers, E.T., Garrison, R.P., Development of a field method for evaluating the service lives of organic vapor cartridges: Results of laboratory testing using carbon tetrachloride. Part II: Humidity effects. Am. Ind. Hyg. Assoc. J. 1990, 51(11), 575-580.

22. Cohen, H.J., Levine, S.P., Garrison, R.P., Development of a field method for determining the service lives of respirator cartridges—part iv: results of field validation trials. American Industrial Hygiene Association Journal 1991, 52(7), 263-270.

23. Cohen, H.J., Garrison, R.P., Development of a Field Method for Evaluating the Service Life of Organic Vapor Cartridges: Results of Laboratory Testing Using Carbon Tetrachloride. Am. Ind. Hyg. Assoc. J. 1989, 50(9), 486-495.

24. Cohen, H.J., Briggs, D.E., Garrison, R.P., Development of a field method for evaluating the service lives of organic vapor cartridges—Part III: Results of laboratory testing using binary organic vapor mixtures. Am. Ind. Hyg. Assoc. J. 1991, 52(1), 34-43.

25. Ackley, M.W., Residence time model for respirator sorbent beds. Am. Ind. Hyg. Assoc. J. 1985, 46(11), 679-689.

26. Janvier, F., Tuduri, L., Cossement, D., Drolet, D., Lara, J., Micropore characterization of activated carbons of respirator cartridges with argon, carbon dioxide, and organic vapors of different vapor pressures. Carbon 2015, 94, 781-791.

27. Werner, M.D., Winters, N.L., Moyer, E.S., A review of models developed to predict gaseous phase activated carbon adsorption of organic compounds. Critical Reviews in Environmental Control 1986, 16(4), 327-356.

28. Jonas, L.A., Boardway, J.C., Meseke, E.L., Prediction of adsorption behavior of activated carbons. J. Colloid Interface Sci. 1975, 50(3), 538-544.

29. Wood, G.O., Moyer, E.S., A Review of the Wheeler Equation and Comparison of Its Applications to Organic Vapor Respirator Cartridge Breakthrough Data. Am. Ind. Hyg. Assoc. J. 1989, 50(8), 400 - 407.

30. Lodewyckx, P., Wood, G.O., Ryu, S.K., The Wheeler–Jonas equation: a versatile tool for the prediction of carbon bed breakthrough times. Carbon 2004, 42(7), 1351-1355.

31. Zhou, C., Jin, Y., Xu, H., Feng, S., Zhou, G., Liang, J., Xu, J., Use of Wheeler–Jonas equation to explain xenon dynamic adsorption breakthrough curve on granular activated carbon. J. Radioanal. Nucl. Chem. 2010, 288(1), 251-256.

32. Jones, J., Smith, M., CBDE Protocol for snowstorm filling of carbon filters bed. CBDE Technical note No.1242, CDE: 1992; p 5.

33. Schwartz, C.E., Smith, J.M., Flow Distribution in Packed Beds. Ind. Eng. Chem. 1953, 45(6), 1209-1218.

34. Wood, G.O., Moyer, E.S., A review and comparison of adsorption isotherm equations used to correlate and predict organiv vapor cartridge capacities Am. Ind. Hyg. Assoc. J. 1991, 52(6), 235-242.

35. Stampfer, J., Respirator canister evaluation for nine selected organic vapors. Am. Ind. Hyg. Assoc. J. 1982, 43(5), 319-328.

36. Wood, G.O., Organic vapor respirator cartridge breakthrough curve analysis. J. Int. Soc. Resp. Prot 1993, 10(4), 5-17.

37. Shiue, A., Den, W., Kang, Y.-H., Hu, S.-C., Jou, G.-t., Lin, C.H., Hu, V., Lin, S.I., Validation and application of adsorption breakthrough models for the chemical filters used in the make-up air unit (MAU) of a cleanroom. Build. environ. 2011, 46(2), 468-477.

38. Lodewyckx, P., Blacher, S., Léonard, A., Use of x-ray microtomography to visualise dynamic adsorption of organic vapour and water vapour on activated carbon. Adsorption 2006, 12(1), 19-26.

39. Léonard, A., Blacher, S., Crine, M., Lodewyckx, P., X-RAY Microtomography: a useful method to study the dynamics of organic and water vapours adsorption on carbon.

40. Lodewyckx, P., Vansant, E.F., Influence of humidity on adsorption capacity from the Wheeler-Jonas model for prediction of breakthrough times of water immiscible organic vapors on activated carbon beds. Am. Ind. Hyg. Assoc. J. 1999, 60(5), 612-617.

Appendix A

Table A. Experimental results of the breakthrough tests of the Mini and OV cartridge.

Parameters						Adsorption capacity		Breakthrough time	
Device	**Type of Exp.**	**Adsorbent**	**Feeding rate (L/min)**	**N**	**Conc. (ppm)**	**We $_{exp}$ (g/g)**	**We $_{calc}$ (g/g)**	**$tb_{10\%}$ (min)**	**$tb_{50\%}$ (min)**
Mini	*Single*	DCM	30	3	490 ± 4	0.097 ± 0.003	0.101 ± 0.007	89 ± 5	108 ± 8
		n-Hexane	30	3	498 ± 16	0.249 ± 0.002	0.249 ± 0.007	241 ± 5	258 ± 4
	Parallel	DCM	30	3	505 ± 11	0.104 ± 0.009	0.106 ± 0.002	93 ± 3	110 ± 3
		n-Hexane	30	4	506 ± 18	0.252 ± 0.002	0.257 ± 0.012	244 ± 6	354 ± 13
		MIBK	30	4	505 ± 17	0.370 ± 0.006	0.404 ± 0.023	313 ± 7	264 ± 5
		Toluene	30	3	517 ± 5	0.386 ± 0.003	0.409 ± 0.012	351 ± 6	382 ± 9
		m-Xylene	30	3	543 ± 11	0.421 ± 0.008	0.448 ± 0.018	325 ± 8	351 ± 11
OV Cartridge	*Single*	DCM	30	3	485 ± 16	0.113 ± 0.003	0.111 ± 0.005	95 ± 2	125 ± 3
		n-Hexane	30	3	504 ± 17	0.269 ± 0.002	0.274 ± 0.007	251 ± 7	294 ± 4
	Parallel	DCM	30	3	505 ± 11	0.114 ± 0.002	0.115 ± 0.003	103 ± 2	125 ± 2
		n-Hexane	30	4	506 ± 18	0.267 ± 0.009	0.269 ± 0.019	251 ± 9	380 ± 12
		MIBK	30	4	505 ± 17	0.395 ± 0.002	0.413 ± 0.028	325 ± 10	288 ± 11
		Toluene	30	3	517 ± 5	0.409 ± 0.003	0.440 ± 0.006	367 ± 23	431 ± 3
		m-Xylene	30	3	543 ± 11	0.430 ± 0.024	0.493 ± 0.009	327 ± 6	399 ± 5

We $_{exp}$ is the experimental adsorption capacity

We $_{calc}$ is the calculated adsorption capacity obtained from the midpoint of the breaktrough curve

N is the number of experiments

$tb_{50\%}$ is the 50%breakthrough time

$tb_{10\%}$ is the 10%breakthrough time

CHAPTER 6: Integrating a Toxicological Approach for Breakthrough Curves of Vapor Mixtures in the Estimation of Respirator Cartridge Service Life‡

6.1 Abstract

The estimation of cartridge service life (CSL) for mixtures of contaminants is a complex task. OSHA-CPL-02-00-158 recommends the use of the additivity principle, which assumes that the entire mixture behaves like a pure system of the most volatile contaminant (i.e., sum up the concentration of the components). Here we present a quantitative risk assessment framework to predict potential human health risk when estimating CSL to avoid vapor gas breakthrough inside the mask, premature change schedules, and unnecessary costs. Simulations using the IAST-Langmuir model combined with the modified Wheeler-Jonas equation allowed the calculation of breakthrough curves for vapor mixtures. Acetone was used as an example of a volatile organic contaminant combined in binary mixture with one of the following: m-xylene, o-xylene, styrene, or toluene. Simulations of exposures to acetone (10-700 ppm) and the other contaminant of lower volatility (500 ppm) through a respiratory cartridge with 50 g of carbon at 25°C and a flow rate of 24 L/min were performed. Outlet concentrations were used to determine the Hazard Index (HI) throughout the exposure. The HI is defined as the sum of concentrations for each mixture component normalized by its Occupational Exposure Limit (OEL) Value (HI > 1 indicates a health risk). Cartridge service life estimations based on the 10% breakthrough times of acetone and the 10% of HI for the mixture were compared. Simulations of breakthrough curves were in agreement with experimental data previously published. At lower acetone concentrations (< 50 ppm), the simulated CSL using 10% HI of the vapor mixture were up to two times greater than the ones calculated following the 10%

‡ This modified version of this chapter was published to The Journal of International Society for Respiratory Protection and was awarded the 2016 Arthur Johnson Young Researcher Award for best paper: Janvier, Florence, Haddad, Sami, and Lara Jaime, The Journal of International Society for Respiratory Protection, Vol 34(1), 10-23.

breakthrough time additive concentration's approach). At higher concentrations of acetone, both approaches gave similar results. The breakthrough time of HI is inversely proportional to the concentration ratio of contaminant 1 (C1), the more volatile, to contaminant 2 (C2), the less volatile contaminant, suggesting that using the HI approach can be useful when $C1/C2 < 2$.

6.2 Introduction

The Respiratory Protection Committee (RPC) of the American Industrial Hygiene Association (AIHA) has identified reliable assessment of respirator performance in the laboratory and workplace environment as a research priority (Ettinger, Janssen, & Metzler, 2009). Because the accuracy of cartridge service life prediction models for organic vapors is influenced by environmental conditions (Nelson & Correia, 1976; Ruch, Nelson, Lindeken, Johnsen & Hodgkins, 1972), several investigations have focused on the effect of moisture (Wood 1985), temperature (Nelson, Correia, & Harder, 1976), flow rate/breathing rate (Coyne, Caretti, Scott, Johnson, & Koh, 2006; Linders, Mallens, van Bokhoven, Kapteijn, & Moulijn, 2003; Nelson & Harder, 1972) and concentration (Nelson & Harder, 1976) on cartridge service life.

In our previous work, we have characterized ten activated carbons from commercially available respirator cartridges by using breakthrough experiments in experimental conditions similar to working environments. We showed that predicted adsorption capacities obtained from the characterization of the micropore volume of activated carbon using organic vapors of different vapor pressure fit well with the experimental data (Janvier, Tuduri, Cossement, Drolet, & Lara, 2015). Additionally, we have applied these aforementioned experimental conditions to the design of a miniaturized cartridge, which was able to mitigate the influence of the effect of flow rate and also allowed a better control on the environmental conditions (temperature, air humidity) (Janvier, Tuduri, Cossement, Drolet, & Lara, 2016).

However, in real working environments, the air is often contaminated with more than one contaminant making the prediction of cartridge service life for vapor mixtures complex. Early works investigated the effects of binary mixtures on respirator cartridge service life and presented qualitative observations (Jonas & Rehrmann, 1972; Nelson & Correia, 1976; Swearengen & Weaver, 1988) but these studies lack thorough understanding of multivapor

adsorption mechanism. In the 1990s Lara, Yoon and collaborators (Lara, Yoon, & Nelson, 1995; Yoon, Nelson, Lara, Kamel, & Fregeau, 1991; Young Hee Yoon, Nelson, & Lara, 1996) developed a mathematical approach for binary mixtures and multivapors. They showed that breakthrough may occur earlier when in mixtures than it would for the single contaminant. Their descriptive model relied on fitting parameters that have to be obtained from experimental data.

Vahdat, Swearengen, and Johnson (1994) developed a simple method for predicting breakthrough curves for binary mixtures based on the Wheeler-Jonas equation and the IAST (Ideal Adsorbed Solution Theory) model combined with the Langmuir equation to obtain adsorption isotherms for each component. This model was successfully applied to binary mixtures of acetone-m-xylene, acetone-styrene, and carbon dioxide-water. Extensive research based on another combination of IAST Dubinin-Radushkevich has been investigated by Wood and Snyder (2007) and resulted in the creation of the program Multivapor ™ available on the National Institute for Occupational Safety and Health (NIOSH) website. Also, Vuong and collaborators (2016) have developed a model based on partial differential equations to predict the breakthrough of binary vapor mixtures.

However, the only existing directive for the estimation of cartridge service life for contaminant mixtures is the OSHA compliance directive *CPL 2-0.120*, *Inspection procedures for the Respiratory Protection Standard*, which recommends the use of the additive concentration effect for multi-component systems, by which the concentration of all the components are summed up and considered to behave as a pure single contaminant for the most volatile contaminant (OSHA, 1998). This approach is simplistic and does not take into account the quantity and toxicity (e.g. cumulative effect) of the contaminants.

Furthermore, the notion that the concentration required to produce a given effect is constant under all concentration-time conditions does not apply because of the displacement phenomenon, where the more volatile contaminant is desorbed by the less volatile contaminant, which has greater affinity with the carbon than the less volatile contaminant.

The framework presented here determines the cartridge service life of binary mixtures by integrating a toxicological approach based on the hazard index (HI) principle to predict potential human health risk to ensure proper use of respirator cartridge while avoiding premature change

schedules and unnecessary costs. To do so, the Vahdat and the Wheeler-Jonas models were employed to predict breakthrough curves of the following binary systems: acetone- m-xylene, acetone- o-xylene, acetone-toluene and acetone-styrene. The IAST (Ideal Adsorbed Solution Theory) - Langmuir equations were used to predict mixture adsorption capacity from the pure single contaminant adsorption data.

6.3 Theory

6.3.1 Langmuir

The Langmuir equation has a simple form and is used extensively in adsorption systems. The Langmuir equation was selected in this study because the calculation is simple and there are abundant adsorption data in the literature for pure components.

Therefore, the adsorption capacity, We for a pure contaminant i using the Langmuir equation is currently used and is expressed in the following form:

$$We = \frac{m_i k_i C}{1 + k_i C} \qquad (6.1)$$

where m and k are Langmuir parameters related to the adsorption capacity and the rate of adsorption for a specific activated carbon-contaminant system, and C is the concentration of the pure contaminant. The Langmuir parameters are commonly determined by fitting experimental data. However, the adsorption isotherm is different for each system, and a set of parameters needs to be determined.

6.3.2 Ideal Adsorbed Solution Theory (IAST)

The Ideal Adsorbed Solution Theory (IAST) is a well-known model to predict the adsorption of gas mixtures by using adsorption data from pure components (Myers & Prausnitz, 1965). The model is based on the thermodynamic equivalence of the spreading pressure of each adsorbent at equilibrium. The spreading pressure, $\prod$, corresponds to the difference in surface tension of a clean surface and an adsorbate-adsorbent interface, considering the same

temperature. The model assumes that the solution is ideal, which means that no interaction between adsorbent–adsorbate is considered and is expressed as:

$$\frac{\Pi A}{RT} = \int_0^{P_i^o} \frac{W_{ei}^0}{P} \qquad (6.2)$$

where A is the area of the adsorbent, W_{ei}^0 is the adsorption capacity of the pure component i, P is the total pressure, T is the temperature, and R is the universal gas constant. Vahdat (1994) successfully applied the Langmuir equation to the IAST model with:

$$\frac{\prod_i A}{RT} = m_i \ln(1 + k_i p_i^0) \qquad (6.3)$$

where p_i^0 is the pure component pressure of component i at the spreading pressure of the mixture. With the postulate that the spreading pressure $\prod$, for each contaminant is equal at the adsorption equilibrium the following equation applies to a binary system:

$$m_1 \ln(1 + k_1 p_1^0) = m_2 \ln(1 + k_2 p_2^0) \qquad (6.4)$$

Additionally, the mole fraction X_1 of component 1 is calculated from:

$$X_1 = \frac{P Y_1}{p_1^0} \qquad (6.5)$$

where Y_1 is the mole fraction of component 1 in the gas phase. A similar equation can be written for component 2.

6.3.3 The Modified Wheeler Jonas Model

The modified Wheeler-Jonas model has been extensively used to describe the adsorption of organic vapors in adsorption beds and is expressed as follows (Jonas & Rehrmann 1973; Wheeler & Robell, 1969; Wood & Moyer, 1989):

$$t_B = \frac{We}{C_o Q}\left[W - \frac{\rho_B Q}{K_v} ln\left(\frac{C_o - C}{C}\right)\right] \quad (6.6)$$

where t_B is the breakthrough time (min), We is the adsorption capacity (g/g), C_o is the inlet concentration (g/cm^3), C (g/cm^3) is the outlet concentration, Q is the flow rate (cm^3/min), W is the amount of activated carbon (g), ρ_B is the packed bed density (g/cm^3), and K_v is the adsorption rate coefficient (min^{-1}), which is dependent on the velocity, u (cm/min).

Wood and Stampfer (1993) proposed an equation based on the fitting of 165 breakthrough curves obtained with 27 hydrocarbons and fluorocarbons with:

$$K_v{}^{-1} = (1 + 0.027u) \times \left[\left(I + S_B \times P_e{}^{-1}\right)\right] \times u^{-1} \quad (6.7)$$

where $S_B = 0.0063 - 0.0055\, ln[(C_0\text{-}C)/C]$, $I = 8.25 \times 10^{-4}$ (min $\cdot\, cm)/s$ and P_e is the molar polarizability (cm^3/mol). In their study, the adsorption rate constant increased linearly with the linear velocity and no size dependence was observed (Wood & Stampfer, 1993).

The Vahdat et al. model (1994 and 1997) describes a series of equations for each zone that is based on the Wheeler-Jonas equation and the IAST model combined with the Langmuir equation to obtain adsorption isotherms for each component. In this model, Component 1 is more volatile or less adsorbed than component 2. The breakthrough curve concentration profile is divided in four distinct zones and is shown in Figure 6.1

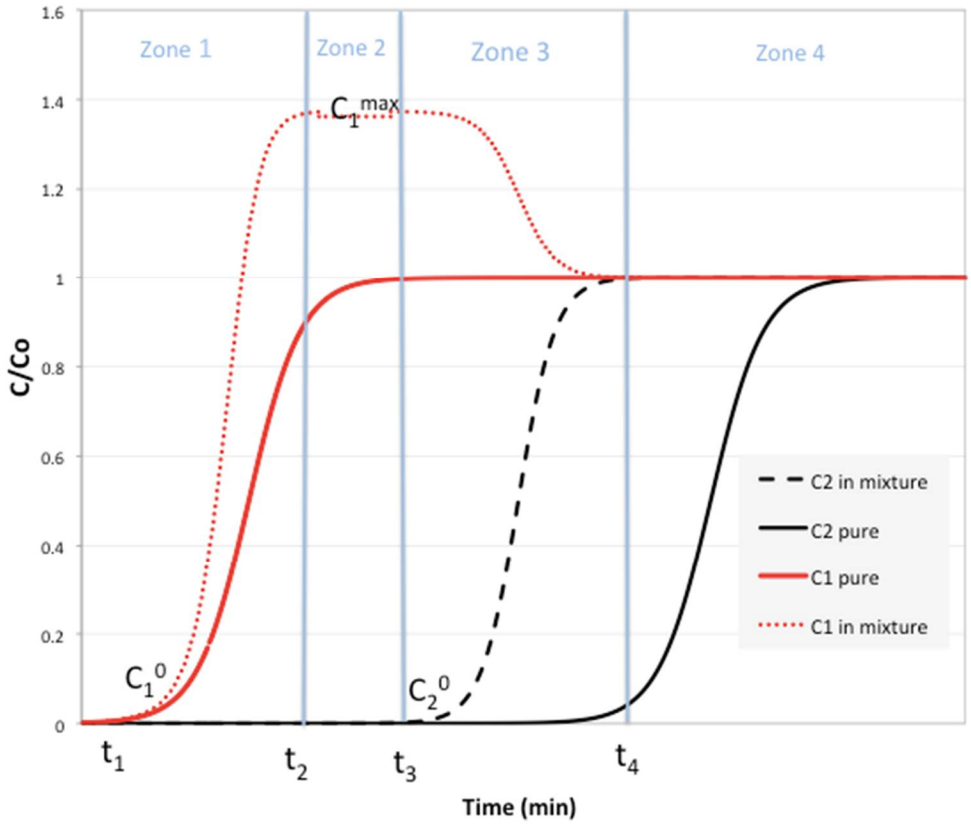

Figure 6.1 Schematic breakthrough curve of a binary system with inlet concentration of contaminant 1 (C_1^o) and contaminant 2 (C_2^o), *and* C_1^{max} is the maximum concentration of component 1 during the desorption phenomenon.

a) **Zone I**

In zone I, the more volatile component 1, which is weakly adsorbed, breaks through. The breakthrough time of this contaminant relates to adsorption capacity W_{e1} and its maximum adsorption capacity, (W_{e1}) at the maximum concentration (C_1^{max}) as follows:

$$t_{b1} = \frac{W_{e1}^{max}}{\frac{C_1^o Q}{W - \frac{\rho_B Q}{K_v} ln\left(\frac{C_1^{max} - C_1}{C_1}\right)} + \frac{C_2^o \rho_B (W_{e1}^{max} - W_{e1})}{W(W_{e2}\rho_B + \varepsilon C_2^o)}} \quad \text{for } t_{b1} < t_2 \qquad (6.8)$$

where ε is the bed porosity, C_1 is the outlet concentration of contaminant 1, C_2^0 is the inlet concentration of contaminant 2.

b) **Zone II**

In Zone II, *Contaminant 1* reaches its maximum concentration (C_1^{max}), which is higher than its initial inlet concentration, C_1^0:

$$C_1 = C_1^{max} \qquad \text{for } t_3 > t > t_2 \qquad (6.9)$$

The maximum concentration can be found from the mass balance equation as follows:

$$C_1^{max} = \frac{2[QC_1^0 t_4 - W(W_{e1}) - \varepsilon V C_1^o - QC_1^o(t_4 - t_3)/2]}{Q[t_3 + t_4 - t_2 - t_1]} \qquad (6.10 - a)$$

where V is the volume of the bed. Initially, C_1^{max} may be approximated by calculating the value with:

$$C_1^{max} = C_1^0 \left(\frac{W_{e1}^0 - W_{e1}}{W_{e2}}\right) C_2^0 \qquad (6.10\text{-b})$$

c) **Zone III**:

In zone III, Contaminant 2, which is more strongly adsorbed, breaks through and reaches its maximum concentration and is described with Eq. 6 by using the adsorption capacity of contaminant 2 in the mixture (W_{e2}) instead of W_e. Contaminant 1's concentration decreases from its maximum concentration (C_1^{max}) and is expressed as follows:

$$C_1 = C_1^{max} - (C_1^{max} - C_1^o)\frac{C_2}{C_2^o} \qquad \text{for } t > t_3 \qquad (6.11)$$

d) **Zone IV**

In zone IV, the carbon bed is saturated with both contaminant 1 and contaminant 2 and breakthrough concentrations are equal to the inlet concentrations C_1^0 and C_2^O, respectively.

Breakthrough curves for each effluent correspond to concentrations that will eventually be inside the worker's mask, especially in the case of a volatile contaminant where contribution to overall risk is considered fairly high (McKone, 1987). To further evaluate the toxicity effect of breakthrough contaminant mixtures and evaluate the potential health risks to workers, it is important to apply risk assessment principles.

6.3.4 Hazard Index

The risk assessment based on the combined action of each component in a chemical mixture may be characterized by using the Hazard index (HI) approach, which was originally proposed by the US Environmental Protection Agency mixture guidelines (US EPA, 1986). This approach is proposed for mixtures containing components having the same toxic effect, in the same organ via the same mode of action. This approach assumes that the components of the mixture are additive in concentration (*or dose)* of the mixture components and is expressed by the sum of hazard quotients calculated of each component. The HI can be calculated as follows:

$$HI = \sum_{i=1}^{n} \frac{D_i}{RfD_i} \qquad (6.12)$$

where the exposure doses (or concentrations) of each component of the mixture (Di) are normalized by the guideline exposure values, i.e., dose or concentration considered safe (e.g. Occupational Exposure Limit value (OEL), reference dose (RfD), etc.). When the hazard index exceeds unity, there may be concern for potential health effects. If HI is less than 1, then it will pose no risk to calculate the breakthrough time of a mixture. The hazard index may incorporate an uncertainty factor (UF) or safety factor of 10, for mixtures of chemicals where little information is known about the potential of interactions amongst components, or if relatively high concentrations of the mixture compounds are present (Drinking Water and Health, Volume 9, 1989). In such cases, it is calculated as:

$$HI = (UF)\sum_{i=1}^{n}\frac{D_i}{RfD_i} \qquad (6.13)$$

Integration of the HI principle in CSL estimation for vapor mixtures is founded on the component-based approach where the toxicity of a known mixture is assessed taking into account the properties of each single contaminant. This means that all components participate in the toxicity even when they are below the "no effect" dose/concentration. Therefore, all time-dependent concentrations are considered in this approach. While any single chemical with an exposure level greater than the OEL value will cause the hazard index to exceed unity, for multiple chemical exposures, the hazard index can also exceed unity even if no single chemical exposure exceeds its OEL. Therefore, when HI is less than 1 and using a safety factor of 10, it will pose no health risk to workers when calculating cartridge service life of a mixture. This translates into longer cartridge service life while taken account of the toxicity of the mixtures compared to the additive principle, which overestimates it and only considers the concentration of the most volatile contaminant. Overall, this approach would mean the change of cartridge would be less frequent, hence, an economic advantage compared to the additive principle while assuring safety for the worker

6.4 Methods

6.4.1 Data Selection

To apply the HI principle, the selection criteria of the binary system were selected on the basis of three factors: (i) the first contaminant is volatile and less harmful compared to contaminant 2; (ii) components of the binary system have to induce a common toxic effect, and (iii) available single component adsorption data are available to solve the quadratic IAST-Langmuir equation. Table 6.1 lists the physical and chemical properties of the contaminants along with their major toxic effects. This study specifically excluded binary mixtures of contaminants where the most volatile component is at the same time the most toxic contaminant.

Table 6.1 Contaminants physicochemical properties and associated toxicity (CNESST, 2015)

Solvent	Density (g/cm^3)	**Boiling point (°C)**	**Vapor Pressure (mm Hg)**	**Odor Threshold (ppm)**	**Major toxic effect**	**OEL (ppm)**
Acetone	0.784	56.29	185	50	Neurotoxicity	500
Toluene	0.866	110.6	22	6.7	Neurotoxicity, Reproductive effect	50
o-Xylene	0.88	144.4	4.97	5.4	Neurotoxicity, Reproductive effect	100
m-Xylene	0.864	139.1	5.9	0.6	Neurotoxicity	100
Styrene	0.906	145	5	0.14	Possible carcinogen, Neurotoxicity	50

The adsorption isotherms of pure contaminants and their binary gas mixtures for the two activated carbons listed in Table 6.2 were fitted with the Langmuir equation. Then, the ideal adsorbed solution theory (IAST) in conjunction with the Langmuir single-component isotherm were used to calculate the adsorption of the mixtures on the two activated carbons at a flow rate of 24 L/min, temperature of 25°C, and carbon weight of 50 g for simulations of exposures to acetone (10-700 ppm) and the other contaminant of lower volatility (500 ppm). Parameters listed in Table 6.2 of Carbon A were used for the simulations and those of Carbon B were used to validate the IAST- Langmuir model with the experimental data.

Table 6.2 Adsorbent data used in the simulation of binary breakthrough curves.

Adsorbent	**Flow rate (L/min)**	**Density (g/cm^3)**	**Temperature (°C)**	**Surface Area (m^2/g)**	**Amount (g)**	**Ref.**

Carbon A	24	0.43	25	1280	50	(Vahdat, 1997)
Carbon B	24	0.45	25	1170	50	(Y H Yoon et al., 1991)

Then, the predicted data of mixture and component gas adsorption and contaminant equilibrium concentration were simulated and analyzed for the following binary mixture systems: acetone/toluene, acetone/m-xylene, acetone/o-xylene, and acetone/styrene. Finally, using the calculated breakthrough concentration as a function of time, a hazard index was calculated using the outlet concentrations of the mixture components to predict the theoretical service life for the safe use of a given respirator cartridge.

6.4.2 Calculations of Breakthrough Curves for Binary Vapor Mixtures

The Microsoft Excel program was used for the calculations using the quadratic equation to solve for the unknown parameters. The pure component pressure of contaminant 1 at the spreading pressure of the mixture, P_1^o was obtained by solving equations 6.4 and 6.5 with:

$$\frac{1 + k_1 P_1^o}{1 + k_2 P_2^o} = \exp\left(\frac{m_2}{m_1}\right) \qquad (6.14)$$

$$X_1 + X_2 = 1 \qquad (6.15)$$

$$\frac{PY_1}{P_1^o} + \frac{PY_2}{P_2^o} = 1 \qquad (6.16)$$

$$x_1 = \frac{PY_1}{P_1^o} \qquad (6.17)$$

To derive implicit quadratic equations, let

$$c = exp(m_2/m_1) \qquad (6.19)$$

Substituting Eq.6.19 into Eq. 6.14 gives:

$$1 + k_1 P_1^0 = c(1 + k_2 P_2^0) \qquad (6.20)$$

$$k_1 P_1^0 - c k_2 P_2^0 + (1 - c) = 0 \qquad (6.21)$$

Rearranging Eq. 6.16 gives:

$$(PY_1P_2^o)/[(P_1^oP_2^o) + (PY_2P_1^o)/(P_1^oP_2^o)] = (P_1^oP_2^o)/(P_1^oP_2^o) \quad (6.21)$$

which can be simplified to :

$$(PY_2P_1^o)/(P_1^o - PY_1) = P_2^o \quad (6.22)$$

Now substituting Eq. 6.22 into Eq.6.21 gives the following quadratic equation:

$$k_1\boldsymbol{P_1^{o\,2}} + (-k_1PY_1 - ck_2PY_2 + 1 - c)\boldsymbol{P_1^o} - (1-c)PY_1 = 0 \quad (6.23)$$

Having the following implicit quadratic solution:

$$\boldsymbol{P_1^o} = \frac{-(-k_1PY_1 - ckPY_2 + 1 - c) \pm \sqrt{(-k_1PY_1 - ckPY_2 + 1 - c)^2 - 4k_1(1-c)PY_1}}{2k_1} \quad (6.24)$$

Because it is a quadratic equation, two solutions are returned. However, only one solution is physically consistent. The major flow chart of the calculations is shown in Figure 6.2. Basically, Langmuir parameters of the pure components are used in combination with the IAST model to determine the adsorption capacities of the individual components in the mixture using the parameters of the adsorption systems (flow rate, pressure, temperature, carbon weight, density, concentration) listed in Table 6.2 for the binary mixture. Then, component 1 and component 2 of the mixture were calculated for each zone of Figure 6.1 using the Vahdat model.

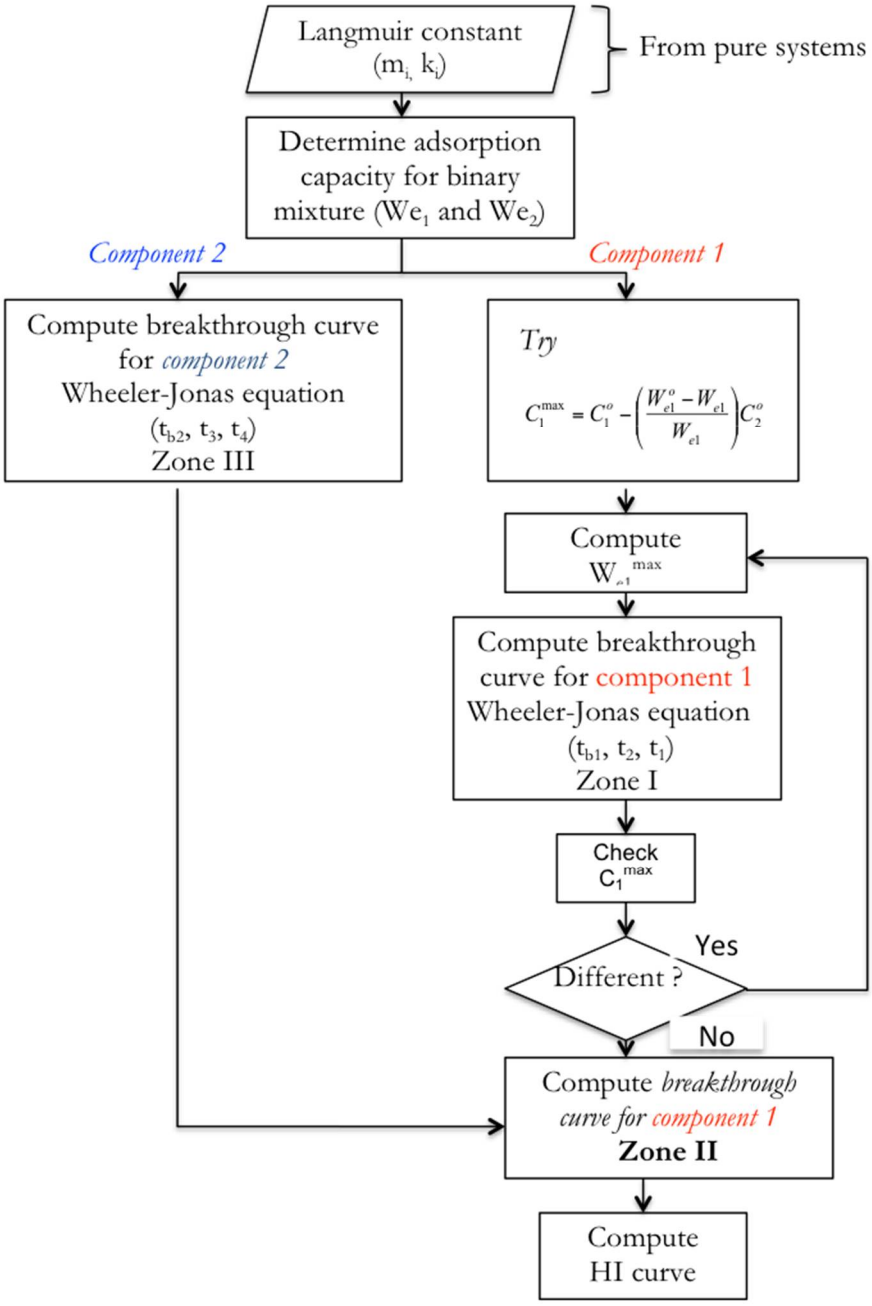

Figure 6.2 Flow chart for calculation of adsorption capacity and breakthrough curve of binary vapors mixtures where C_1^{max} can initially be estimated and checked with equations 6.10-a and 6.10-b.

6.5 Results and Discussion

6.5.1 Validation of Prediction Model

Using single contaminant adsorption data, IAST, and parameters of binary vapor mixtures, breakthrough curves of the binary systems of acetone/m-xylene using the Vahdat model were validated against previously published data (Lara et al., 1995; Vahdat et al., 1994) and the comparison is shown Table 6.3. All three simulations revealed reproducibility of the experimental data and closely matched the Vahdat Model.

Table 6.3 Comparison of predicted maximum concentration ratios of acetone with experimental data and the Vahdat Model (1994).

Concentration (ppm)		C^1_{max}/C^o_1		
			Vahdat Model	
Acetone	m-Xylene	Experimental[20]	(1994)	This Study
749	260	1.21	1.23	1.21
474	490	1.55	1.55	1.54
248	730	2.37	2.33	2.31

C^1_{max} is the maximum concentration of contaminant 1 and C^o_1 is the inlet concentration of contaminant 1

An example of the above resulting adsorption breakthrough curves in the binary system of acetone/m-xylene are shown in Figure 6.3. The additive principle curve, which considers that the mixtures behave as a pure contaminant by summing up the concentration of each component to acetone, was also computed. Because acetone is weakly adsorbed compared to m-xylene, the breakthrough of the former occurs early and is desorbed by the strongly adsorbed m-xylene according to the competing adsorption effect. Therefore, acetone is displaced by m-xylene and enters the gas stream, causing outlet concentration of acetone to increase beyond its inlet concentration.

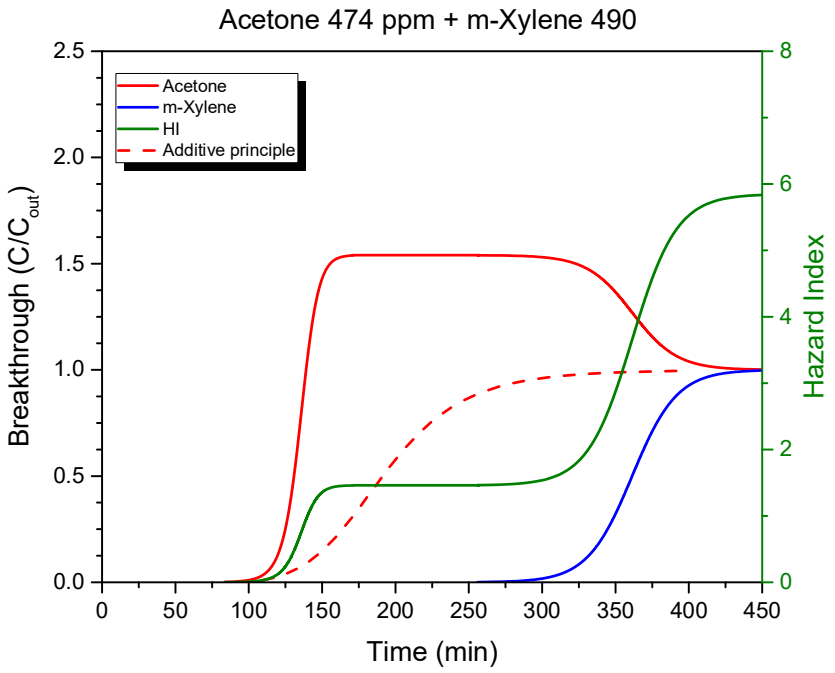

Figure 6.3 Hazard index and breakthrough curve for acetone (474 ppm) and m-xylene (490 ppm) on respirator cartridge in the binary system. The additive principal curve is calculated by adding the sum of the concentration of each component to acetone.

6.5.2 Effect of Concentration Ratio on the Hazard Index (HI)

The HI curves for the breakthrough concentration fractions presented in Table 6.3, were computed and are plotted in Figure 6.4. Two distinctive plateaus are observed for all HI plots: the first one occurs on the onset of the breakthrough of contaminant 2 (m-xylene); the second one at the maximum concentration of acetone. Depending on the concentration ratio of acetone to m-xylene, the shape of the HI curve varied and its positions shifted (see Figure 6.4).

When the concentration of acetone was about three times less than m-xylene ($C_1/C_2 = 0.34$), the HI curve increased steeply and its characteristic curve shifted to the right. When the concentration of acetone was almost equal to that of m-xylene ($C_1/C_2 = 0.97$), spreading of HI curve occurred and the curve shifted to the left of HI plot of $C_1/C_2 = 0.34$. Then, when the acetone concentration was 2.8 times that of m-xylene, the HI curve decreased and exhibited the most spreading along the x-axis.

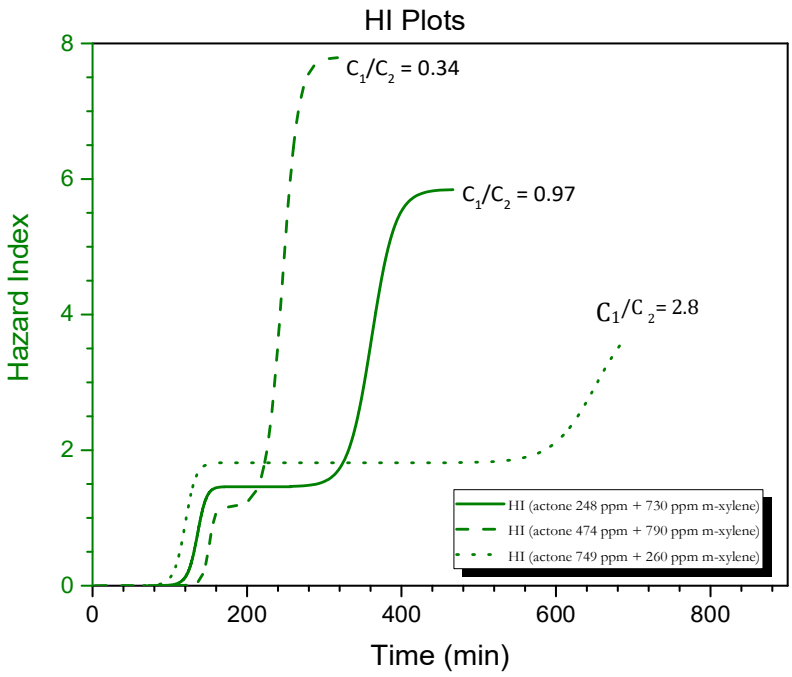

Figure 6.4 Effect of the concentration ratio of acetone (C_1) to m-xylene (C_2) on the Hazard index curve.

In this scenario, when HI > 1, breakthrough time values pose an unreasonable health risk and occur before the breakthrough of the second contaminant, m-xylene. As stated in the U.S. EPA (1986) guidelines, the hazard index should be interpreted as an approximation of the non-carcinogenic risk posed by exposure to the mixture and not considered as an absolute risk value.

6.5.3 Simulations

Results of the of breakthrough curves for the binary vapor mixtures of acetone/o-xylene at various concentration scenarios for acetone while the concentration of o-xylene remained fixed at 500 ppm are shown in Figure 6.5. A protection factor of 10, which replaces the uncertainty factor, was included into HI. At very low concentrations of acetone (< 25 ppm), a marked difference of about 100 minutes is observed between the 10% breakthrough times ($t_b10\%$) and 10% HI breakthrough times for the binary system of acetone/o-xylene. Above the concentration of 50 ppm of acetone, the 10% HI breakthrough times are not significantly different to the calculated 10% breakthrough times. However, when the protection factor is not considered, a difference of up to 170 min below 400 ppm is observed. When the concentration of acetone is

equivalent or greater to the concentration of o-xylene, all breakthrough time indicators (t_b10%, t_b 10%HI, t_b HI) are more or less the same.

The results of the HI breakthrough times for the binary vapor mixtures of acetone/toluene are shown in Figure 6.6. When the concentration of acetone is 10 ppm, a difference of more than 100 min between t_b 10% and t_b 10% HI is observed. If the uncertainty factor of 10 for HI is removed, a difference up to 170 minutes is seen between t_b 10% and t_b HI when the concentration of acetone is below 225 ppm in the binary system of acetone/toluene.

The results of the HI breakthrough times for the binary vapor mixtures of acetone/styrene are shown in Figure 6.7. For various inlet concentrations of acetone, the HI breakthrough times for the adsorption mixture showed no significant difference between the t_b10% and t_b10% HI. However, when the concentration of toluene is 305 ppm and the concentration of acetone is 503 ppm, the difference between t_b10% and t_b HI is up to 240 minutes.

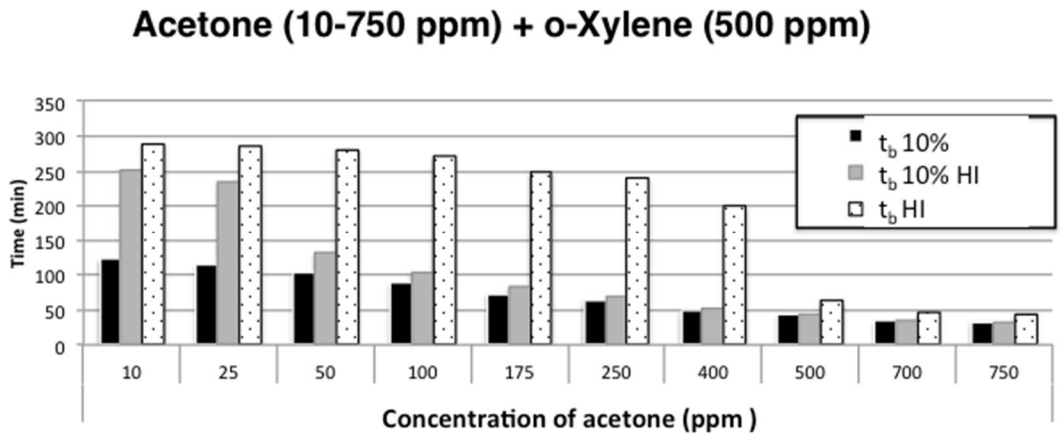

Figure 6.5 Comparison of cartridge service life using 10% breakthrough time (t_b 10%), hazard index (HI), and t_b10 % HI when HI = equal 1 for the binary system of acetone/o-xylene.

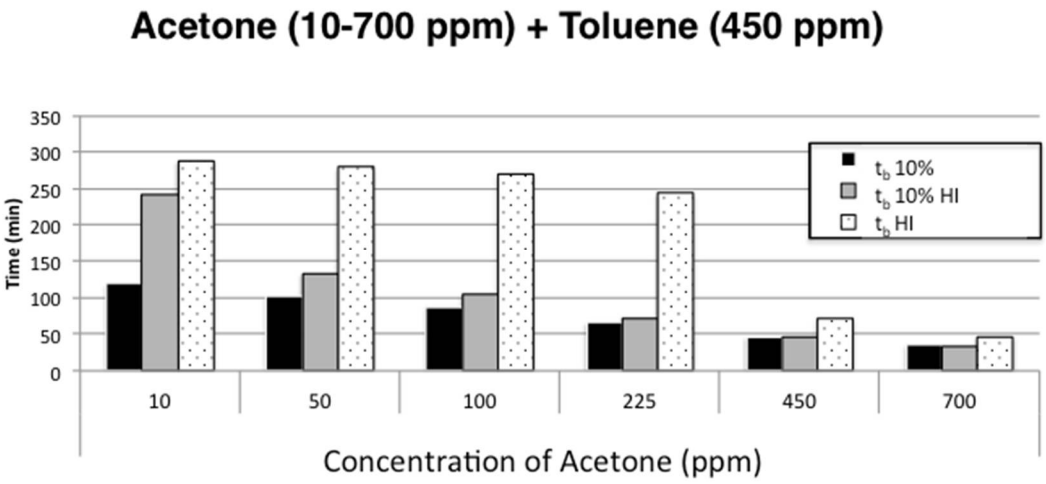

Figure 6.6 Comparison of cartridge service life using 10% breakthrough time (t_b 10%), hazard index (HI), and t_b10 % HI when HI = equals to 1 for the binary system of acetone/toluene.

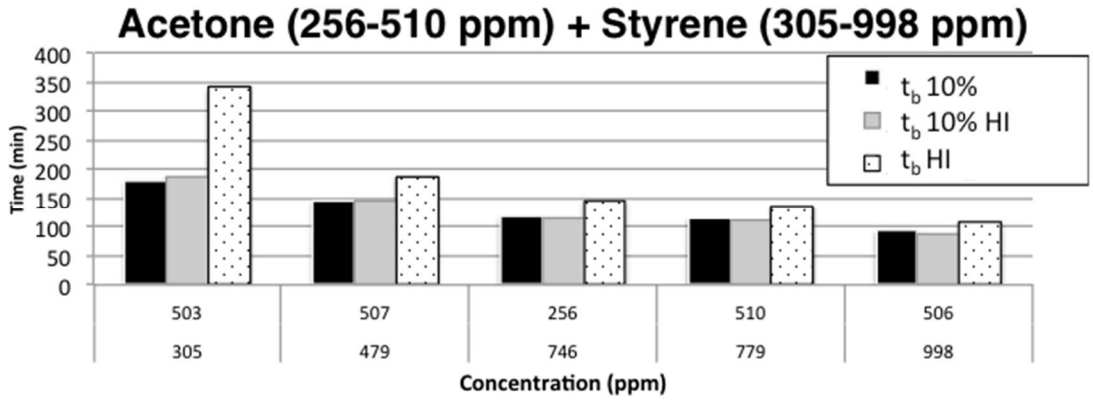

Figure 6.7 Comparison of cartridge service life using 10% breakthrough time (t_b 10%), hazard index (HI), and t_b10 % HI when HI = equals to 1 for the binary system of acetone/styrene.

6.5.4 Effect of the Concentration Ratio on HI

The effect of the concentration ratio of contaminant 1 (C_1) to contaminant 2 (C_2) on the breakthrough time when HI=1 (t_b *HI*=1) was studied in Figure 6.8. The relationship appears to be inversely proportional; as C_1/C_2 increases, t_b HI=1 decreases. The asymptote is reached around C_1/C_2 =2 for vapor mixtures of acetone + m-xylene and acetone + styrene, whereas for binary systems of acetone + o-xylene and acetone + toluene it occurs earlier C_1/C_2 = 1.5 and C_1/C_2 =1, respectively. This result implies that using the breakthrough time when HI =1 to calculate the cartridge service life for binary systems would be more useful at low concentration fractions of contaminant 1 to contaminant 2.

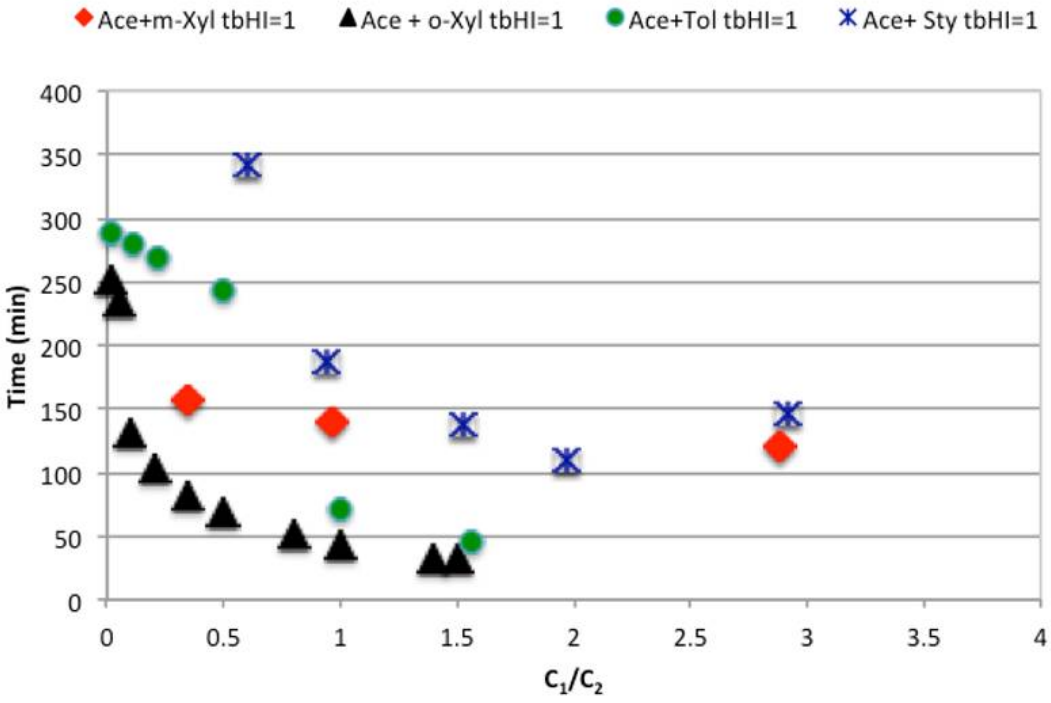

Figure 6.8 Effect of C1/C2 on t_b *HI = 1* for binary systems

6.6 Conclusions

Breakthrough curves of mixture contaminants were simulated using the Vahdat model and agreed well with the experimental data for the binary system of acetone and m-xylene. The results obtained highlight the importance of integrating a toxicological approach to predict mixture breakthrough curves for binary vapor mixtures particularly at low concentration fraction for contaminant 1 ($C_1/C_2 < 2$). The simulated cartridge service life using the breakthrough times of 10% HI were up to two times greater than the 10% breakthrough times of acetone in the mixture. At higher concentrations of acetone, both approaches gave similar results. The HI approach is a useful tool to characterize the risk related to exposures to mixtures of contaminants. Its use in combination with breakthrough time prediction models can assure a safe use of respirators and optimize estimation of cartridge service life while reducing the cost of changing cartridges. The HI approach should be considered in future development of predictive software tools.

Acknowledgments

F.J acknowledges financial support from IRSST, FRSQ (Fonds de recherche du Québec-Santé), Institut de recherche en santé publique de l'Université de Montréal (IRSPUM) and ÉSPUM (École de santé publique de l'Université de Montréal).

6.7 References

Commission des normes de l'équité de la santé et de la sécurité du travail. (2015). Répertoire Toxicologique.

Coyne, K., Caretti, D., Scott, W., Johnson, A., & Koh, F. (2006). Inspiratory flow rates during hard work when breathing through different respirator inhalation and exhalation resistances. Journal of Occupational and Environmental Hygiene, 3, 490–500.

Drinking Water and Health, Volume 9. (1989). Washington, D.C.: National Academies Press. doi:10.17226/773

Ettinger, H., Janssen, L., & Metzler, R. (2009). Respiratory Protection Committee Identifies Research Priorities. Synergist, 20, 26–27.

Janvier, F., Tuduri, L., Cossement, D., Drolet, D., & Lara, J. (2015). Micropore characterization of activated carbons of respirator cartridges with argon, carbon dioxide, and organic vapors of different vapor pressures. Carbon, 94, 781–791.

Janvier, F., Tuduri, L., Cossement, D., Drolet, D., & Lara, J. (2016). Systematic evaluation of the adsorption of organic vapors onto a miniaturized cartridge device using breakthrough tests in parallel experiment with a full size respirator cartridge. Adsorption Science & Technology, 34, 287–306.

Jonas, L. A., & Rehrmann, J. A. (1972). The kinetics of adsorption of organo-phosphorus vapors from air mixtures by activated carbons. Carbon, 10, 657–663.

Jonas, L. A., & Rehrmann, J. A. (1973). Predictive equations in gas adsorption kinetics. Carbon, 11, 59–64.

Lara, J., Yoon, Y. H., & Nelson, J. H. (1995). The Service Life of Respirator Cartridges with Binary Mixtures of Organic Vapors. Journal of the International Society for Respiratory Protection, 13, 7–26.

Linders, M. J. G., Mallens, E. P. J., van Bokhoven, J. J. G. M., Kapteijn, F., & Moulijn, J. A. (2003). Breakthrough of Shallow Activated Carbon Beds Under Constant and Pulsating Flow. AIHA Journal, 64, 173–180.

McKone, T. E. (1987). Human exposure to volatile organic compounds in household tap water: the indoor inhalation pathway. Environmental Science & Technology, 21, 1194–1201.

Myers, A. L., & Prausnitz, J. M. (1965). Thermodynamics of mixed-gas adsorption. AIChE Journal, 11, 121–127.

Nelson, G., & Harder, C. (1972). Respirator cartridge efficiency studies IV. Effects of steady-state and pulsating flow. American Industrial Hygiene Association Journal, 33, 797–805.

Nelson, G. O., & Correia, A. N. (1976). Respirator cartridge efficiency studies: VIII. Summary and conclusions. American Industrial Hygiene Association Journal, 37, 514–525.

Nelson, G. O., Correia, A. N., & Harder, C. A. (1976). Respirator cartridge efficiency studies: VII. Effect of relative humidity and temperature. American Industrial Hygiene Association Journal, 37, 280–288.

Nelson, G. O., & Harder, C. A. (1976). Respirator cartridge efficiency studies: VI. Effect of concentration. American Industrial Hygiene Association Journal, 37, 205–216.

OSHA. (1998). Inspection procedures for the Respiratory Protection Standard. CPL 02-00-120.

Ruch, W. E., Nelson, G. O., Lindeken, C. L., Johnsen, R. G., & Hodgkins, D. J. (1972). Respirator Cartridge Efficiency Studies. American Industrial Hygiene Association Journal, 33, 105–109.

Swearengen, P. M., & Weaver, S. C. (1988). Respirator Cartridge Study Using Organic-Vapor Mixtures. American Industrial Hygiene Association Journal, 49, 70–74.

US EPA. (1986). Guidelines for the Health Risk Assessment of Chemical Mixtures. Fed. Reg., 51, 34014–34025.

Vahdat, N. (1997). Theoretical study of the performance of activated carbon in the presence of binary vapor mixtures. Carbon, 35, 1545–1557.

Vahdat, N., Swearengen, P. M., & Johnson, J. S. (1994). Adsorption Prediction Of Binary-Mixtures On Adsorbents Used In Respirator Cartridges And Air-Sampling Monitors.

American Industrial Hygiene Association Journal, 55, 909–917.

Vuong, F., Chauveau, R., Grevillot, G., Marsteau, S., Silvente, E., & Vallieres, C. (2016). Predicting the lifetime of organic vapor cartridges exposed to volatile organic compound mixtures using a partial differential equations model. Journal of Occupational and Environmental Hygiene.

Wheeler, A., & Robell, A. J. (1969). Performance of fixed-bed catalytic reactors with poison in the feed. Journal of Catalysis, 13, 299–305.

Wood, G. O. (1985). Effects of air temperatures and humidities on efficiencies and lifetimes of air-purifying chemical respirator cartridges tested against methyl iodide. American Industrial Hygiene Association Journal, 46, 251–6.

Wood, G. O., & Moyer, E. S. (1989). A Review of the Wheeler Equation and Comparison of Its Applications to Organic Vapor Respirator Cartridge Breakthrough Data. American Industrial Hygiene Association Journal, 50, 400–407.

Wood, G. O., & Snyder, J. L. (2007). Estimating service lives of organic vapor cartridges III: Multiple vapors at all humidities. Journal of occupational and environmental hygiene, 4(5), 363-374.

Wood, G. O., & Stampfer, J. F. (1993). Adsorption rate coefficients for gases and vapors on activated carbons. Carbon, 31, 195–200.

Yoon, Y. H., Nelson, J. H., & Lara, J. (1996). Respirator Cartridge Service-Life: Exposure to Mixtures. American Industrial Hygiene Association Journal, 57, 809–819.

Yoon, Y. H., Nelson, J. H., Lara, J., Kamel, C., & Fregeau, D. (1991). A Theoretical Interpretation Of The Service Life Of Respirator Cartridges For The Binary Acetone Meta-Xylene System. American Industrial Hygiene Association Journal, 52, 65–74.

Commission Des Normes De L'équité De La Santé Et De La Sécurité Du Travail. (2015). Répertoire Toxicologique.

Coyne, K., Caretti, D., Scott, W., Johnson, A., & Koh, F. (2006). Inspiratory Flow Rates During Hard Work When Breathing Through Different Respirator Inhalation And Exhalation Resistances. Journal Of Occupational And Environmental Hygiene, 3, 490–500.

Drinking Water And Health, Volume 9. (1989). Washington, D.C.: National Academies Press. Doi:10.17226/773

Ettinger, H., Janssen, L., & Metzler, R. (2009). Respiratory Protection Committee Identifies Research Priorities. Synergist, 20, 26–27.

Janvier, F., Tuduri, L., Cossement, D., Drolet, D., & Lara, J. (2015). Micropore Characterization Of Activated Carbons Of Respirator Cartridges With Argon, Carbon Dioxide, And Organic Vapors Of Different Vapor Pressures. Carbon, 94, 781–791.

Janvier, F., Tuduri, L., Cossement, D., Drolet, D., & Lara, J. (2016). Systematic Evaluation Of The Adsorption Of Organic Vapors Onto A Miniaturized Cartridge Device Using Breakthrough Tests In Parallel Experiment With A Full Size Respirator Cartridge. Adsorption Science & Technology, 34, 287–306.

Jonas, L. A., & Rehrmann, J. A. (1972). The Kinetics Of Adsorption Of Organo-Phosphorus Vapors From Air Mixtures By Activated Carbons. Carbon, 10, 657–663.

Jonas, L. A., & Rehrmann, J. A. (1973). Predictive Equations In Gas Adsorption Kinetics. Carbon, 11, 59–64.

Lara, J., Yoon, Y. H., & Nelson, J. H. (1995). The Service Life Of Respirator Cartridges With Binary Mixtures Of Organic Vapors. Journal Of The International Society For Respiratory Protection, 13, 7–26.

Linders, M. J. G., Mallens, E. P. J., Van Bokhoven, J. J. G. M., Kapteijn, F., & Moulijn, J. A. (2003). Breakthrough Of Shallow Activated Carbon Beds Under Constant And Pulsating Flow. AIHA Journal, 64, 173–180.

Mckone, T. E. (1987). Human Exposure To Volatile Organic Compounds In Household Tap Water: The Indoor Inhalation Pathway. Environmental Science & Technology, 21, 1194–1201.

Myers, A. L., & Prausnitz, J. M. (1965). Thermodynamics Of Mixed-Gas Adsorption. Aiche Journal, 11, 121–127.

Nelson, G., & Harder, C. (1972). Respirator Cartridge Efficiency Studies IV. Effects Of Steady-State And Pulsating Flow. American Industrial Hygiene Association Journal, 33, 797–805.

Nelson, G. O., & Correia, A. N. (1976). Respirator Cartridge Efficiency Studies: VIII. Summary And Conclusions. American Industrial Hygiene Association Journal, 37, 514–525.

Nelson, G. O., Correia, A. N., & Harder, C. A. (1976). Respirator Cartridge Efficiency Studies: VII. Effect Of Relative Humidity And Temperature. American Industrial Hygiene Association Journal, 37, 280–288.

Nelson, G. O., & Harder, C. A. (1976). Respirator Cartridge Efficiency Studies: VI. Effect Of Concentration. American Industrial Hygiene Association Journal, 37, 205–216.

OSHA. (1998). Inspection Procedures For The Respiratory Protection Standard. CPL 02-00-120.

Ruch, W. E., Nelson, G. O., Lindeken, C. L., Johnsen, R. G., & Hodgkins, D. J. (1972). Respirator Cartridge Efficiency Studies. American Industrial Hygiene Association Journal, 33, 105–109.

Swearengen, P. M., & Weaver, S. C. (1988). Respirator Cartridge Study Using Organic-Vapor Mixtures. American Industrial Hygiene Association Journal, 49, 70–74.

US EPA. (1986). Guidelines For The Health Risk Assessment Of Chemical Mixtures. Fed. Reg., 51, 34014–34025.

Vahdat, N. (1997). Theoretical Study of The Performance of Activated Carbon in the Presence of Binary Vapor Mixtures. Carbon, 35, 1545–1557.

Vahdat, N., Swearengen, P. M., & Johnson, J. S. (1994). Adsorption Prediction Of Binary-Mixtures On Adsorbents Used In Respirator Cartridges And Air-Sampling Monitors. American Industrial Hygiene Association Journal, 55, 909–917.

Vuong, F., Chauveau, R., Grevillot, G., Marsteau, S., Silvente, E., & Vallieres, C. (2016). Predicting The Lifetime Of Organic Vapor Cartridges Exposed To Volatile Organic Compound Mixtures Using A Partial Differential Equations Model. Journal Of Occupational And Environmental Hygiene.

Wheeler, A., & Robell, A. J. (1969). Performance Of Fixed-Bed Catalytic Reactors With Poison In The Feed. Journal Of Catalysis, 13, 299–305.

Wood, G. O. (1985). Effects Of Air Temperatures And Humidities On Efficiencies And Lifetimes Of Air-Purifying Chemical Respirator Cartridges Tested Against Methyl Iodide. American Industrial Hygiene Association Journal, 46, 251–6.

Wood, G. O., & Moyer, E. S. (1989). A Review Of The Wheeler Equation And Comparison Of Its Applications To Organic Vapor Respirator Cartridge Breakthrough Data. American Industrial Hygiene Association Journal, 50, 400–407.

Wood, G. O., & Stampfer, J. F. (1993). Adsorption Rate Coefficients for Gases And Vapors On Activated Carbons. Carbon, 31, 195–200.

Yoon, Y. H., Nelson, J. H., & Lara, J. (1996). Respirator Cartridge Service-Life: Exposure To Mixtures. American Industrial Hygiene Association Journal, 57, 809–819.

Yoon, Y. H., Nelson, J. H., Lara, J., Kamel, C., & Fregeau, D. (1991). A Theoretical Interpretation of the Service Life of Respirator Cartridges for the Binary Acetone Meta-Xylene System. American Industrial Hygiene Association Journal, 52, 65–74.

CHAPTER 7: CONCLUSIONS

Based on the three papers presented in Chapter 4, 5, and 6, this chapter discusses the major results and their contributions to prediction models for cartridge service life. A discussion of limitations and plausible explanations for unexpected results also are presented. Finally, this chapter highlights some avenues for possible future research based on the implications of this study.

7.1 Summary of Findings and Contributions

The underlying theme of this thesis was to optimize prediction models for respirator cartridge service life necessary to protect workers against harmful organic vapors. Three specific research objectives were targeted by this project and resulted in three publications. The first paper in Chapter 4 presented a novel approach to characterize activated carbons with a multi-vapor adsorption isotherm obtained from five organic vapors of different vapor pressures. The second paper, in Chapter 5, presented an approach to characterize the cartridge service life using a Mini cartridge. A description and the demonstration of the validity and accuracy of the Mini cartridge approach are discussed. Finally, the last paper presented in Chapter 6 showed the application of a toxicology approach in the prediction of cartridge service life for exposure to mixtures of contaminants.

7.1.1 Characterization of Activated Carbon

Because prediction models are recommended to estimate cartridge service life, experimental data are necessary for parameterization and validation of models. In particular, knowledge of the micropore volume and structural constant B are essential carbon parameters for the prediction of the adsorption capacity in the Wheeler-Jonas model [150]. To do so, in Chapter 4, a fundamental investigation was conducted to characterize the textural properties (surface area, micropore volume, and pore size distribution) of ten commercially activated carbons contained in respirator cartridges with three types of adsorbents: Ar at 87.3 K, CO_2 at 273 K and by using a multi organic vapor adsorption isotherm obtained from breakthrough data

at 294 K, 40% relative humidity (RH), and at 500 ppm for toluene, n-hexane, DCM, MIBK, and m-xylene.

The originality of this research is in the approach of using a multi-vapor adsorption isotherm obtained from breakthrough data with different organic solvents of varying boiling points to characterize the microstructure of activated carbon. As such, a point in the adsorption isotherm, representing the adsorption capacity, which is an important parameter in the prediction of cartridge service life could be used to predict respirator cartridge service life for any other organic solvents without prior experimentation. The organic vapors chosen gave a relative vapor pressure range of 9×10^{-4}- 0.1 and exhibited the characteristic Type I adsorption isotherm typical for microporous adsorbates as validated with the Langmuir equation.

The experimental adsorption capacities (We_{exp}) obtained by gravimetric measurement were slightly lower than the calculated adsorption capacities (We_{calc}) obtained from the mid point of the curve. The difference between the We_{exp} and We_{calc} was more pronounced for the less volatile and hydrophobic contaminants (m-xylene, toluene, and MIBK). Because a blank experiment (no contaminant) performed at the same experimental conditions showed that the activated carbons used in the OV cartridges contained less than 0.7% of water when the air humidity was 40% RH, this value was considered negligible. This finding is agreement with studies, which have showed that RH values below 50% have no significant effect on the breakthrough of organic vapors in OV cartridges [68,100]. Therefore, the discrepancy was interpreted as due to the successful displacement of water by the less volatile contaminant compared to the low boiling solvents of DCM and n-hexane causing $We_{calc.} > We_{exp.}$ This finding agrees with Lodewyckx [151], that demonstrated the loss of adsorption capacity by volume exclusion for the more volatile contaminant, which is not able to replace the more strongly adsorbed water molecules.

The multi-vapor adsorption isotherms were constructed with the calculated adsorption capacities (We_{calc}) and the experimental adsorption capacities (We_{exp}). The values of adsorption capacities of the activated carbons increased with the decreasing order of their vapor pressure as follows: DCM <n-hexane <MIBK≤ toluene ≤ m-xylene. Therefore, because of the hydrophobic nature of the microporous graphene layers of activated carbon, non-polar solvents are more strongly adsorbed [17]. However, when the volume occupied by the adsorbed vapor

was computed by dividing the liquid volume of the organic vapor by the micropore volume obtained with the Argon data, the order was as follows: DCM> n-hexane> toluene>MIBK> m-xylene. This results showed that molecular size of the adsorbent must be considered in the adsorption capacity [152].

The predicted DR equation [153], which relates the adsorption capacity to the micropore volume of activated carbon, was used to compare the Ar and OV data. In general, the predicted structural constants B_{calc} and B_{exp} showed up to 57% difference from Wood's universal constant b =3.56 x 10^{-5} mol^2 cal^{-2} $(cm^3/mol)^{1.8}$ [74,154]. Whereas, the predicted micropore volumes obtained with the We_{exp} were within 0-19% of the Ar data. The micropore volume data predicted with Ar data were smaller than the OV data. This important outcome, further demonstrates the hindrance in the diffusion within micropores due to low kinetic energy and low temperature of Ar, thus giving preference for the OV approach.

Overall, the predicted adsorption capacities obtained with the multi-OV adsorption data and structural constant B were in a good agreement with the experimental data whereas a large discrepancy up to 89% was observed with the predicted adsorption capacities obtained with Ar data and the universal relative constant b = 3.56 x 10-5 mol^2 cal^{-2} $(cm3/mol)^{1.8}$. Thus, this thesis demonstrated the importance in integrating the characterization of the micropore structure of the activated carbons respirator cartridges obtained from experimental conditions similar to its application in the workplace.

The characterization of the ten activated carbon samples with Ar at 87.3 K exhibited the characteristic type I adsorption isotherm as confirmed by fitting of the Langmuir equation. The range of micropore volume was 400-500 cm^3/g and increased with the specific BET surface area as opposed to with the total pore volume, which is indicative of the micropores being the preferred adsorption sites. The analysis of the pore size distribution (PSD) of the activated carbon obtained with Ar at 87.3 K showed late pore filling and slow diffusion for the micropore range of < 20 Å. Whereas the PSD of CO_2 at 273 K revealed the readily accessibility of the adsorbent in the narrow micropores (widths < 7 Å). Also, the PSD with DFT and CO_2 provided unique structural information about the activated carbons.

Therefore, this study showed that narrow micropores may be involved and may play a significant role in the adsorption of organic vapors. Thus, this study provided further understanding of the mechanism of organic vapor adsorption unto activated carbons.

This study could thus have an impact on the preparation and selection of activated carbon in terms of the micropore distribution and micropore volume to improve the optimal filtering capacity of the organic vapor cartridges.

7.1.2 Mini Cartridge

This thesis postulated a novel experimental design using a Mini cartridge device to simulate the behaviour of a full size cartridge provides more precise data of the surface properties of the activated carbons. Thus, Chapter 5 presented the validation of the Mini approach with a series of repeatability and reproducibility tests.

The carbon loading of the Mini was achieved by the snow filling method [155], which is used in the industry to fill the respirator cartridges. The reproducibility of the carbon packed bed thickness of the Mini for the OV cartridge 3M6001 was 1.66 ± 0.05 cm for N= 23 suggesting that the predetermined amount of carbon added to the Mini was packed identically to the corresponding cartridge. Although the equivalent flow rate of the Mini to match the breakthrough profile of the full size cartridge was not achieved completely, it still provided overall a good estimation of the breakthrough curve of the respirator cartridge.

Even though the asymmetry of the breakthrough curves is reported by others [94] to be an effect that originates from the kinetics of the adsorber [27], the Mini breakthrough curve study showed that symmetrical breakthrough curves were achieved for all contaminants. This indicates that the geometry of the cartridge or face velocity is the dominating factor affecting the symmetry of breakthrough profiles. Therefore, utilizing the Mini to characterize the activated carbon breakthrough curve is preferred as it removed the inconsistency in the linearity of the airflow profile in the OV cartridge.

The stability and reliability of the experimental set-up for the single and parallel experiments were confirmed by the superposition of triplicate curves of both the Mini and OV cartridge. The unique experimental set-up of the parallel experimental design allowed for the

Mini to be exposed to identical environmental conditions to that of the OV cartridge, thus removing experimental errors and allowing a real time comparison.

Similarly to the OV cartridge data, the We_{calc} values obtained with the Mini were larger than the We_{exp} values which revealed that this is an adsorbate effect that is not related to the flow in the cartridge. The adsorption capacities We_{calc}, which were obtained from the mid-point of the breakthrough curves obtained with the Mini were slightly lower than the ones obtained with the OV cartridges. However, the differences were within the experimental error. The t_b 10% obtained with the Mini were also within experimental error with the ones of the OV cartridge results. Whereas greater discrepancy was observed for the t_b 50% in particularly for the less volatile contaminants, which required more time to reach complete saturation.

Breakthrough simulations were used to assess the performance of the Mini in predicting respirator cartridge breakthrough curves by applying the Wheeler-Jonas equation to the Mini breakthrough data. Overall, the results showed that the Mini data was suitable to predict cartridge service life of respirator cartridges but simulating the entire shape of the OV cartridge remained a challenge.

The use of a Mini cartridge allowed acquisition of accurate and reliable breakthrough data under controlled conditions (with several variables, air flow rates, temperature, humidity, that may affect the final results), which could translate to a significant reduction of the amount of solvent used.

Once the repeatability and reproducibility study was validated for the cartridge 3M6001, this experimental approach was extended to ten other respirator cartridges where parallel experiments were performed at 40% RH at 500 pm for DCM, n-hexane, MIBK, toluene and m-xylene and the findings are reported in the IRSST report [156].

7.1.3 Application of the findings to an online software prediction tool

Application of the organic vapor respirator cartridge breakthrough data from this thesis was used to feed the IRSST online prediction tool SATURISK (http://www.irsst.qc.ca/saturisk/) for the 11 tested cartridges. Though, the mini cartridge studies proved promising, there are still some questions unanswered. Therefore, the input parameters of the micropore volume obtained

from the multi- vapor adsorption isotherm and the corresponding structural constants of the full size respirator cartridge were utilized in SATURISK. This tool will potentially help 300,000 + workers in Quebec to safely predict cartridge service life for over 195 solvents.

7.1.4 Toxicological Approach for Mixtures

Predicting cartridge service life for multi contaminants is complicated and often it will be only defined as the breakthrough of the most volatile contaminant. In Chapter 6, a toxicity approach was introduced using the hazard index (HI) principle [129], which considers the additivity principle by computing the sum of concentrations for each mixture component normalized by its Occupational Exposure Limit (OEL). Contaminants were chosen on the basis of available Langmuir single component data [123] able to solve the simple quadratic equation of the Langmuir-IAST equation[157]. First, simulations were validated with previously reported data of Lara and collaborators [20,115,116]. Simulations of exposures with acetone as the volatile contaminant with a concentration range of 10-700 ppm and the other contaminant of lower volatility at 500 ppm through a respiratory cartridge with 50 g of carbon at 25°C and at flow rate of 24 L/min were performed. Under the binary systems and conditions selected, this study demonstrated that the cartridge service life estimation based on the HI breakthrough times is useful when the first contaminant to elute is volatile or has a boiling point lower than 65°C (e.g. acetone) and at low concentration (< 50 ppm). A safety factor of 10% of the HI = 1 breakthrough times was chosen as a protection measure to ensure safe use of respirators and gave up to twice the 10% breakthrough times when the concentration of acetone was below 50 ppm.

Also, this study showed that that the calculated breakthrough time for binary mixtures of contaminants based on HI is inversely proportional to the concentration ratio of contaminant 1 (C1) to contaminant 2 (C2), and applicable when C1/C2 < 2. The use of the HI approach to predict cartridge service of mixtures in these conditions is suitable.

The use of this approach will provide a toxicological basis on the service life of the cartridges while providing a better management of the change schedule for cartridges as well as offering a better protection to workers.

7.2 Research Limitations

Although the research has reached its aims, there were unavoidable limitations to this study as discussed in the individual chapters. First, because, of time limit, the research was conducted with only few organic vapors, at a specified concentration and experimental conditions. Therefore, to generalize the applicability of the universal adsorption isotherm to all organic vapors, especially for polar solvents where the interaction of water would have to be considered, more organic vapors should have been tested. Second, the transposition of the Mini to the full size cartridge posed some limitations in terms of the shape and difference in the flow profile. Consequently, breakthrough profiles of the Mini differed than that of the full size cartridge in particular for the less volatile contaminants. A flow correction factor, which takes into account the geometry of the cartridge, should have been introduced. Last, the third paper aimed to integrate a toxicological approach for mixture contaminants by using the IAST- Langmuir equations. However, using the quadratic equations to solve the two unknown variables presented only limited options of binary systems and concentrations that fitted this model. Using a sophisticated program to simultaneously solve multivariable would have provided a broader range of concentrations and systems to analyse. Furthermore, the study on mixture of contaminants did not examine all scenarios. For examples, when the most volatile component of the mixture is at the same time the most toxic, would the toxicological approach be applicable? However, examining such questions was beyond the scope of this study as several toxic contaminants have specific PPE regulations depending on the jurisdictions and for many of these cases, the use of the additivity concentration principle is safer.

7.3 Future Works

The work presented in this thesis offers multiple avenues for future research in organic vapors respirator cartridge service life prediction models. As Chapter 4 demonstrated, the characterization of the micropore volume and structural constant of activated carbon can be

achieved with a multi- OV adsorption isotherm obtained from breakthrough data. To further test this approach, other organic vapors should be tested to broaden the range of P/P_o.

Moreover, a brief study shown in Appendix I, shows that a relationship between the 10 % breakthrough times and the narrow micropores may exist. Finding a means to incorporate narrow micropore data into prediction models may be an avenue worth investigating.

Also, it may be possible to apply the same characterization approach demonstrated in this thesis to other types of activated carbon such as new "multi-gas" impregnated activated carbons (IACs) with zinc and copper based impregnates [158][159] to gain insight on the adsorption of their compounds and development of prediction models.

An area in which further developments are needed is the effect of surface chemistry on the adsorption of organic vapors [17]. Many activated carbons are comprised of hydrophilic surfaces where several oxygen, hydrogen, nitrogen, and other elements can be found in the carbon surface, in the form of single atoms and/or functional groups, which may influence their adsorption properties. Chemical interactions between organic molecules and carbon surfaces in humid condition can be significant and, in some cases, may overwhelm physical interactions [17]. Mechanistic information on the chemical interaction should be investigated in isotherms models and mathematical models.

While the study of the Mini cartridge presented in Chapter 5 showed that suitable adsorption capacity and 10% breakthrough time of a full size respirator cartridge can be reproduced, conducting a breakthrough flow profile study inside the cartridge may be beneficial to extend a correctional flow factor in the calculation of the flow rate of the Mini.

Even if no breakthrough experiments with mixtures of contaminants were performed in this thesis, the use of previously published data has allowed to explore the consideration of the toxicity of contaminants as criteria to define in the cartridge service life determinations and the need for more research in this area. In order to apply the proposed approach presented in Chapter 6, several mixture systems containing more than two contaminants should be investigated with different solvents and a more advanced and complex solution system of the Langmuir-IAST equation by iteration should be considered. Moreover, other studies have shown that other models such IAST-DR [160] or IAST Freundlich [161] are useful for mixtures

contaminants. Unquestionably, experimental data to validate this approach and the general applicability to more complex systems is desirable.

7.4 General Conclusion

In summary, predictive models to estimate the cartridge service life are necessary to ensure the best protection of workers against toxic organic vapors and require confidence in the mathematical model to predict accurate service life for a specific carbon, under a well-defined environment. However, they do require some experimental data due to the complexity of the phenomenon of adsorption and predictive behaviour due to the nature of different activated carbons, the broad range of contaminants and environmental conditions. Collectively, the use of a multi-vapor adsorption isotherm, of a Mini cartridge device, and the integration of the toxicity approach are all new elements, which aided the optimization of predictive models in respirator cartridge service life.

7.5 References

1 Vézina E. Cloutier, S. Stock, K., Lippel, É. Fortin et autres (2011). M. Enquête québécoise sur des conditions de travail, d'emploi et de sécurité du travail (EQCOTESST). Institut de recherche Robert-Sauvé en santé et sécurité du travail, Institut national de santé public Québec, Montréal: IRSST; 2011. p. 756.

2 US Department of Health and Human Services Centers for Disease Control and Prevention, National Center for Health Statistics PHS. National Center for Health Statistics. 2010 National Health Interview Survey (NHIS) public use data release. *NHIS survey description.* Hyattsville, Maryland; 2011.

3 Calvert GM, Luckhaupt SE, Sussell A, Dahlhamer JM, Ward BW. The prevalence of selected potentially hazardous workplace exposures in the US: Findings from the 2010 National Health Interview Survey. *Am J Ind Med* Wiley Subscription Services, Inc., A Wiley Company; 2013; **56**: 635–46.

4 OSHA. Safety and Health Topics | Chemical Hazards and Toxic Substances - Controlling Exposures. [Online]. Available: https://www.osha.gov/SLTC/hazardoustoxicsubstances/control.html. [Accessed: 12-Jan-2016].

5 Lynge E, Anttila A, Hemminki K. Organic solvents and cancer. *Cancer Causes Control*

1997; **8**: 406–19.

6 Chen R, Seaton A. A Meta-analysis of Mortality among Workers Exposed to Organic Solvents. *Occup Med (Chic Ill)* 1996; **46**: 337–44.

7 Spencer PS, Schaumburg HH. Organic solvent neurotoxicity: Facts and research needs. *Scand J Work Environ Health* Scandinavian Journal of Work, Environment & Health; 1985; **11**: 53–60.

8 Baker E. A review of recent research on health effects of human occupational exposure to organic solvents. A critical review. *J Occup Med* 1994; **36**: 1079–92.

9 Vyskocil A, Truchon G, Leroux T, Lemay F, Gendron M, Gagnon F, Majidi N El, Boudjerida A, Lim S, Emond C, Viau C. A weight of evidence approach for the assessment of the ototoxic potential of industrial chemicals. *Toxicol Ind Health* 2012; **28**: 796–819.

10 Semple S. Dermal exposure to chemicals in the workplace: just how important is skin absorption? *Occup Environ Med* 2004; **61**: 376–82.

11 Gérin M, Bégin D. Substitution des solvants en milieu de travail: élaboration d'un outil pour l'intervention: rapport LR098. Montréal: Institut de recherche en santé et sécurité du travail; 1995.

12 Regulation respecting occupational health and safety. Québec: Éditeur officiel du Québec.; p. O.C. 885-2001, 45.

13 Occupational Safety and Health Administration. Respiratory Protection. *29 CFR 1910.134*. Federal Register: Department Of Labor; 1998.

14 United States Department of Labor (USDOL) B of LS (BLS)/National I for OS and H (NIOSH). Respirator Use in the Private Sector Firms, 2001. Washington; 203AD.

15 Doney BC, Groce DW, Campbell DL, Greskevitch MF, Hoffman WA, Middendorf PJ, Syamlal G, Bang KM. A Survey of Private Sector Respirator Use in the United States: An Overview of Findings. *J Occup Environ Hyg* Taylor & Francis; 2005; **2**: 267–76.

16 Johnson SJ. Insight: Respiratory Protection Most cited, and Most Necessary. *Synerg* 2012; **February**: 18–9.

17 Bradley R. Recent Developments in the Physical Adsorption of Toxic Organic Vapours by Activated Carbons. *Adsorpt Sci Technol* 2011; **29**: 1–28.

18 Nelson GO, Correia AN. Respirator cartridge efficiency studies: VIII. summary and conclusions. *Am Ind Hyg Assoc J* Taylor & Francis; 1976; **37**: 514–25.

19 NIR, #160, Ido, SUZIN, Yaacov, KAPLAN, Doron. The effect of airflow pattern on filter breakthrough in physical adsorption. Kidlington, ROYAUME-UNI: Elsevier; 2002.

20 Lara J, Yoon YH, Nelson JH. The Service Life of Respirator Cartridges with Binary Mixtures of Organic Vapors. *J Int Soc Respir Prot* 1995; **13**: 7–26.

21 Lara J, Vennes M. Guide des appareils de protection respiratoire utilisés au Québec. [Montréal]: Commission de la santé et de la sécurité du travail du Québec; 1999.

22 Rose-Pehrsson SL, Williams ML. Integration of Sensor Technologies into Respirator Vapor Cartridges as End-of-Service-Life Indicators: Literature and Manufacturer's Review and Research Roadmap. 2005; .

23 Favas G. End of Service Life Indicator (ESLI) for Respirator Cartridges. Part 1: Literature Review. Defence D of, editor. Australian Goverment: Defence Science and Technology Organisaton Victoria (Australia) Human Protection and Performance Div ; 2005. p. 49.

24 Wheeler A, Robell AJ. Performance of fixed-bed catalytic reactors with poison in the feed. *J Catal* 1969; **13**: 299–305.

25 Jonas LA, Rehrmann JA. The kinetics of adsorption of organo-phosphorus vapors from air mixtures by activated carbons. *Carbon N Y* 1972; **10**: 657–63.

26 Yoon YH, Nelson JH. Application of Gas Adsorption Kinetics I. A Theoretical Model for Respirator Cartridge Service Life. *Am Ind Hyg Assoc J* Taylor & Francis; 1984; **45**: 509–16.

27 Wood GO. Organic Vapor Respirator Cartridge Breakthrough Curve Analysis. *J Int Soc Respir Prot* 1993; **10**: 400–7.

28 Lodewyckx P, Vansant EF. Estimating the overall mass transfer coefficient k(v) of the Wheeler-Jonas equation: A new and simple model. *Aihaj* 2000; **61**: 501–5.

29 Grevillot G, Marsteau S, Vallieres C. A Comparison of the Wheeler-Jonas Model and the Linear Driving Force at Constant-Pattern Model for the Prediction of the Service Time of Activated Carbon Cartridges. *J Occup Environ Hyg* 2011; **8**: 279–88.

30 An Act respecting occupational health and safety. Quebec: Éditeur officiel du Québec; 1979 p. CQLR, S-2.1.

31 An Act Respecting Industrial Accidents and Occupational Diseases, CQLR c A-3.001. CanLII; Accessed on Septemer 2016.

32 Québec. Regulation respecting occupational health and safety. *RJ-510068*. Éditeur officiel du Québec; 2002. p. O.C. 885-2001, 45.

33 Canadian Standards Association. Z94.4-93 Selection, Use, and Care of Respirators. 1993. p. 72.

34 Z94.4-11EN.book - CSA_Z94.4-11_Selection_Care_Use_of_Respirators.pdf. [Online]. Available: http://www.drivercheck.ca/wp-content/uploads/2014/12/CSA_Z94.4-11_Selection_Care_Use_of_Respirators.pdf. [Accessed: 18-Nov-2015]

35 Bollinger N. NIOSH Respirator Decision Logic. Cincinnati: NIOSH Publications Dissemination; 2004.

36 Lara Vennes, M J. Guide des Guide pratique de protection respiratoire, 2e édition. Commission de la santé et de la sécurité du travail du Québec; 2003.

37 OSHA Technical Manual (OTM) | Section VIII: Chapter 2: Respiratory Protection. *OSHA Instruction TED 01-00-015 [TED 1-0.15A]*. OSHA Instruction TED 01-00-015 [TED 1-0.15A]. [Online]. Available: https://www.osha.gov/dts/osta/otm/otm_viii/otm_viii_2.html. [Accessed: 07-Dec-2015]

38 National Institute for Occupational Safety and Health and National Personal Protective Technology Laboratory. CDC - NIOSH NPPTL CEL Cautions and Limitations.

39 Moyer ES. Review of Influential Factors Affecting the Performance of Organic Vapor Air-Purifying Respirator Cartridges. *Am Ind Hyg Assoc J* Taylor & Francis; 1983; **44**: 46–51.

40 Nguyen C, Do DD. A New Method for the Characterization Of Porous Materials. *Langmuir* American Chemical Society; 1999; **15**: 3608–15.

41 Kim J-W, Sohn M-H, Kim D-S, Sohn S-M, Kwon Y-S. Production of granular activated carbon from waste walnut shell and its adsorption characteristics for Cu2+ ion. *J Hazard Mater* 2001; **85**: 301–15.

42 Rodriguez-Reinoso F. Activated Carbon and Adsorption. Buschow KHJ, Cahn RW, Flemings MC, Ilschner B, Kramer EJ, Mahajan S, editors. *Encyclopedia of Materials - Science and Technology, Volumes 1-11*. Elsevier; 2001. p. 22–35.

43 Derbyshire F, Jagtoyen M, Thwaites M. Activated carbons-production and applications. *Porosity in carbons* Edward Arnold; 1995; **252**.

44 Marsh H, Reinoso FR. Activated Carbon. Elsevier; 2006.

45 Rodríguez-Reinoso F, Molina-Sabio M. Activated carbons from lignocellulosic materials by chemical and/or physical activation: an overview. *Carbon N Y* 1992; **30**: 1111–8.

46 Bansal RC, Goyal M. Activated Carbon Adsorption. CRC Press; 2005.

47 Bering BP, Dubinin MM, Serpinsky V V. Theory of volume filling for vapor adsorption. *J Colloid Interface Sci* Elsevier; 1966; **21**: 378–93.

48 Rodríguez-reinoso F. The role of carbon materials in heterogeneous catalysis. *Carbon N Y* 1998; **36**: 159–75.

49 Fletcher AJ, Kennedy MJ, Zhao XB, Bell JB, Thomas KM. Adsorption of Organic Vapour Pollutants on Activated Carbon. In: Mota JP, Lyubchik S, editors. *Recent Advances in Adsorption Processes for Environmental Protection and Security*. Springer Netherlands; 2008. p. 29–54.

50 Lodewyckx P. Adsorption on activated carbon: One underlying mechanism? *Recent Adv Adsorpt Process Environ Prot Secur* 2008; : 19–28.

51 Everett DH. IUPAC' Manual of Symbol and Terminology for Physicochemical Quantities and Units, Appendix, Definitions, Terminology and Symbols in Colloid and Surface Chemistry, Part I. *Pure Appl Chem* 1972; **31**: 579.

52 Brennan JK, Bandosz TJ, Thomson KT, Gubbins KE. Water in porous carbons. *Colloids Surfaces A Physicochem Eng Asp* 2001; **187**–**188**: 539–68.

53 Lodewyckx P, Vansant EF. Water isotherms of activated carbons with small amounts of surface oxygen. *Carbon N Y* 1999; **37**: 1647–9.

54 Bradley RH, Rand B. On the Physical Adsorption of Vapors by Microporous Carbons. *J Colloid Interface Sci* 1995; **169**: 168–76.

55 Polanyi M. The Potential Theory of Adsorption. *Science (80-)* 1963; **141**: 1010–3.

56 Polanyi M. Section III.-Theories of the adsorption of gases. A general survey and some additional remarks. Introductory paper to section III. *Trans Faraday Soc* The Royal Society of Chemistry; 1932; **28**: 316–33.

57 Manes M, Hofer LJE. Application of the Polanyi adsorption potential theory to adsorption from solution on activated carbon. *J Phys Chem* American Chemical Society; 1969; **73**: 584–90.

58 Wood GO, Stampfer JF. Adsorption rate coefficients for gases and vapors on activated carbons. *Carbon N Y* 1993; **31**: 195–200.

59 Rodríguez-Reinoso F, Molina-Sabio M. Textural and chemical characterization of microporous carbons. *Adv Colloid Interface Sci* 1998; **76–77**: 271–94.

60 Prakash J, Nirmalakhandan N, Speece RE. Prediction of Activated Carbon Adsorption Isotherms for Organic Vapors. *Environ Sci Technol* American Chemical Society; 1994; **28**: 1403–9.

61 Silvestre-Albero J, Silvestre-Albero A, Rodríguez-Reinoso F, Thommes M. Physical characterization of activated carbons with narrow microporosity by nitrogen (77.4K), carbon dioxide (273K) and argon (87.3K) adsorption in combination with immersion calorimetry. *Carbon N Y* 2012; **50**: 3128–33.

62 Okeola FO, Odebunmi EO. Freundlich and Langmuir Isotherms Parameters for Adsorption of Methylene Blue by Activated Carbon Derived from Agrowastes. *Adv Nat Appl Sci* 2010; **4**: 281–8.

63 Brunauer S, Deming LS, Demingn WE, Teller E. On a Theory of the van der Walls Adsorption of Gases. *J Am Chem Soc* 1940; **62**: 1723–32.

64 Sing KSW. Reporting physisorption data for gas/solid systems with special reference to the determination of surface area and porosity (Recommendations 1984). *Pure Appl Chem* 1985; **57**: 603–19.

65 Yu FD, Luo LA, Grevillot G. Adsorption isotherms of VOCs onto an activated carbon monolith: Experimental measurement and correlation with different models. *J Chem Eng Data* 2002; **47**: 467–73.

66 Langmuir I. The Constitution and Fundamental Properties of Solids And Liquids. Part I. Solids. *J Am Chem Soc* American Chemical Society; 1916; **38**: 2221–95.

67 Brunauer S, Emmett PH, Teller E. Adsorption of Gases in Multimolecular Layers. *J Am Chem Soc* American Chemical Society; 1938; **60**: 309–19.

68 Werner MD, Winters NL, Moyer ES. A review of models developed to predict gaseous phase activated carbon adsorption of organic compounds. *Crit Rev Environ Control* Taylor & Francis; 1986; **16**: 327–56.

69 Rouquerol F, Rouquerol J, Sing K. Adsorption by Powders and Porous Solids: Principles, Methodology and Applications. New York: Academic Press Inc.; 1999.

70 Dubinin MM. The Potential Theory of Adsorption of Gases and Vapors for Adsorbents

with Energetically Nonuniform Surfaces. *Chem Rev* 1960; **60**: 235–41.

71 Stoeckli F. Recent developments in Dubinin's theory. *Carbon N Y* 1998; **36**: 363–8.

72 Wood GO, Moyer ES. A review and comparison of adsorption isotherm equations used to correlate and predict organiv vapor cartridge capacities . *Am Ind Hyg Assoc J* Taylor & Francis; 1991; **52**: 235–42.

73 Wood GO. Affinity coefficients of the Polanyi/Dubinin adsorption isotherm equations - A review with compilations and correlations. *Carbon N Y* 2001; **39**: 343–56.

74 Wood GO. Activated Carbon Adsorption Capacities for Vapors. *Carbon N Y* 1992; **30**: 593–9.

75 Haynes WM. CRC handbook of chemistry and physics. 93rd ed. *Handbook of chemistry and physics*. Boca Raton, Fla.: CRC; 2013.

76 Wu JF, Claesson A, Fangmark I, Hammarstrom LG. A systematic investigation the Wheeler-Jonas equation for of the overall rate coefficient in adsorption on dry activated carbons. *Carbon N Y* 2005; **43**: 481–90.

77 Seaton NA, Walton J. A new analysis method for the determination of the pore size distribution of porous carbons from nitrogen adsorption measurements. *Carbon N Y* Elsevier; 1989; **27**: 853–61.

78 Lowell S, Shields JE, Thomas MA, Thommes M. Characterization of Porous Solids and Powders: Surface Area, Pore Size and Density. Springer Science & Business Media; 2012.

79 Landers J, Gor GY, Neimark A V. Density functional theory methods for characterization of porous materials. *Colloids Surfaces A Physicochem Eng Asp* Elsevier; 2013; **437**: 3–32.

80 Grévillot G, Vallières C. Design of Adsorption Cartridges for Personnal Protection from Toxic GasesBiodefence. In: Mikhalovsky S, Khajibaev A, editors. Springer Netherlands; 2011. p. 159–68.

81 Wood GO. Reviews of Models for Adsorption of Single Vapors, Mixtures of Vapors, and Vapors at High Humidities on Activated Carbon for Applications Including Predicting Service Lives of Organic Vapor Respirator Cartridges. report LANL, editor. 2000.

82 Wood GO. A review of the effects of covapors on adsorption rate coefficients of organic vapors adsorbed onto activated carbon from flowing gases. *Carbon N Y* 2002; **40**: 685–94.

83 M. A. S. D. Barros PAA and EAS. Mass Transfer - Advances in Sustainable Energy and Environment Oriented Numerical Modeling. Nakajima H, editor. InTech; 2013.

84 Wood GO. Estimating service lives of air-purifying respirator cartridges for reactive gas removal. *J Occup Environ Hyg* 2005; **2**: 414–23.

85 Yoon YH, Nelson JH. Breakthrough Time and Adsorption Capacity of Respirator Cartridges. *Am Ind Hyg Assoc J* 1992; **53**: 303–16.

86 Bohart GS, Adams. EQ. Some Aspects of The Behavior of Charcoal with Respect to Chlorine.1. *J Am Chem Soc* 1920; **42**: 523–44.

87 Mecklenburg W. Layer Filtration, A Contribution to the Theory of the Gas Mask. *Chem Abtr* 1926; **20**: 531.

88 Klotz I. The adsorption wave. *Chem Rev* 1946; **39**: 241–68.

89 Lodewyckx P, Wood GO, Ryu SK. The Wheeler–Jonas equation: a versatile tool for the prediction of carbon bed breakthrough times. *Carbon N Y* 2004; **42**: 1351–5.

90 Wood GO. Estimating service lives of organic vapor cartridges. *Am Ind Hyg Assoc* 1994; **55**: 11–5.

91 Wood GO, Moyer ES. A Review of the Wheeler Equation and Comparison of Its Applications to Organic Vapor Respirator Cartridge Breakthrough Data. *Am Ind Hyg Assoc J* Taylor & Francis; 1989; **50**: 400–7.

92 Wood GO, Lodewyckx P. An extended equation for rate coefficients for adsorption of organic vapors and gases on activated carbons in air-purifying respirator cartridges. *Aiha J* 2003; **64**: 646–50.

93 Wood GO. Quantification and application of skew of breakthrough curves for gases and vapors eluting from activated carbon beds. *Carbon N Y* 2002; **40**: 1883–90.

94 G.O W. Quantification and application of skew of breakthrough curves for gases and vapors eluting from activated carbon beds. *Carbon N Y* 2002; **40**: 1883–90.

95 Gleuckauf Jic, Coates JI. The influence of incomplete equilibrium on the front boundary of chromatograms and the effectiveness of separation. *J Chem Soc* 1947; **1315**: e21.

96 Grévillot G, Marsteau S, Vallières C. A Comparison of the Wheeler-Jonas Model and the Linear Driving Force at Constant-Pattern Model for the Prediction of the Service Time of Activated Carbon Cartridges. *J Occup Environ Hyg* 2011; **8**: 279–88.

97 Jonas LA, Boardway JC, Meseke EL. Prediction of adsorption behavior of activated carbons. *J Colloid Interface Sci* 1975; **50**: 538–44.

98 Nelson G, Harder C. Respirator cartridge efficiency studies IV. Effects of steady-state and pulsating flow. *Am Ind Hyg Assoc J* 1972; **33**: 797–805.

99 Nelson GO, Correia AN, Harder CA. Respirator cartridge efficiency studies: VII. effect of relative humidity and temperature. *Am Ind Hyg Assoc J* Taylor & Francis; 1976; **37**: 280–8.

100 Nelson GO, Harder CA. Respirator cartridge efficiency studies: VI. Effect of concentration. *Am Ind Hyg Assoc J* 1976; **37**: 205–16.

101 Rehrmann JA, Jonas LA. Dependence of gas adsorption rates on carbon granule size and linear flow velocity. *Carbon N Y* 1978; **16**: 47–51.

102 Trout D, Breysse PN, Hall T, Corn M, Risby T. Determination of organic vapor respirator cartridge variability in terms of degree of activation of the carbon and cartridge packing density. *Am Ind Hyg Assoc J* 1986; **47**: 491–6.

103 Léonard A, Wullens H, Blacher S, Marchot P, Toye D, Crine M, Lodewyckx P. In situ observation of wall effects in activated carbon filters by X-ray microtomography. *Sep Purif Technol* 2008; **64**: 127–30.

104 Lodewyckx P, Blacher S, Leonard A. Use of x-ray microtomography to visualise dynamic adsorption of organic vapour and water vapour on activated carbon. *Adsorpt Int Adsorpt Soc* 2006; **12**: 19–26.

105 Wood GO. Effects of air temperatures and humidities on efficiencies and lifetimes of air-purifying chemical respirator cartridges tested against methyl iodide. *Am Ind Hyg Assoc J* 1985; **46**: 251–6.

106 Tanaka S, Tanaka M, Kimura K, Nozaki K, Seki Y. Breakthrough Time of a Respirator Cartridge for Carbon Tetrachloride Vapor Flow of Workers' Respiratory Patterns. *Ind Health* 1996; **34**: 227–36.

107 Suzin Y, Nir I, Kaplan D. The effect of flow pattern on adsorption of dimethyl methyl phosphonate in activated carbon beds and canisters. *Carbon N Y* 2000; **38**: 1129–33.

108 Tanaka S, Haneda M, Tanaka M, Kimura K, Seki Y. Breakthrough Times for Vapors of Organic Solvents with Low Boiling Points in Steady-state and Pulsating Flows on Respirator Cartridges. *Ind Health* 1996; **34**: 125–31.

109 Cothran T. Service life software for organic vapor cartridges. *Occup Health Saf* 2000; **69**: 84–90.

110 Nelson GO, Harder CA. Respirator Cartridge Efficiency Studies: V. Effect of Solvent Vapor. *Am Ind Hyg Assoc J* American Industrial Hygiene Association Journal; 2010; .

111 Jonas LA, Sansone EB, Farris TS. The effect of moisture on the adsorption of chloroform by activated carbon. *Am Ind Hyg Assoc J* 1985; **46**: 20–3.

112 Werner MD. The Effects of Relative Humidity on the Vapor Phase Adsorption of Trichloroethylene by Activated Carbon. *Am Ind Hyg Assoc J* Taylor & Francis; 1985; **46**: 585–90.

113 Lodewyckx P, Vansant EF. The influence of humidity on the overall mass transfer coefficient of the Wheeler-Jonas equation. *Aihaj* 2000; **61**: 461–8.

114 Swearengen PM, Weaver SC. Respirator Cartridge Study Using Organic-Vapor Mixtures. *Am Ind Hyg Assoc J* 1988; **49**: 70–4.

115 Yoon YH, Nelson JH, Lara J, Kamel C, Fregeau D. A Theoretical Interpretation of the Service Life of Respirator Cartridges for the Binary Acetone Meta-Xylene System. *Am Ind Hyg Assoc J* 1991; **52**: 65–74.

116 Yoon YH, Nelson JH, Lara J. Respirator Cartridge Service-Life: Exposure to Mixtures. *Am Ind Hyg Assoc J* Taylor & Francis; 1996; **57**: 809–19.

117 Myers Al, Valenzuela D. Computer algorithm and graphical method for calculating adsorption equilibria of gas mixtures. *J Chem Eng Japan* 1986; **19**: 392–6.

118 Myers AL, Prausnitz JM. Thermodynamics of mixed-gas adsorption. *AIChE J* 1965; **11**: 121–7.

119 Guggenheim EA. The theoretical basis of Raoult's law. *Trans Faraday Soc* Royal Society of Chemistry; 1937; **33**: 151–6.

120 Kim D, Cai Z, Sorial GA. Determination of gas phase adsorption isotherms—a simple constant volume method. *Chemosphere* 2006; **64**: 1362–8.

121 OSHA Instruction. [Online]. Available: https://www.osha.gov/OshDoc/Directive_pdf/CPL_02-00-158.pdf. [Accessed: 23-Nov-2015].

122 Vahdat N, Swearengen PM, Johnson JS. Adsorption Prediction Of Binary-Mixtures On Adsorbents Used In Respirator Cartridges and Air-Sampling Monitors. *Am Ind Hyg Assoc J* 1994; **55**: 909–17.

123 Vahdat N. Theoretical study of the performance of activated carbon in the presence of binary vapor mixtures. *Carbon N Y* 1997; **35**: 1545–57.

124 Valenciano R, Aylón E, Izquierdo MT. A Critical Short Review of Equilibrium and Kinetic Adsorption Models for VOCs Breakthrough Curves Modelling. *Adsorpt Sci Technol* Multi Science Publishing; 2015; **33**: 851–70.

125 McKone TE. Human exposure to volatile organic compounds in household tap water: the indoor inhalation pathway. *Environ Sci Technol* ACS Publications; 1987; **21**: 1194–201.

126 Klaassen CD. Casarett & Doull's Toxicology: The Basic Science of Poisons, Seventh Edition. McGraw Hill Professional; 2007.

127 Cassee FR, Groten JP, Bladeren PJ van, Feron VJ. Toxicological Evaluation and Risk Assessment of Chemical Mixtures. *Crit Rev Toxicol* 1998; **28**: 73–101.

128 Mumtaz M, editor. Principles and Practice of Mixtures Toxicology . 2010.

129 US EPA. Guidelines for the Health Risk Assessment of Chemical Mixtures. *Fed Reg* 1986; **51**: 34014–25.

130 Groten JP, Feron VJ, Sühnel J. Toxicology of simple and complex mixtures. *Trends Pharmacol Sci* 2001; **22**: 316–22.

131 Drinking Water and Health, Volume 9. Washington, D.C.: National Academies Press; 1989.

132 CDC - NIOSH - NPPTL - Certified Equipment List. [Online]. Available: https://www.cdc.gov/niosh/npptl/topics/respirators/cel/ [Accessed: 07-Dec-2015]

133 Donald M, Wan Ying S, Kuo-Ching M, Sum Chi L. Aldehydes and Ketones. *Handbook of Physical-Chemical Properties and Environmental Fate for Organic Chemicals, Second Edition*. CRC Press; 2006. p. 2583–686.

134 Donald M, Wan Ying S, Kuo-Ching M, Sum Chi L. Aliphatic and Cyclic Hydrocarbons. *Handbook of Physical-Chemical Properties and Environmental Fate for Organic Chemicals, Second Edition*. Boca Raton: CRC Press; 2006. p. 61–404.

135 Donald M, Wan Ying S, Kuo-Ching M, Sum Chi L. Halogenated Aliphatic Hydrocarbons. *Handbook of Physical-Chemical Properties and Environmental Fate for Organic Chemicals, Second Edition*. Boca Raton: CRC Press; 2006. p. 921–1256.

136 Silvestre-Albero A, Rico-Francés S, Rodríguez-Reinoso F, Kern AM, Klumpp M, Etzold BJM, Silvestre-Albero J. High selectivity of TiC-CDC for CO2/N2 separation. *Carbon N Y* 2013; **59**: 221–8.

137 Baertsch CD, Funke HH, Falconer JL, Noble RD. Permeation of Aromatic Hydrocarbon Vapors through Silicalite−Zeolite Membranes. *J Phys Chem* American Chemical Society; 1996; **100**: 7676–9.

138 Ferreira AFP, Mittelmeijer-Hazeleger MC, Granato MA, Martins VFD, Rodrigues AE, Rothenberg G. Sieving di-branched from mono-branched and linear alkanes using ZIF-8: experimental proof and theoretical explanation. *Phys Chem Chem Phys* 2013; **15**: 8795–804.

139 Samoto H, Fukui Y, Ukai H, Okamoto S, Takada S, Ohashi F, Moriguchi J, Ezaki T, Ikeda M. Field survey on types of organic solvents used in enterprises of various sizes. *Int Arch Occup Environ Health* Springer-Verlag; 2006; **79**: 558–67.

140 Commission des normes de l'équité de la santé et de la sécurité du travail. Répertoire Toxicologique. 2015.

141 Ettinger H, Janssen L, Metzler R. Respiratory Protection Committee Identifies Research Priorities. *Synergist* 2009; **20**: 26–7.

142 Ruch WE, Nelson GO, Lindeken CL, Johnsen RG, Hodgkins DJ. Respirator Cartridge Efficiency Studies. *Am Ind Hyg Assoc J* Taylor & Francis; 1972; **33**: 105–9.

143 Coyne K, Caretti D, Scott W, Johnson A, Koh F. Inspiratory flow rates during hard work when breathing through different respirator inhalation and exhalation resistances. *J Occup Environ Hyg* 2006; **3**: 490–500.

144 Linders MJG, Mallens EPJ, van Bokhoven JJGM, Kapteijn F, Moulijn JA. Breakthrough of Shallow Activated Carbon Beds Under Constant and Pulsating Flow. *AIHA J* Taylor & Francis; 2003; **64**: 173–80.

145 Janvier F, Tuduri L, Cossement D, Drolet D, Lara J. Micropore characterization of activated carbons of respirator cartridges with argon, carbon dioxide, and organic vapors of different vapor pressures. *Carbon N Y* 2015; **94**: 781–91.

146 Janvier F, Tuduri L, Cossement D, Drolet D, Lara J. Systematic evaluation of the adsorption of organic vapors onto a miniaturized cartridge device using breakthrough tests in parallel experiment with a full size respirator cartridge. *Adsorpt Sci Technol* 2016; **34**: 287–306.

147 Vuong F, Chauveau R, Grevillot G, Marsteau S, Silvente E, Vallieres C. Predicting the lifetime of organic vapor cartridges exposed to volatile organic compound mixtures using a partial differential equations model. *J Occup Environ Hyg* Taylor & Francis; 2016; .

148 OSHA. Inspection procedures for the Respiratory Protection Standard. *CPL 02-00-120*. 1998.

149 Jonas LA, Rehrmann JA. Predictive equations in gas adsorption kinetics. *Carbon N Y* 1973; **11**: 59–64.

150 Wood GO. Estimating Service Lives of Organic Vapor Cartridges. *Am Ind Hyg Assoc J*

Taylor & Francis; 1994; **55**: 11–5.

151 Lodewyckx P, Vansant EF. Influence of humidity on adsorption capacity from the Wheeler-Jonas model for prediction of breakthrough times of water immiscible organic vapors on activated carbon beds. *Am Ind Hyg Assoc J* 1999; **60**: 612–7.

152 Reid CR, Thomas KM. Adsorption Kinetics and Size Exclusion Properties of Probe Molecules for the Selective Porosity in a Carbon Molecular Sieve Used for Air Separation. *J Phys Chem B* American Chemical Society; 2001; **105**: 10619–29.

153 Dubinin MM. No Title. *Chem. and Phys. of Carbon*. New York: EL. Walker, Jr. (Ed.),Mercel Dekker; 1966.

154 Wood GO. D-R Plots and Typical Parameters for Several OV and Multigas Cartridges and Canisters. *J Int Soc Respir Prot* 2009; **26**: 71–81.

155 Jones J, Smith ME. CBDE Protocol for snowstorm filling of carbon filters bed. *CBDE Technical note No.1242*. CDE; 1992.

156 Tuduri L, Janvier F, Cloutier Y, Poulin J, Cossement D, Drolet D, Lara J. Optimisation de SATURISK, l'outil de calcul du temps de service des cartouches de protection respiratoire contre les vapeurs organiques. *Études et recherches*. Montréal: IRSST; 2015.

157 Tarafder A, Mazzotti M. A Method for Deriving Explicit Binary Isotherms Obeying the Ideal Adsorbed Solution Theory. *Chem Eng Technol* 2012; **35**: 102–8.

158 Smith JWH, Romero JV, Dahn TR, Dunphy K, Sullivan B, Mallay M, Croll LM, Reynolds JH, Andress C, Dahn JR. The effect of heating temperature and nitric acid treatments on the performance of Cu- and Zn-based broad spectrum respirator carbons. *J Colloid Interface Sci* 2011; **364**: 178–94.

159 Romero J V, Smith JWH, Sullivan BM, Croll LM, Dahn JR. SO2 and NH3 gas adsorption on a ternary ZnO/CuO/CuCl2 impregnated activated carbon evaluated using combinatorial methods. *ACS Comb Sci* ACS Publications; 2011; **14**: 31–7.

160 Wood GO. Review and comparisons of D/R models of equilibrium adsorption of binary mixtures of organic vapors on activated carbons. *Carbon N Y* Elsevier; 2002; **40**: 231–9.

161 Wu J, Xie Z, Guo K, Claesson O. Measurement and Prediction of the Adsorption of Binary Mixtures of Organic Vapours on Activated Carbon. *Adsorpt Sci Technol* 2001; **19**: 737–49.

ANNEXE I

Fig. A1 shows that as the size of the narrow micropore volume increased, so did the breakthrough time, however, at around 0.20 cm^3/g, there seems to be an optimal value where the increase of the narrow pore size has no effect on the breakthrough time. This trend was observed across all five OV tested but only three vapors are shown here for clarity. The influence of the pore size on breakthrough time was only observed for the narrow micropores.

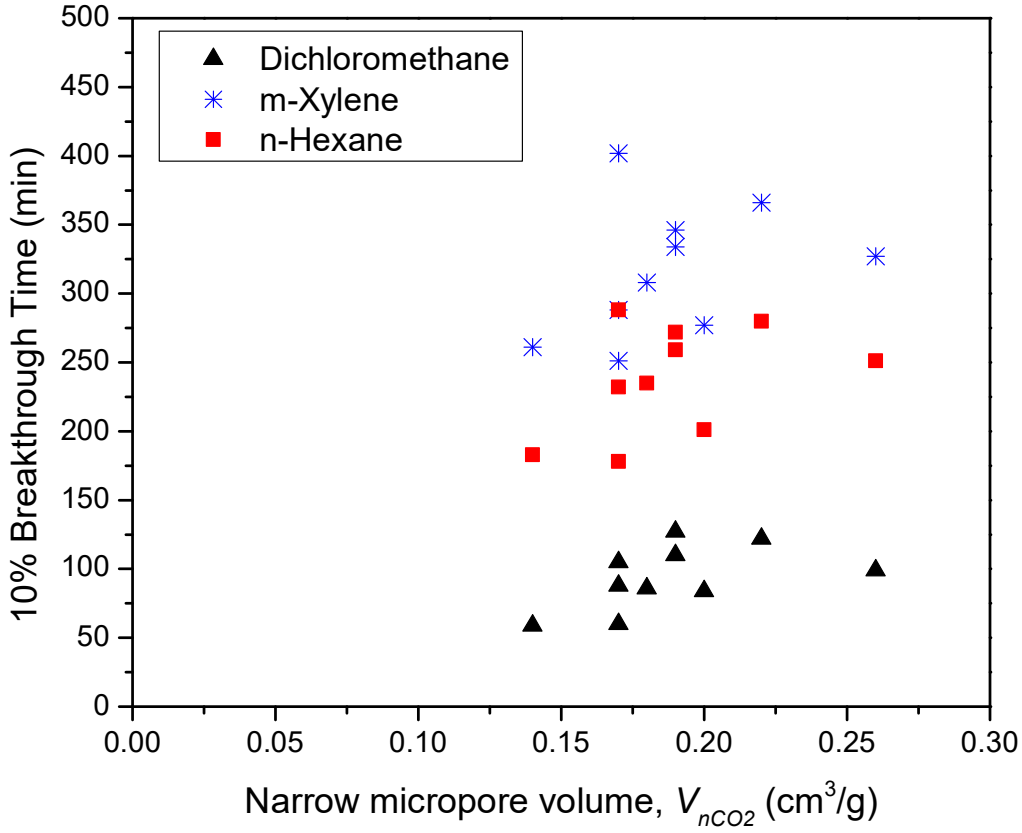

Fig. A1-Relationship between the breakthrough time and the narrow micropore volume for the series of activated carbon OV cartridges studied.